2018

Development And Characterization Of Novel Raf Dimer Inhibitors To Target Brafv600e Inhibitor Resistance

Michael Joseph Grasso
University of Pennsylvania, michaelgrasso4@gmail.com

Development And Characterization Of Novel Raf Dimer Inhibitors To Target Brafv600e Inhibitor Resistance

Abstract
ABSTRACT

BRAF is a notable oncoprotein within the MAPK signaling pathway, which is a pathway that sends a signal from the surface of a cell to the nucleus of a cell via phosphorylation cascades. This pathway regulates cell growth, differentiation, and survival. BRAF is known to be mutated in about 50% of melanomas, and less frequently in a wide variety of other cancers, making BRAF a bona-fide target for therapy. In melanoma, a single V600E activation segment mutation (BRAFV600E) accounts for ~90% of BRAF mutant malignant tumors. BRAFV600E selective inhibitors, such as vemurafenib, extend the survival of patients in the clinic, however most patients develop drug resistance and progress at a median of 6 months. One mode of resistance is "paradoxical activation" of RAF heterodimers. In this mechanism, a drug-bound BRAF protomer dimerizes with either BRAFWT or CRAFWT, allosterically stimulating kinase activity and leading to hyper-activation of the MAPK pathway.

The first part of this thesis involves my efforts to develop bivalent BRAF inhibitors to target paradoxical activation of active RAF dimers. We successfully chemically linked two BRAFV600E selective vemurafenib inibitors and found that this bivalent inhibitor stabilized an inactive face-to-face BRAF dimer conformation. We then extended this strategy to pan-RAF inhibitor TAK632 to target BRAFWT and CRAFWT in cells. Interestingly, this bivalent molecule was unable to "trap" two BRAF molecules in the same face-to-face conformation as the bivalent vemurafenib inhibitor, but also uncovered that the monovalent TAK632 depends on induction of active conformation BRAF dimers to be able to potently inhibit RAF.

The last part of this thesis involved the development of a high throughput screen to discover novel inhibitors that can disrupt the complex between BRAF and its downstream substrate MEK. We were able to design a high throughput TR-FRET assay to identify 15 novel inhibitors that can inhibit BRAF/MEK dimerization. Together, our studies identify novel RAF dimer inhibitors that can be used as chemical probes to further understand BRAF signaling through RAF dimerization in melanoma and other BRAF-related cancers. These studies also highlight a novel method of targeting paradoxical activation and RAF dimerization for melanoma therapy.

Degree Type
Dissertation

Degree Name
Doctor of Philosophy (PhD)

Graduate Group
Chemistry

First Advisor
Ronen Marmorstein

Keywords
BRAF, cancer, crystallography, inhibitor

Subject Categories
Biochemistry

DEVELOPMENT AND CHARACTERIZATION OF NOVEL RAF DIMER INHIBITORS TO TARGET BRAF^{V600E} INHIBITOR RESISTANCE

Michael J. Grasso

A DISSERTATION

in

Chemistry

Presented to the Faculties of the University of Pennsylvania

in

Partial Fulfillment of the Requirements for the

Degree of Doctor of Philosophy

2018

Supervisor of Dissertation

_____

Ronen Marmorstein, Ph.D.
George W. Raiziss Professor of Biochemistry and Biophysics

Graduate Group Chairperson

_____

Dr. Gary A. Molander
Hirschmann-Makineni Professor of Chemistry

Dissertation Committee
Dr. David W. Christianson, Roy and Diana Vagelos Professor in Chemistry and Chemical Biology, Committee Chair
Dr. Jeffrey D. Winkler, Merriam Professor of Chemistry
Dr. Emmanuel Skordalakes, Associate Professor of Gene Expression and Regulation
Dr. E. James Petersson, Associate Professor of Chemistry

Dedicated to Mom and Dad

Acknowledgements

First and foremost, I have to thank Ronen for being not only an incredible mentor in science but also being incredibly supportive in anything I wished to achieve. I was able to learn so much from being in his lab, and he took steps to ensure that not just my techniques at the bench improved but also my writing, speaking, and critical thinking skills improved as well. He has also been incredibly patient and his open-door policy allowing me to barge in at any second to ask him about an experiment or a paper or any other number of things has helped me immensely. I also need to thank my committee members Dr. David Christianson, Dr. Emmanuel Skordalakes, Dr. E. James Petersson, and Dr, Jeffrey Winkler for their encouragement, constructive criticisms, and overall help in my graduate studies. Dr. Jeffrey Winkler, Dr. Jessie Villanueva, and Dr. Donita Brady have also been great collaborators who not only helped with my work but also took time out to help give me advice on my career, and I can't stress enough how helpful it has been to have these people around to support me.

The lab has been an incredibly great environment to learn techniques, and my mentor Dr. Jasna Maksimoska was great in teaching me all that she knows about protein purification, crystallization, and assay development. After Jasna left, I also "adopted" Dr. John Domsic and Dr. Adam Olia as my surrogate mentors, and they also helped teach me too many techniques to count. Dr. Michael Ricketts, Dr. Robert Magin, Dr. Yadilette Rivera-Colon, Dr. Ryan Emptage, Dr. Austin Vogt, and everyone else in the lab has also been incredibly helpful in teaching me or just helping me with a problem I was having that day. To Sravya, Alaina, Natalie, Kiara, and Kristen: You guys were awesome rotation students and I've learned so much from you. Thanks for putting up with me. To Michelle,

Shuai, Minu, and Julianne, you guys have been amazing collaborators and I'm so glad I got to work with you.

My friends have also helped me keep my sanity over the last couple of years. Melissa, Sam, Mike, Matt G., Angela, Kate, Alex, Jackie, Carmen, Shane, Jane, Rob, Yady, Jason, Emily, Cheryl, and Gleb: you guys have made life not suck when things have been pretty bad, and I can't thank you enough for that. Special thanks to Matt Barry for being an amazing roommate. I also need to thank Angel Payan because he asked to be mentioned by name specifically.

Lastly, my family has been incredibly supportive through everything that I've done. Living close to home meant I got to see my parents, grandparents, aunts, and uncles way more often than the average person and it has been great. Going to Rocco's on a Saturday night and then going over Grandpop Mike's afterwards for a cup of coffee and a UFC fight, a baseball game or even Family Feud will be a memory I will always cherish. Mommom Do, Poppop Moon, and everyone else helped so much just by being there when I needed them. I also was able to visit my sister Corinne and brother-in-law Matt twice (!!) in England, and whether we traveled to Edenborough or just toured castles in the English countryside, its been great. And even though I haven't met her in person yet, I have to thank Amelia for being adorable. Finally, I need to thank my parents for helping me become who I am and keeping me from driving myself crazy. My first year things didn't go as planned, and when I thought that I was going to get kicked out of grad school, my father was the one who was stuck trying to calm me down. He managed to do it (I don't know how), and I can't ever thank him or my mother enough for all of their help and support.

ABSTRACT

DEVELOPMENT AND CHARACTERIZATION OF NOVEL RAF DIMER INHIBITORS TO TARGET BRAF^{V600E} INHIBITOR RESISTANCE

Michael J. Grasso

Ronen Marmorstein

BRAF is a notable oncoprotein within the MAPK signaling pathway, which is a pathway that sends a signal from the surface of a cell to the nucleus of a cell via phosphorylation cascades. This pathway regulates cell growth, differentiation, and survival. BRAF is known to be mutated in about 50% of melanomas, and less frequently in a wide variety of other cancers, making BRAF a bona-fide target for therapy. In melanoma, a single V600E activation segment mutation (BRAF^{V600E}) accounts for ~90% of BRAF mutant malignant tumors. BRAF^{V600E} selective inhibitors, such as vemurafenib, extend the survival of patients in the clinic, however most patients develop drug resistance and progress at a median of 6 months. One mode of resistance is "paradoxical activation" of RAF heterodimers. In this mechanism, a drug-bound BRAF protomer dimerizes with either BRAF^{WT} or CRAF^{WT}, allosterically stimulating kinase activity and leading to hyper-activation of the MAPK pathway.

The first part of this thesis involves my efforts to develop bivalent BRAF inhibitors to target paradoxical activation of active RAF dimers. We successfully chemically linked two BRAF^{V600E} selective vemurafenib inibitors and found that this bivalent inhibitor stabilized an inactive face-to-face BRAF dimer conformation. We then extended this strategy to pan-RAF inhibitor TAK632 to target BRAF^{WT} and CRAF^{WT} in cells.

Interestingly, this bivalent molecule was unable to "trap" two BRAF molecules in the same face-to-face conformation as the bivalent vemurafenib inhibitor, but also uncovered that the monovalent TAK632 depends on induction of active conformation BRAF dimers to be able to potently inhibit RAF.

The last part of this thesis involved the development of a high throughput screen to discover novel inhibitors that can disrupt the complex between BRAF and its downstream substrate MEK. We were able to design a high throughput TR-FRET assay to identify 15 novel inhibitors that can inhibit BRAF/MEK dimerization. Together, our studies identify novel RAF dimer inhibitors that can be used as chemical probes to further understand BRAF signaling through RAF dimerization in melanoma and other BRAF-related cancers. These studies also highlight a novel method of targeting paradoxical activation and RAF dimerization for melanoma therapy.

Table of Contents

List of Tables

List of Figures

Chapter 1-the MAPK Signaling Pathway and Cancer

1.1 Phosphorylation

Protein kinases are enzymes that modify other proteins by adding phosphate groups to them to either regulate activity, localization, or interactions between various molecules. Kinases are involved in a large percentage of the signal transduction within eukaryotic cells, sending signals either from the surface of a cell to the nucleus of a cell, or managing cross talk between different cell types (Manning, Whyte, Martinez, & Hunter, 2002). One of the first protein kinases to be discovered was cAMP-dependent protein kinase (PKA) in 1968, leading the way for further analysis and classification of these essential and complex enzymes (Walsh, Perkins, & Krebs, 1968). The further discovery of Src led to the elucidation that while existing kinases were known to phosphorylate serine and threonine, Src was a tyrosine kinase, opening the door for different mechanisms of phosphorylation (Hunter, 2009). Furthermore, in 1982, sequence screening led to the discovery that PKA is related to Src gene kinases, establishing that these proteins stemmed from a common ancestor (Barker & Dayhoff, 1982).

These discoveries led to the illumination of the protein kinome, one of the largest eukaryotic families of proteins, corresponding to close to 2% of the entire genome (**Figure 1**) (Taylor & Kornev, 2011). As more kinases were discovered through the surge of cloning technologies, a study was performed to map conserved regions of the catalytic domains through alignment and amino acid sequence similarities to elucidate properties and functions of the catalytic core (S. Hanks, Quinn, & Hunter, 1988). This study revealed 11 highly conserved subdomains within the catalytic region of the kinase, later expanded to 12 regions (S. K. Hanks & Hunter, 1995). With primary structure alone, a phylogenic tree was adapted, allowing predictions of function and substrates just by looking at conserved

residues, as well as reflecting evolution stemming from gene duplication events or from speciation.

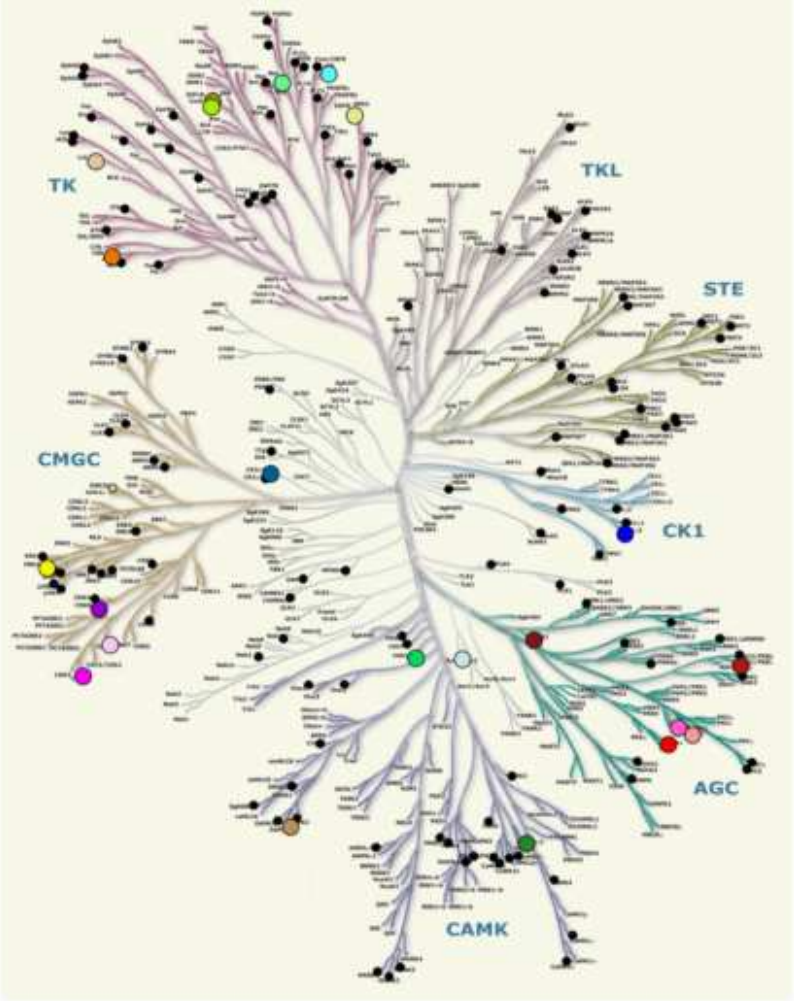

Figure 1 The human kinome.

Black circles represent publicly available structures. The 7 subfamilies are as follows: AGC (Containing PKA, PKG, PKC families), CAMK (Calcium/calmodulin dependent protein kinase), CK1 (Casein kinase 1), CMGC (Containing CDK, MAPK, GSK3, and CLK families), STE (Homologs of yeast sterile 7, sterile 11, sterile 20 kinases), TK (tyrosine kinases), and TLK (tyrosine kinase-like). Figure taken from (Taylor & Kornev, 2011).

In 1991, the first crystal structure of a kinase, PKA, was solved, allowing for the previously classified subdomains to be mapped to corresponding secondary structure (Knighton et al., 1991). This crystal structure resolved the now common kinase catalytic domain, consisting of a smaller N-terminal lobe (N-lobe) and a larger, C-terminal lobe (C-lobe) with a cleft being formed between the two lobes. This cleft is the site of catalysis, with substrate, ATP and Mg binding between the two lobes. Five β strands encompass the majority of the N-lobe, with an α helix on the surface. The C-lobe, in contrast, is composed mostly of α helices (Knighton et al., 1991). While kinase structures may differ slightly from enzyme to enzyme, the main structural motifs are present in all human kinase structures (Taylor & Kornev, 2011). Because kinases regulate signal transduction, they are often linked to disease as mutations in these enzymes can cause aberrant cell growth, as well as halt or hyper activate important mechanisms needed for survival (Ochoa, Bradley, & Beltrao, 2018). These initial studies on kinase structure and function paved the way for drug development to target a wide variety of diseases and enzymatic pathways.

1.2 Kinase inhibitor development

One of the first molecules developed for the inhibition of kinase activity is Staurosporine, a natural product isolated from bacteria *Streptomyces* (Omura et al., 1977). It was discovered to hit important kinases such as PKA and v-src p60 with half maximal inhibitory concentration (IC_{50})'s in the low nanomolar range (Nakano et al., 1987). This inhibitor was later found to be an ATP-competitive inhibitor, binding in the pocket ATP binds to trigger a phosphorylation event. However, it was also found to lack selectivity, hitting many kinases known in the human kinome (Karaman et al., 2008). While this inhibitor lacks the selectivity needed to be a fruitful molecule in the clinic, it brought about

the need for selectivity testing, as the initial sequence alignments and structure studies shed light on the similarities of structures within the human kinome, despite very different targets and pathways. Staurosporine is also a useful tool in research, and even led to the FDA approval of Midostaurin, a semi-synthetic stauro sporine analog used for treatment of acute myeloid leukemia (AML) (Weisberg et al., 2002).

In 2001, the first kinase small molecule inhibitor, imatinib (Gleevec) was approved by the FDA (Müller, Chaikuad, Gray, & Knapp, 2015). The clinical success of imatinib led to optimism in the field of drug discovery and kinase inhibition, as it was shown to treat patients with chronic myelogenous leukemia (CML) (Jänne, Gray, & Settleman, 2009). While success in the clinic is not easy to come by, kinase inhibitors' impressive results in a variety of cancers as well as the potential that comes from such a large enzyme family lends to the importance in the field of medicinal chemistry and pharmacology (Knapp & Sundström, 2014).

Out of the class of inhibitors currently available, there are four classes of kinase inhibitors. ATP mimetic inhibitors that bind in the ATP active site cleft make up the first two classes of kinase inhibitors, whereas those that stabilize an "active" state are type I inhibitors and those that stabilize an "inactive" state are type II inhibitors (Müller et al., 2015). The classification of "active" versus "inactive" comes from the position of the DFG motif, a conserved three residue patch in almost all kinases that is involved in magnesium binding and stabilization near the active site pocket. When the motif is flipped inward, this is considered an active conformation, whereas the flipping outward to open up an allosteric pocket refers to a type II, inactive conformation (**Figure 2**) (Treiber & Shah, 2013). Kinases are known to be highly dynamic and thought to alternate between the active and

inactive states when not bound to any substrate or inhibitor. These different classes of inhibitor can stabilize either state through by extending to occupy not only the ATP binding region but also an accompanying allosteric pocket within the binding cleft (Treiber & Shah, 2013). Type III kinase inhibitors are allosteric inhibitors that bind to a region other than the ATP site. While these are less common than types I and II, there have been examples of type III that have been approved by the FDA, such as Trametinib (Salama & Kim, 2013). Type IV inhibitors, meanwhile, bind to surface pockets of the kinase to block protein-protein interactions. This class of kinase inhibitor is the least studied of the four (Müller et al., 2015). Through the utilization of these four different classes, more selective inhibitors can be developed to produce highly potent and selective molecules targeting specific pathways involved in diseases such as many different types of cancer.

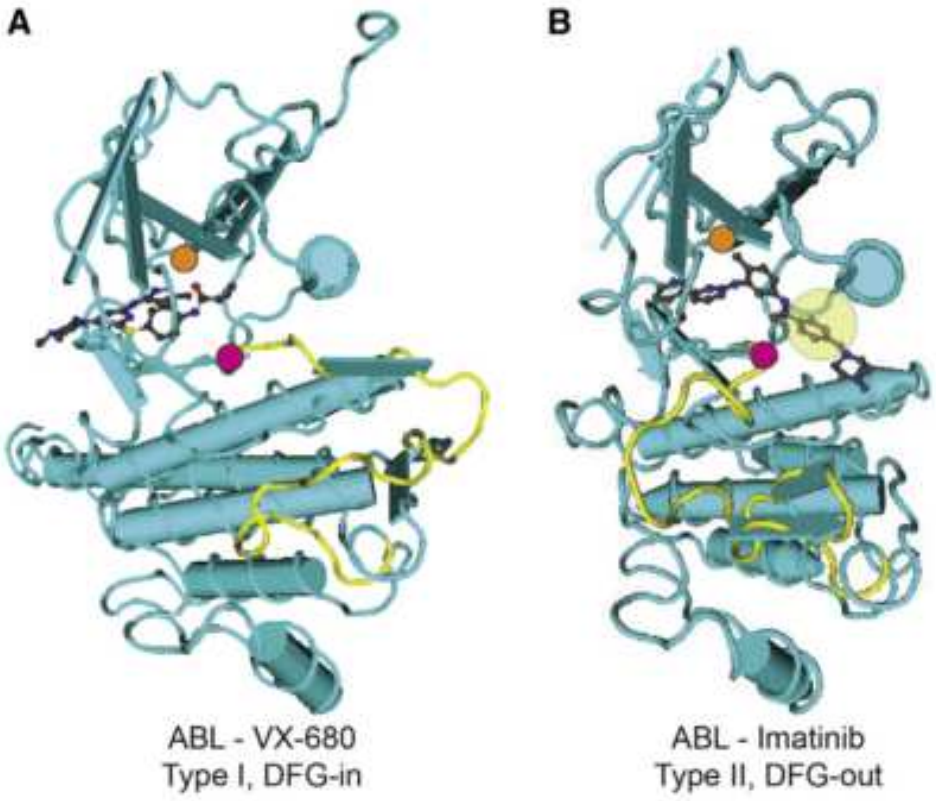

Figure 2 DFG-in versus DFG-out.

Figure A, left, shows protein kinase ABL bound to inhibitor VX-680, a type I inhibitor that stabilizes a DFG-in, active conformation, flipping the activation segment (yellow) to the right. Figure B, right, shows ABL bound to type II inhibitor Imatinib, stabilizing a DFG-out, inactive conformation, flipping the activation segment (yellow) to the left. Both figures show the inhibitors in black sticks. The gatekeeper residue is shown by an orange circle, and the DFG motif is shown by a magenta circle. Figure taken from (Treiber & Shah, 2013).

1.3 MAPK/ERK Signaling Pathway

The mitogen-activated protein kinase (MAPK) signaling pathway is a family of kinases that help to send a signal from the surface of a cell to either the nucleus or cytoplasm of a cell to regulate cell growth, survival, and differentiation (Wellbrock, Karasarides, & Marais, 2004). These signals are sent through the activation and process of a cascade of three kinases that trigger one another in succession. The most upstream kinases are MAPK kinase kinases (MAPKKK) which are serine/threonine kinases that phosphorylate and activate the MAPK kinase (MAPKK) dual specificity serine/threonine/tyrosine kinases, which then phosphorylate the final kinases in the cascade, the MAPKs, which have many different substrates within the nucleus as well as the cytoplasm (Acosta & Kadkol, 2016; Wellbrock et al., 2004). Within the MAPK signaling pathway family lies four distinct cascades, named after their downstream MAPKs; the extracellular signal regulated kinases 1/2 (ERK1/2), Jun amino-terminal kinases 1/2/3 (JNK1/2/3), p38-MAPK, and extracellular signal regulated kinase 5 (ERK5). These pathways are usually regulated by growth factors binding to receptor tyrosine kinases (RTKs) but can also be initiated via stress (Acosta & Kadkol, 2016). RTK's contain an extracellular binding region capable of binding growth factors, as well as a transmembrane domain and an intracellular domain that contains a kinase domain. Growth factor binding activates the intracellular kinase domain, allowing for dimerization and trans-phosphorylation to trigger recruitment of adaptor proteins to further initiate pathway activation (Katz, Amit, & Yarden, 2007). Adaptor proteins can bind to phosphorylated regions of RTKs as well as guanine-nucleotide exchange factors (GEFs), which bind GTPases and allow release of GDP and, in turn, initiate binding of GTP. This GTP binding

can activate the GTPase, which allows for activation of the MAPKKK, triggering the phosphorylation cascade (Acosta & Kadkol, 2016).

One of the most studied MAPK signaling pathways is the ERK1/2 pathway, due to its heavy involvement in cancer and disease, and the terms "ERK1/2 pathway" and MAPK signaling pathway" are often used interchangeably referring to ERK1/2 (Wellbrock et al., 2004). In 1983, the isolation of the v-raf oncogene from a mouse retrovirus was reported, and was later found to be a serine/threonine kinase (Moelling, Heimann, Beimling, Rapp, & Sander, 1984; Rapp et al., 1983). V-raf's cellular homologue, CRAF, was later discovered in human cells and characterized as a proto-oncogene (Bonner et al., 1985). The corresponding protein CRAF would later be characterized as a MAPKKK in the ERK1/2 MAPK signaling pathway, however the discovery of the CRAF gene paved the way to this discovery (Hugo Lavoie & Therrien, 2015; Wellbrock et al., 2004). While human homologues ARAF and BRAF were discovered shortly thereafter, little was known other than that they were proto-oncogenes whose corresponding proteins had kinase activity (Huleihel et al., 1986; Ikawa et al., 1988). In 1987, ERK, then known as MAP-kinase due to its ability to phosphorylate microtubule associated protein 2 (MAP-2), was discovered and characterized as being activated by growth factors such as insulin (Boulton et al., 1991; Ray & Sturgill, 1987; Rossomando, Payne, Weber, & Sturgill, 1989). ERK1/2's MAPKK, MEK1, was soon discovered, and this was connected to the RAF proteins when MEK1 was found to be a substrate of CRAF (Crews & Erikson, 1992; Kyriakis et al., 1992). ERK1/2 activation was found to be initiated by insulin, and this was corroborated with studies connecting CRAF with receptor tyrosine kinases and RAS, the upstream GTPase (Chuang et al., 1994; Kolch, Heidecker, Lloyd, & Rapp, 1991; Morrison,

Kaplan, Rapp, & Roberts, 1988). The relationship between RAS and RAF was further elucidated when RAS was found to interact directly with the amino (N) -terminus of RAF, activating it, and soon a clearer picture of the ERK1/2 signaling pathway was revealed (Dent, Reardon, Morrison, Sturgill, & Iol, 1995; Vojtek, Hollenberg, & Cooper, 1993; X. F. Zhang et al., 1993). Upon binding of growth factors, receptor tyrosine kinases can dimerize and activate one another, initiating bonding of adaptor protein GRB2, which can then bind guanine-nucleotide exchange factor SOS, which can interact and stimulate GTP binding and activation of RAS. This activation stimulates N-terminal binding to the RAF proteins, triggering the phosphorylation cascade of RAF phosphorylating MEK and MEK phosphorylating ERK (**Figure 3**). (Acosta & Kadkol, 2016; Hugo Lavoie & Therrien, 2015; Wellbrock et al., 2004).

ERK1 is the first of the MAPK proteins to be discovered, and ERK2 was cloned shortly thereafter (Boulton et al., 1991). These proteins share 83% amino acid sequence identity (Boulton et al., 1991; Cargnello & Roux, 2011). After activation via RTK and RAS stimulation of the RAF-MEK-ERK phosphorylation cascade, ERK proteins can either phosphorylate their targets in the cytoplasm or be imported to the nucleus to phosphorylate nuclear substrates (Cargnello & Roux, 2011; R. H. Chen, Sarnecki, & Blenis, 1992). A recent proteomics study reported that ERK has over 600 direct target sites, highlighting the immense scope of ERKs functionality (Ünal, Uhlitz, & Blüthgen, 2017). ERK mainly controls cell proliferation through its target phosphorylation, and can do so by multiple mechanisms, but is also known to regulate transcription factors such as Elk-1 (Cargnello & Roux, 2011).

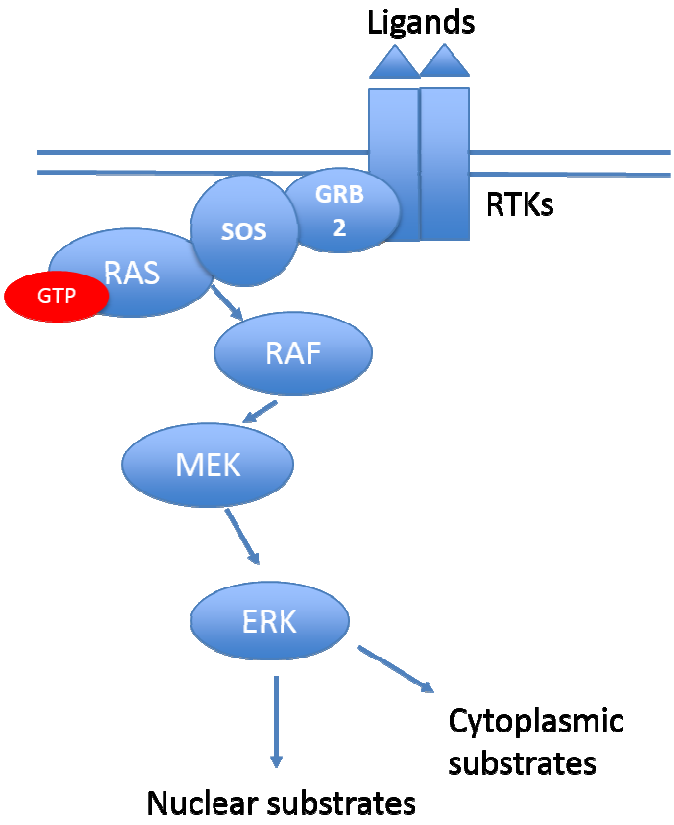

Figure 3 MAPK/ERK signaling pathway.

A schematic illustrating the ERK1/2 signaling pathway, in which growth factor binding stimulates RTK dimerization and activation of the RTK kinase domain. This allows adaptor GRB2 to bind and recruit SOS, which can bind and activate RAS by promoting GTP binding. RAS-GTP binding to RAF proteins then stimulates a phosphorylation cascade in which RAF proteins activate MEK and MEK activates ERK. This figure is adapted from (Wellbrock et al., 2004).

1.4 BRAF and Cancer

The ERK1/2 pathway has been heavily studied since its discovery due to its involvement in cell proliferation, as well as its hyper-activation in about 30% of tumor cell lines (Hoshino et al., 1999). In the late 1990's and early 2000's, RAS was the focal point of many researchers' studies due to its mutations in 15% of all human cancers. However, it was soon discovered that BRAF, one of the three homologues of the RAF proteins, had a high frequency of mutations in cancers such as melanoma (60%), colorectal cancers (18%) and gliomas (11%), among others (Davies et al., 2002; Wellbrock et al., 2004). While many different BRAF mutations can be found in cancers, a majority of them are found in the kinase domain. Of these mutations, 98.4% occur at the specific residue valine 600. Of those mutations, 97.8% of them are one specific point mutation: a glutamate instead of the valine (V600E) (**Figure 4**) (Hugo Lavoie & Therrien, 2015).

While BRAF has become a focus due to its major role in cancer, particularly melanoma, the other RAF homologues, ARAF and CRAF, also play an important role in ERK1/2 signaling. Although the three homologues differ in protein sequence, they have three conserved regions, CR1, CR2, and CR3 (**Figure 5**). CR1 consists of two particular regions, a RAS binding domain (RBD) that acts as an auto regulatory domain and frees up the kinase domain for activation after binding RAS, and a cysteine rich domain (CRD) (Tran, Wu, & Frost, 2005). The CR2 domain acts as regulatory domain that can bind 14-3-3 proteins upon phosphorylation by kinases such as PKA (Cook & McCormick, 1993; Muslin, Tanner, Allen, & Shaw, 1996), and CR3 is the kinase domain (Hugo Lavoie & Therrien, 2015).

Interestingly, BRAF mutations are much more predominant in cancer patients than in CRAF or ARAF, and this is due to sequences within the kinases right before the kinase domain (Forbes et al., 2011; Wellbrock et al., 2004). The RAF kinases are regulated not just by RAS binding but also by multiple phosphorylation events, and one of these occurs on an N-terminal acidic (NtA) region right before the kinase domain that requires a negative charge in order to activate the kinases. In ARAF and CRAF, these sequences are SSYY (residues 299-302 in ARAF and 338-341 in CRAF), and must be phosphorylated by SRC kinases on the tyrosine residues and casein kinase 2 (CK2) on serine residues (Diaz et al., 1997; Ritt et al., 2007; Williams, Roberts, & Li, 1992). In contrast, BRAF has the sequence SSDD in its NtA region, resulting in less phosphorylation events needed for activation (Marais, Light, Paterson, Mason, & Marshall, 1997). Moreover, negative charge is needed for CK2 to phosphorylate the serine residue in the NtA region, meaning its phosphorylation of BRAF is unregulated whereas ARAF and CRAF are SRC-dependent (**Figure 5**) (Ritt et al., 2007). BRAF, therefore, only needs RAS binding to its N-terminus and phosphorylation on its activation segment to be activated (Hugo Lavoie & Therrien, 2015). This "priming" of RAF activation leads to a more activated kinase than ARAF or CRAF (Wellbrock et al., 2004). This also explains BRAF's V600E mutation, as this mimics activation segment phosphorylation, which is otherwise required on residues T599 and S602 in BRAF (B. H. Zhang & Guan, 2000). While all three RAF isoforms are known to phosphorylate MEK, to what degree and how these three kinases function together is not completely understood. Many studies have shown evidence that BRAF:CRAF heterodimers exist in cells and exhibit higher activity than respective RAF homodimers,

and one particular study suggests that ARAF can act as a scaffolding protein to regulate these heterodimers (Hugo Lavoie & Therrien, 2015; Rebocho & Marais, 2013).

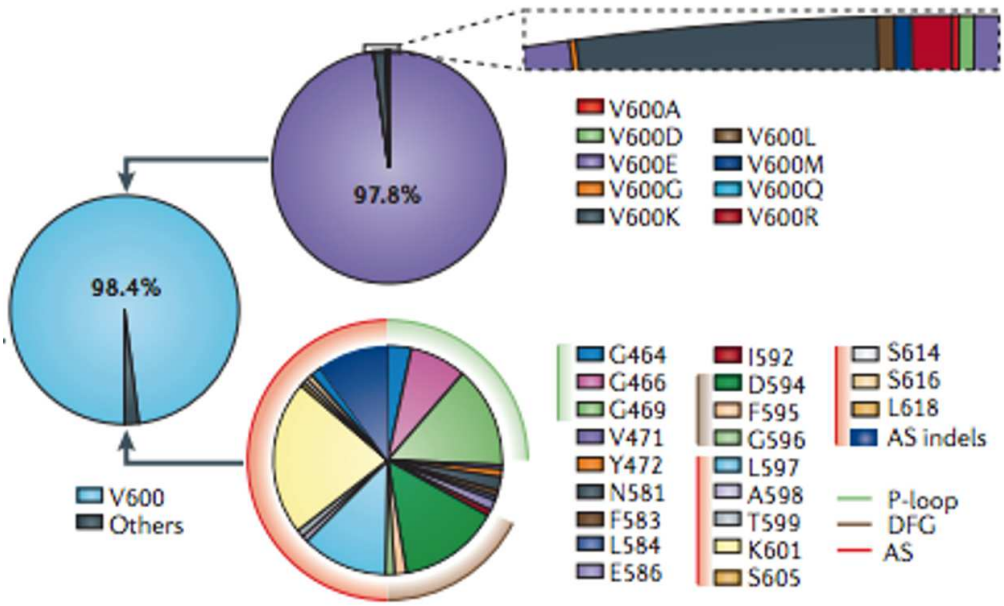

Figure 4 Mutations in BRAF.

Pie graph showing the prevalence of point mutations at residue 600, primarily V600E. Taken from (Hugo Lavoie & Therrien, 2015)

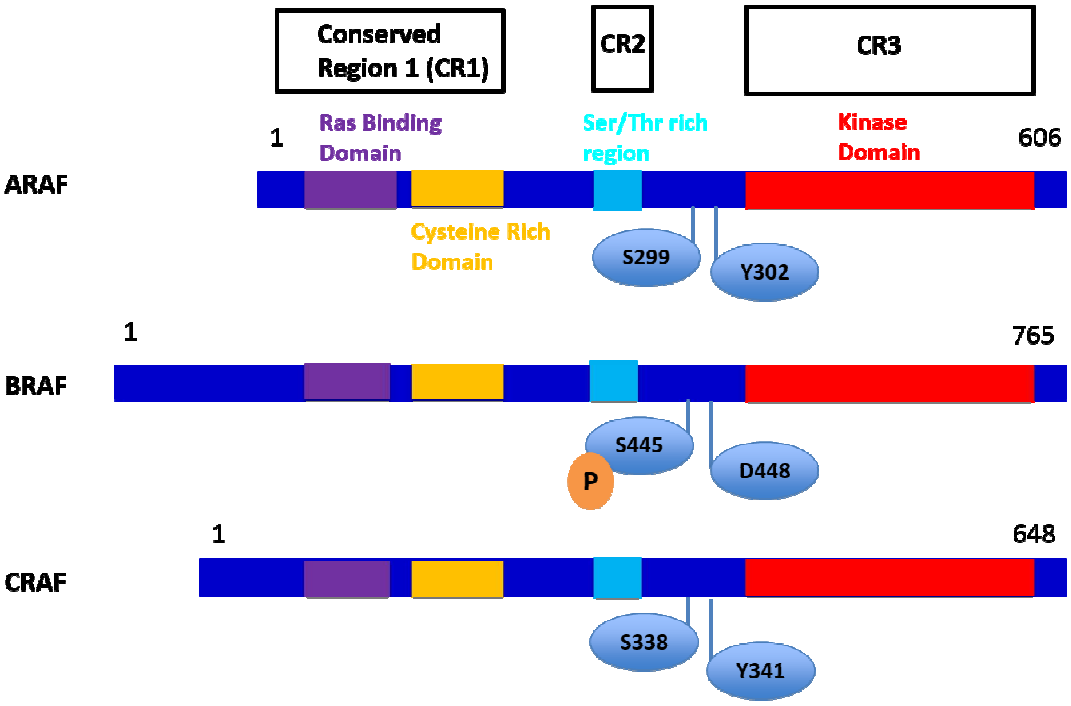

Figure 5 RAF homologues and conserved regions.

The three RAF homologues, ARAF, BRAF, and CRAF, shown via conserved regions in their protein sequences. CR1 contains a Ras Binding Domain (purple) and a cysteine rich domain (orange). CR2 contains a serine/threonine rich region (cyan) that can be phosphorylated to promote binding by 14-3-3 proteins. CR3 is the conserved kinase domain (red). NtA residues needed for activation in all three homologues are shown. Figure is adapted from (Wellbrock et al., 2004).

In 2004, the first crystal structure of the BRAF kinase domain was solved by co-crystallizing with one of the first kinase inhibitors, Sorafenib (Wan et al., 2004). The kinase domain, crystallized with an inhibitor, was well resolved except for the N terminus (Q433-S447) and the activation segment from residue K601 to Q612 (Wan et al., 2004). This crystal structure confirmed that BRAF adopts the canonical kinase structure shown in **Figure 2**, with an N-lobe and a larger C-lobe, and the inhibitor inhabiting the cleft between the two lobes. Due to structural comparisons to a previous c-Abl crystal structure, it was determined that this inhibitor was establishing an inactive form of the kinase, with a DFG-out conformation (Wan et al., 2004) (**Figure 6**). Despite being in the inactive conformation and the activation segment being mostly disordered, the authors proposed that $BRAF^{V600E}$ is able to initiate an active conformation by forming a salt bridge with lysine 507 in the αC-helix, stabilizing an activation segment flipped in the active conformation. Further crystal structures bound to inhibitors stabilizing the active form later confirmed this (Wan et al., 2004; Xie et al., 2009) (**Figure 7**).

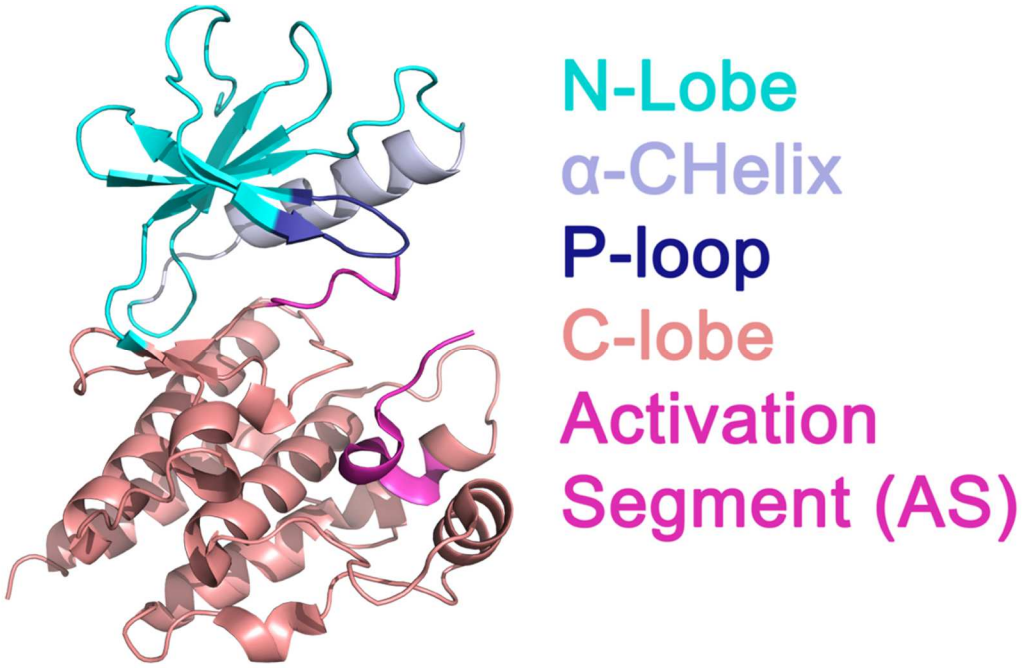

Figure 6 Crystal structure of the BRAF kinase domain.

Crystal structure of $BRAF^{WT}$ kinase domain, color coded with different structural domains of kinases. PDB accession code 1UWH.

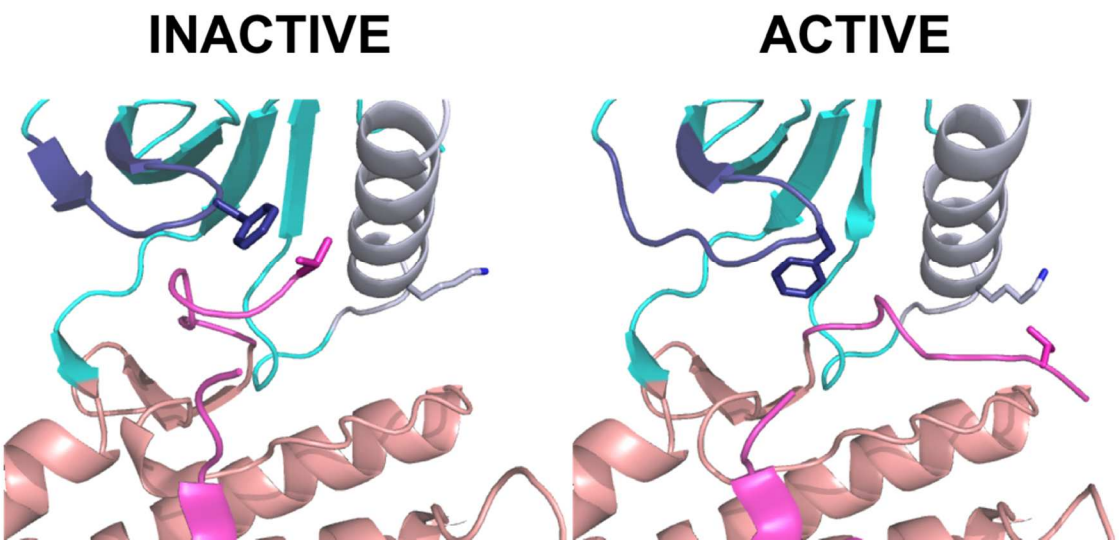

Figure 7 Inactive vs. active forms of BRAF.

Crystal structure of $BRAF^{WT}$ kinase domain in the inactive conformation (left, PDB ID 1UWH) compared to $BRAF^{WT}$ kinase domain in the active conformation (right, PDB ID 3Q4C), demonstrating the possibility of V600E mutations forming salt bridges with K507.

When the RAF kinases were first discovered, little was known about their complex activation mechanism. As mentioned above, RAS interaction with the RAS binding domain (RBD) of RAF proteins are known to activate RAF, but despite a crystal structure of the RAF RBD interacting with RAS being solved in 2015, the exact mechanism as to how this activation occurs is not clearly understood (Fetics et al., 2015). In 1996, it was discovered that artificial induction of RAF dimerization in cells stimulated its activity (Farrar, Alberola-Ila, & Perlmutter, 1996). RAS was later found to promote dimeric complexes between BRAF and CRAF as well as respective homodimers, and oncogenic mutations other than V600E were found to impair kinase activity but stimulate CRAF

activation in vivo, hinting at a dimerization dependent mechanism for activation (Rushworth, Hindley, Neill, & Kolch, 2006; Wan et al., 2004). As more crystal structures of BRAF became publicly available on the PDB, it became evident that the asymmetric unit of these crystals comprised two kinase domains making notable contacts with one another in a conserved manner. While this was first thought to be an artifact of crystal packing, the conserved nature of this interaction hinted at biological relevance (Rajakulendran, Sahmi, Lefrançois, Sicheri, & Therrien, 2009). A key residue, R509, lies at the center of this interface and forms contacts to the partner subunit's backbone residues of R506 and T508 (Rajakulendran et al., 2009) (**Figure 8**). Mutation of this residue to a histidine (R509H) has been shown to deplete dimerization in vitro (Rajakulendran et al., 2009). While the exact mechanism of dimerization-dependent RAF mechanism is still not completely understood, it is thought that the stabilization of a closed conformation between the N and C lobes and the alignment of two regions of hydrophobic residues spanning several kinases can lead to kinase closure and activation (Kornev, Haste, Taylor, & Ten Eyck, 2006). In RAF, the stabilization of this closed conformation is thought to be governed by the αC-helix (light grey in **Figures 6 and 7**), as R509 lies on the C terminal tip of this helix (Hugo Lavoie & Therrien, 2015; Rajakulendran et al., 2009).

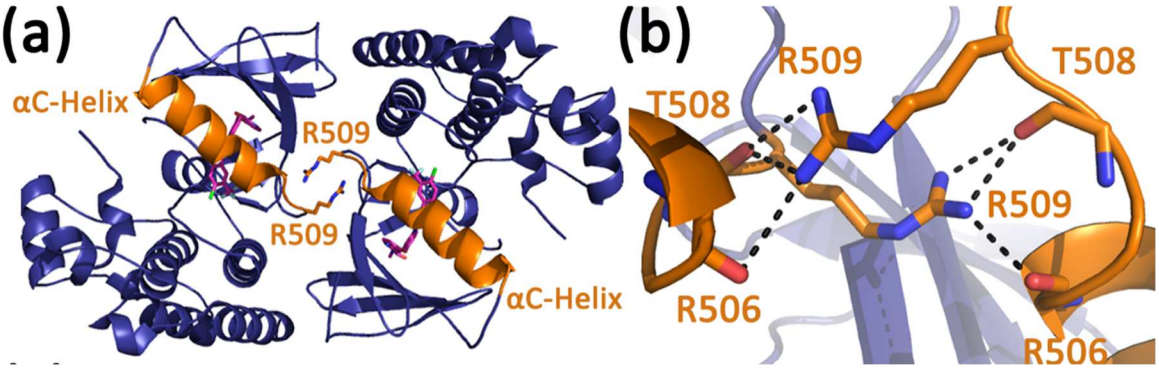

Figure 8 R509 dimerization stabilization in BRAF.

Figure (a) Illustrates the side to side dimerization interface of the RAF kinases, while (b) is a close-up of R509 interactions with T508 and R506. This figure is taken from (Grasso et al., 2016).

The crucial nature of αC-helix conformation in dimerization activation of BRAF was further elucidated with the first monomeric structure of the BRAF kinase domain, which illustrated an αC-helix conformation significantly shifted "outward" compared to those of known dimeric crystal structures (Thevakumaran et al., 2014) (**Figure 9**). This crystal structure also demonstrated that, despite the activation segment being in a DFG-in, active, conformation, the activation segment was more resolved than other structures and displayed a helical conformation(AS-H1) that is thought to be inactive, as it forms multiple contacts with the αC-helix, therefore stabilizing its inactive form (Thevakumaran et al., 2014) (**Figure 9**).

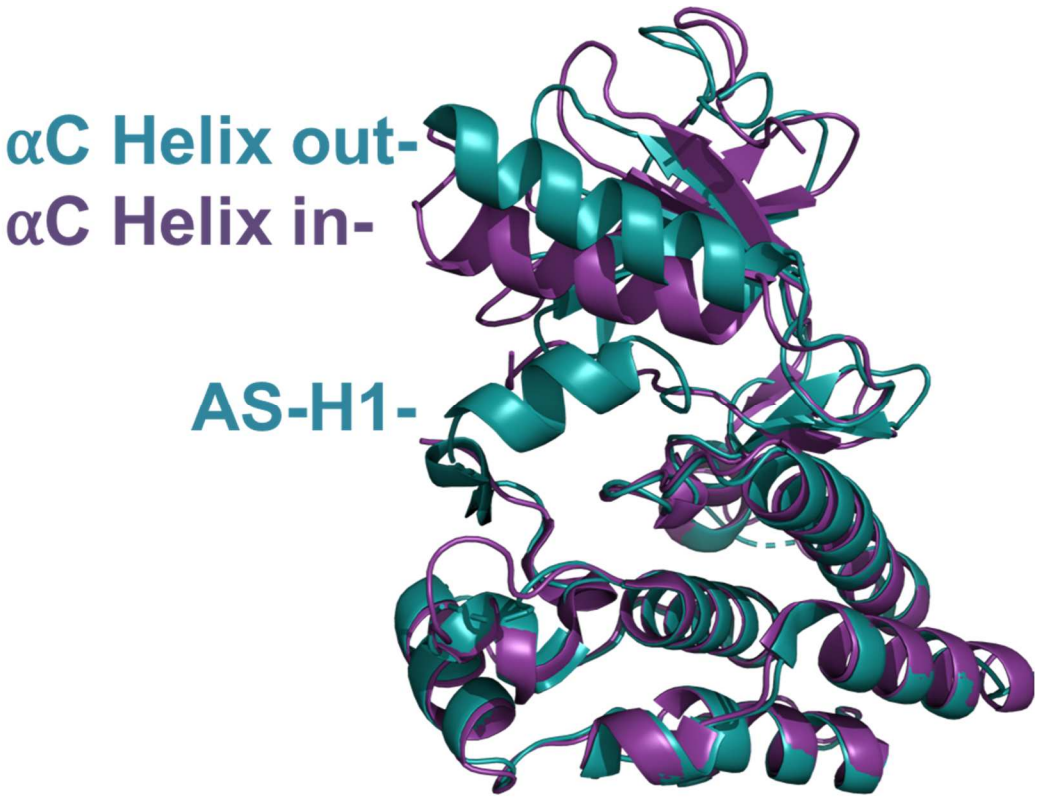

Figure 9 Monomeric BRAF crystal structure shows αC-helix shift.

Monomeric BRAF crystal structure (blue, PDB ID 4WO5) aligned with dimeric BRAF (purple, PDB ID 1UWH), showing a shift in the αC-helix and the formation of AS-H1.

A recent study from 2013 helped elucidate BRAF's interactions on downstream activity of the MAPK pathway by crystallizing the complex of BRAF with its substrate MEK (Haling et al., 2014). The crystal structure demonstrated that at high concentrations, the complex is a hetero-tetramer, with two BRAF molecules forming a side-to-side dimeric interaction, and MEK molecules on each BRAF molecule, making face-to-face interactions (**Figure 10**). The interactions are stabilized mostly through the activation segments of both kinases (magenta, **Figure 11**) , as well as their G-helices (cyan, **Figure 11**) (Haling et al., 2014). The activation segment of BRAF is stabilized in an active, DFG-in conformation

despite no inhibitor binding, and the conformation demonstrates that V600E mutations can indeed stabilize this conformation with a salt-bridge to K507 and thereby strengthen the complex. Interestingly, this complex has a very strong interaction with a K_D of ~43 nM, and it is thought that phosphorylation of MEK1 by BRAF weakens the interaction (Haling et al., 2014).

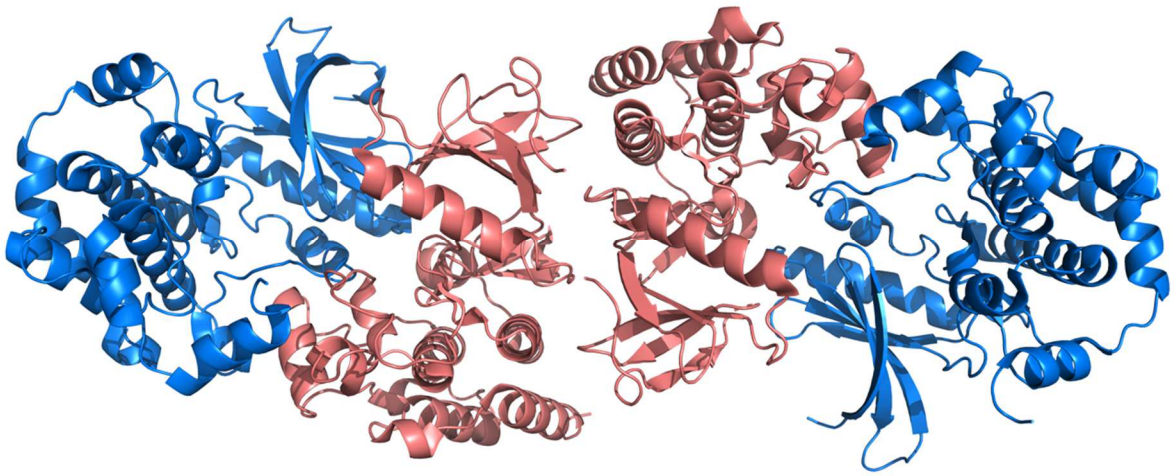

Figure 10 BRAF:MEK complex.

The crystal structure of MEK (blue) bound to a biologically relevant BRAF dimer (salmon), forming a hetero-tetrameric structure (PDB ID 4MNE).

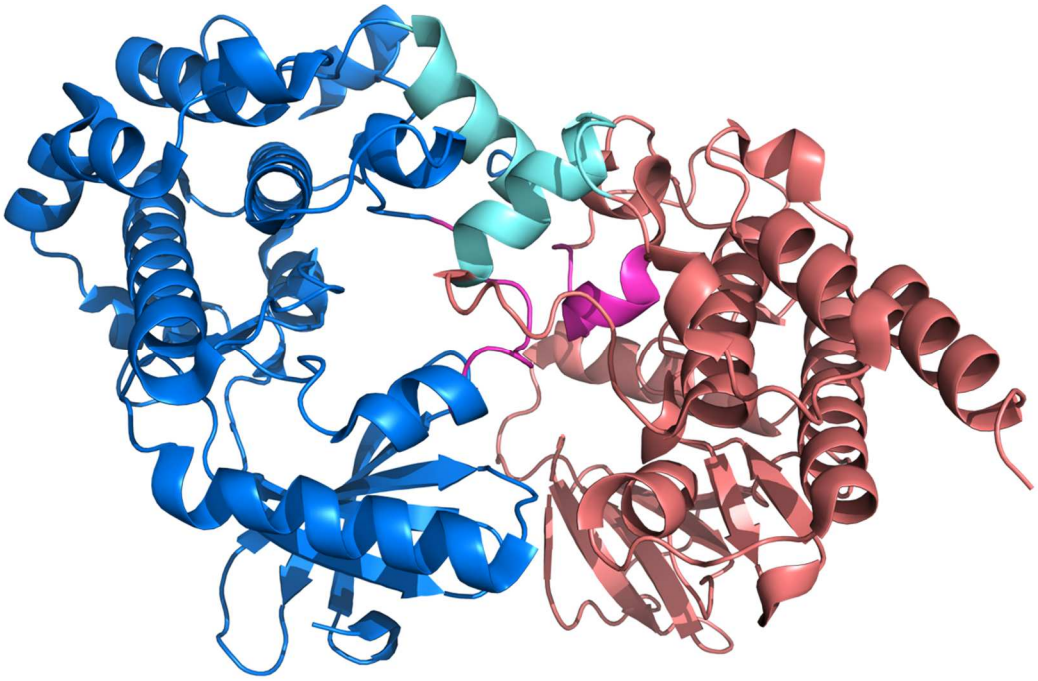

Figure 11 BRAF:MEK complex interactions.

The crystal structure of MEK (blue) bound to BRAF (salmon) shows their activation segments (magenta) make extensive contacts, as well as their G-helices (cyan) (PDB ID 4MNE).

1.5 BRAF Inhibitors and Cancer

As it was being discovered that RAF kinases would be a suitable target in cancer treatment, the first available inhibitor, Sorafenib (BAY43-9006) was being developed by Bayer (Lyons, Wilhelm, Hibner, & Bollag, 2001; Wan et al., 2004). Sorafenib is a pan-RAF inhibitor, targeting $CRAF^{WT}$, $BRAF^{WT}$, and $BRAF^{V600E}$. Sorafenib was found to be extremely potent against the RAF kinases, with recorded IC_{50} values in the low nanomolar

range (S. Wilhelm & Chien, 2002). The inhibitor bound the DFG-out, inactive conformation, and is ATP-competitive, binding in the cleft between the N and C lobes of the kinase. However, its lack of selectivity within the RAF kinases, as well as its ability to hit certain RTK's upstream, led to issues in the clinic and side effects (S. M. Wilhelm et al., 2004). The need for a mutant specific RAF inhibitor was apparent, and after extensive "scaffold-like" drug discovery techniques, vemurafenib was first synthesized in 2005 (**Figure 12**) (Bollag et al., 2012). Vemurafenib binds to BRAF in the active, DFG-in conformation, thus displaying selectivity for the $BRAF^{V600E}$ mutant over $BRAF^{WT}$ (Bollag et al., 2010, 2012; Tsai et al., 2008a). However, in the clinic, patients receiving high enough doses of vemurafenib often regressed after 6 months, and tumors return (**Figure 12**) (Bollag et al., 2010, 2012).

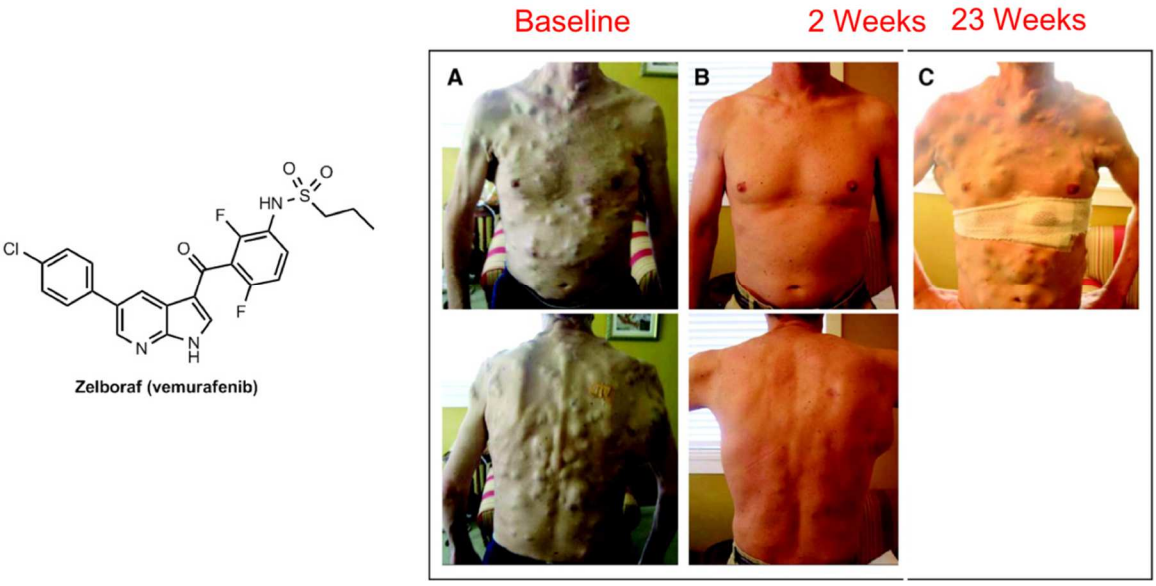

Figure 12 Resistance in melanoma patients treated with vemurafenib.

Image of patient treated with vemurafenib and after ~6 months, developed cutaneous metastatic deposits due to inhibitor resistance. Adapted from (Wagle et al., 2011).

Interestingly, the crystal structure of BRAF-bound vemurafenib consists of BRAF in the biologically relevant dimer conformation, but one protomer is bound to inhibitor while the other is not (**Figure 13**) (Bollag et al., 2010). A difference in the αC-helix is present between the two protomers, and it is thought that inhibitor binding promotes dimerization, and this dimerization forces the αC-helix in the conformation shown in grey in **Figure 13**, keeping a second vemurafenib molecule from binding in that active site (Bollag et al., 2010, 2012; P. I. Poulikakos, Zhang, Bollag, Shokat, & Rosen, 2010). Indeed, at sub-saturating concentrations of inhibitor, ERK signaling in cells is increased, and this phenomenon is called "transactivation" or "paradoxical activation" (P. I. Poulikakos et al., 2010; P. Poulikakos & Rosen, 2011). Further studies have shown that in the presence of oncogenic RAS, kinase dead BRAF mutants can bind and activate CRAF and other BRAF protomers. This mechanism is also true for inhibited BRAF molecules (Heidorn et al., 2010). Examining the process of transactivation, it was found that BRAF has the potential to transactivate other BRAF and CRAF molecules while CRAF cannot, and this is due to the NtA motif that is "primed" with its sequence SSDD, whereas CRAF and ARAF require phosphorylation to activate their NtA motifs (Hu et al., 2013). Furthermore, this activation is dimerization dependent, as R509H mutations block any ERK activation (Hu et al., 2013). The current model of transactivation is shown in **Figure 14**, in which inhibitor bound RAF can allosterically activate another RAF molecule that is not bound to inhibitor when active RAS is present (P. Poulikakos & Rosen, 2011).

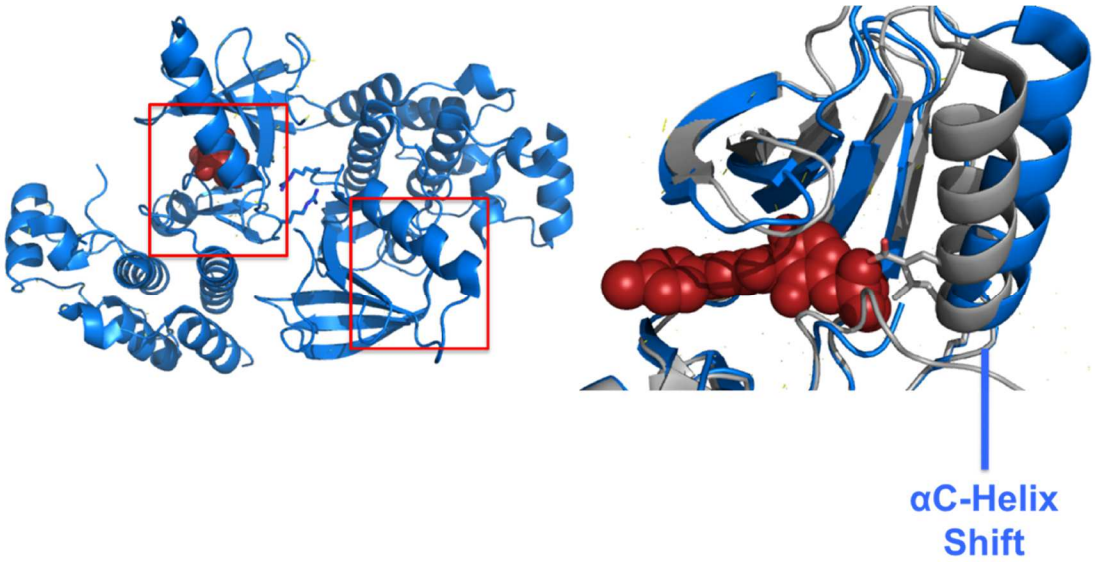

Figure 13 Vemurafenib binding.

Crystal structure of Vemurafenib bound to $BRAF^{V600E}$ shows only one molecule of the BRAF dimer bound to vemurafenib, and the other is left free with its αC-helix in a conformation promoting dimerization but blocking inhibitor binding (PDB ID 3OG7).

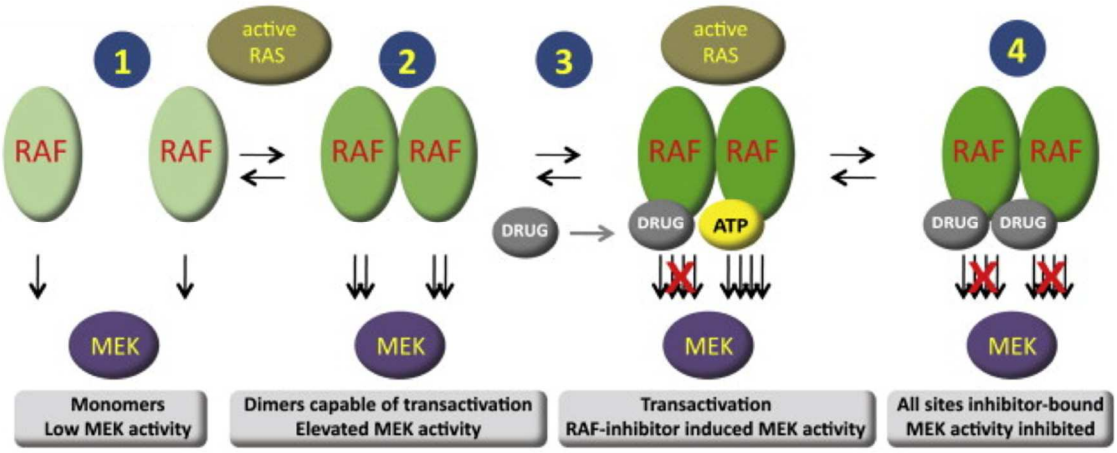

Figure 14 Transactivation model.

Illustration of transactivation, in which without activated RAS, RAF is mainly monomeric and has low activity. When active RAS is present, MEK phosphorylation is elevated to basal level. At sub-saturating levels of inhibitor such as vemurafenib, one molecule of a RAF dimer can activate the other molecule allosterically, inducing MEK phosphorylation and ERK signaling. Figure is taken from (P. Poulikakos & Rosen, 2011).

Resistance to BRAF inhibitors develops ~6 months after melanoma cell lines are persistently exposed to these drugs, and interestingly, these resistant cell-lines also demonstrate resistance to other BRAF inhibitors, indicating that most existing BRAF inhibitors act under the same mechanism to promote resistance (Villanueva, Vultur, & Herlyn, 2011). Some common resistance pathways are RTK, N-RAS, and CRAF upregulation, N-RAS mutations, and expression of a specific splice variant of BRAF (Nazarian et al., 2010; P. I. Poulikakos et al., 2011; Villanueva et al., 2011). All of these resistance mechanisms go hand in hand with transactivation and dimerization, as the

increase in RTK's, RAS, and CRAF, as well as N-RAS mutations, increase the presence of RAF dimers in cells. Also, the splice variant of BRAF cuts out the RBD of the BRAF N-terminus, hindering RAS regulation and allowing for aberrant dimerization of BRAF (P. I. Poulikakos et al., 2011). In 2015, "paradox breaker" inhibitors were developed, which modify vemurafenib to reduce the amount of transactivation of the ERK pathway in cells (C. Zhang et al., 2015). Despite these positive results, however, the crystal structures of these inhibitors bound to BRAF still demonstrate one protomer bound and the other unbound in an activated αC-helix conformation, leading to the possibility of inhibitor resistance developing (Karoulia et al., 2016; C. Zhang et al., 2015). Extensive studies of RAF inhibitors have concluded that certain inhibitors can induce dimerization by favoring a "closed" conformation of the N- and C- lobes of the kinase, and αC-helix-"in" favoring inhibitors such as sorafenib promote dimerization while αC-helix-"out" inhibitors such as vemurafenib do not (Karoulia et al., 2016; H Lavoie et al., 2013). These studies shed a light on the current mechanisms of transactivation, however there is a current need for not only inhibitors that can circumvent transactivation but also more information on how this pathway functions and how to avoid further resistant pathways.

1.6 Dissertation Objectives

While much work has been done to elucidate BRAF as a cancer target and develop drugs targeting RAF kinases, many questions still need to be answered due to the discovery of inhibitor resistance in BRAF-mutant cancers. Can small molecule inhibitors be developed to target transactivation? If so, which means would be most effective? Would these small molecule inhibitors have downstream effects on the MAPK pathway, and could

they elucidate more intricacies in ERK signaling that have yet to be discovered? Answering these questions will not only provide options for clinical treatments for melanoma as well as many other cancers but will also provide useful molecular probes to elucidate inhibitor mechanisms *in vitro* and in cells.

The focus of my dissertation is to develop and characterize novel small molecule inhibitors targeting BRAF-mutant melanoma and other cancers. Exploiting BRAF's propensity for transactivation via dimerization, I aimed to develop two novel classes of inhibitors that utilize different techniques to target inhibitor resistance within the MAPK signaling pathway. I first characterized and used structure-based inhibitor design to improve upon a bivalent class of BRAF inhibitors that can target two BRAF molecules at once using type I, mutant specific inhibitor vemurafenib. I then utilized the same technique to develop a class of bivalent BRAF inhibitors using a type II, pan-RAF inhibitor TAK632. Finally, I developed and optimized a high-throughput screen to identify small molecules that can disrupt the interaction between BRAF and its downstream substrate MEK. Through these studies, I have:

(1) Determined that chemically-linked dimeric vemurafenib inhibitors can stabilize a biologically irrelevant dimeric form with an inactive αC-helix conformation

(2) Bivalent TAK632 inhibitors cannot stabilize this biologically irrelevant conformation, but monovalent TAK632 can stabilize the biologically relevant dimeric form even in the presence of mutations within the dimer interface

(3) Small molecule inhibitors identified in my FRET-based high throughput screen affect BRAF/MEK dimerization.

In conclusion, these small molecules can be used to further probe BRAF dimerization and its role in MAPK signaling and inhibitor resistance.

Chapter 2- Chemically Linked Vemurafenib Inhibitors Promote an Inactive BRAF^{V600E} Conformation

This research was performed in collaboration with Dr. Michelle Estrada, Dr. Minu Samanta, Dr. Christian Ventocilla, and Dr. Jasna Maksimoska of the University of Pennsylvania. Dr. Estrada and Dr, Ventocilla performed the synthesis of inhibitors, Dr. Samanta carried out cell-based experiments, and Dr. Maksimoska performed initial first-generation enzymatic assays. Repeated with permission from Grasso, M., Estrada, M. A., Ventocilla, C., Samanta, M., Maksimoska, J., Villanueva, J., Winkler, J., and Marmorstein, R. (2016). Chemically Linked Vemurafenib Inhibitors Promote an Inactive BRAFV600E Conformation. *ACS Chemical Biology*, *11*, 2876–2888.

2.1 Introduction

BRAF is a notable oncoprotein within the MAPK signaling pathway due to its proclivity to mutations in cancer as compared to other RAF proteins ARAF and CRAF. 60% of melanomas in particular carry a BRAF mutation, and 90% of those mutations are a particular point mutation of valine to glutamic acid at residue 600 (V600E) (Davies et al., 2002; Wellbrock et al., 2004). $BRAF^{V600E}$-selective inhibitors have therefore become a topic of interest in the fields of drug discovery, and two inhibitors in particular, vemurafenib and dabrafenib, have been approved by the FDA based on overall extended survival in patients with metastatic $BRAF^{V600E}$ melanoma (Bollag et al., 2012; King et al., 2013; Rheault et al., 2013). However, almost all patients develop drug resistance within about 6 months of treatment through diverse mechanisms (Anforth et al., 2012; P. Poulikakos & Rosen, 2011; Villanueva et al., 2013). While combination therapies of MEK and BRAF inhibitors have been approved by the FDA to help counteract MAPK reactivation, resistance can still develop and this strategy has limited activity in a subset of melanomas with acquired resistance to RAF or MEK inhibitor monotherapy, particularly in the context of increased MAPK signaling (Flaherty et al., 2012; Johnson et al., 2014).

Resistance pathways, while diverse, appear to stem from the phenomenon of "paradoxical activation" or "transactivation" in which drug-bound BRAF in an inactive conformation is able to allosterically shift the associated non-drug bound wild-type BRAF or CRAF subunit into an activated conformation to promote MAPK signaling (P. I. Poulikakos et al., 2010). Consistent with the importance of RAF dimerization, a single R509H mutation that disrupts BRAF dimerization is shown to prevent transactivation (Rajakulendran et al., 2009). These studies highlight the importance of RAF dimerization

and suggest that novel approaches to specifically target RAF dimers may have therapeutic value. In the study reported here, we used $BRAF^{V600E}$ dimers in the active conformation as a model system to ask if chemically linked vemurafenib inhibitors could shift RAF dimers into an inactive conformation. We show that chemically linked vemurafenib inhibitors promote an inactive $BRAF^{V600E}$ dimeric conformation, implicating that a similar strategy can be employed to target $BRAF^{V600E}/RAF^{WT}$ dimers for inhibition of transactivation in the MAPK pathway.

2.2 Results

2.2.1 Chemically linked vemurafenib molecules specifically and potently disrupt active $BRAF^{V600E}$ dimers

Vemurafenib was the first selective BRAF inhibitor approved to treat $BRAF^{V600E}$ melanoma based on efficacy and improved overall survival; however, responses are transient due to the emergence of resistance in virtually all patients, demonstrating the necessity for more effective drugs/therapies, particularly those that directly address the issue of transactivation (Bollag et al., 2010; Tsai et al., 2008a). Therefore, we hypothesized that two vemurafenib molecules chemically linked in an appropriate fashion could inhibit a RAF dimer and thus prevent paradoxical activation. Of the 45 BRAF kinase domain crystal structures available in the PDB, only one (4WO5) (Thevakumaran et al., 2014) is not present in what is presumed to be a biologically relevant dimer (**Figure 15a**). In the BRAF dimer, residue Arg509 makes dimer-stabilizing H-bonds to the backbone carbonyl oxygens of T508 and R506 of the other BRAF subunit of the dimer, which contributes to orienting the αC-helix in a conformation that facilitates catalysis (**Figure 15b**) (Thevakumaran et al., 2014). The dimer structures reveal that the kinase active sites face

away from each other and are separated by about ~30Å (**Figure 15a**). Based on this observation, we reasoned that a linker of ~ 30Å could enable an inhibitor to bind both active sites of the observed dimer simultaneously, while a shorter linker might also be able to "trap" BRAF into another, potentially inactive dimer conformation. With this in mind, we prepared linked vemurafenib molecules in which the tether contained 2 (~10Å) to 6 (~30Å) polyethylene glycol (PEG) units (**Figure 15c**).

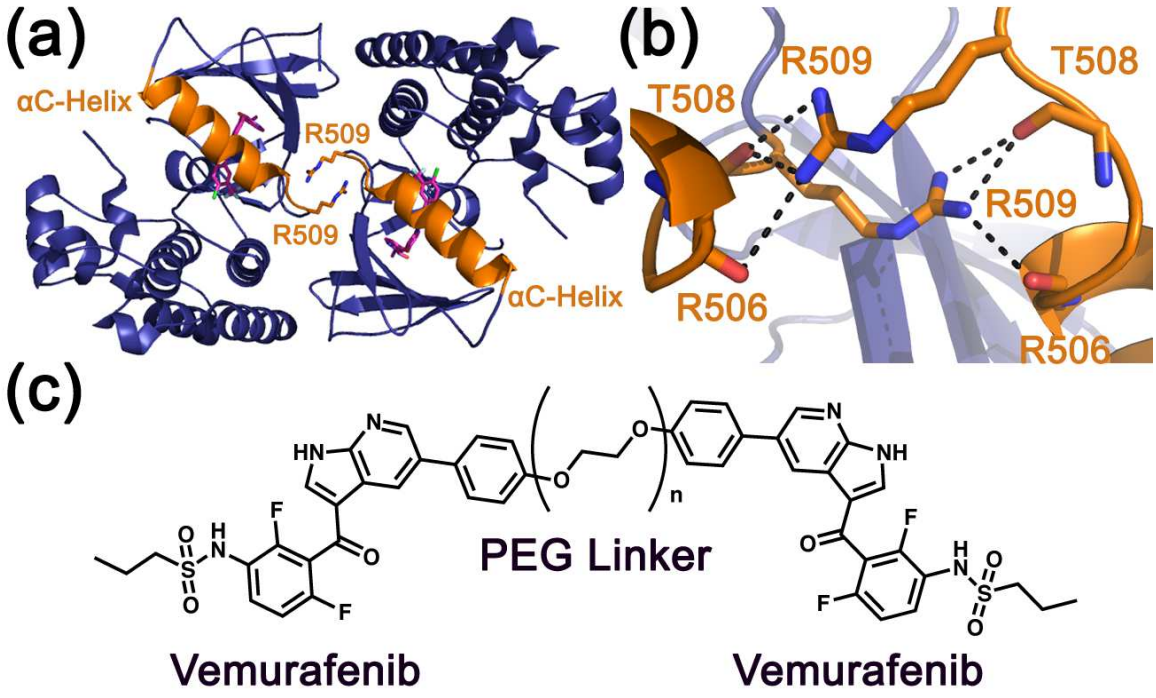

Figure 15 Structure of BRAF kinase domain and rationale for linked vemurafenib BRAF inhibitors.

(a) Structure of the $BRAF^{WT}$ kinase domain crystallized with Sorafenib (accession code 1UWH). The αC-Helix and R509 residue are highlighted in orange. (b) Close up of BRAF dimer interactions mediated by R509. (c) Initial scaffold for vemurafenib linked inhibitors where n equals the number of polyethylene glycol moiety groups.

The potencies of the linked vemurafenib inhibitors against $BRAF^{V600E}$ and $BRAF^{WT}$ were evaluated *in vitro* using an ELISA assay that measures phosphorylation of the BRAF substrate GST-MEK1. We found that all but the linked compound with the fewest PEG units (Vem-2-Vem) had potencies within 2-fold of unlinked PLX4720 (an analogue of vemurafenib without a phenyl group, referred to herein as PLX) inhibitor against $BRAF^{V600E}$. In control studies, we also demonstrated that PLX4720 (PLX) and PLX4032 (Vemurafenib, or Vem) have potencies within about 2-fold of each other (**Figure 16).** Interestingly, all of the linked compounds had considerably poorer potency against $BRAF^{WT}$ (**Figures 17a and 17b,** respectively). These data demonstrate that the potency of the chemically linked vemurafenib inhibitors against $BRAF^{V600E}$ is relatively insensitive to linker length between 3 and 6 units. Unexpectedly, linkers of all lengths significantly reduced the potency of vemurafenib against $BRAF^{WT}$, suggesting that the linked vemurafenib inhibitors are binding to two $BRAF^{V600E}$ subunits in a way that differed from the active dimer conformation. This hypothesis was also corroborated by the data showing that all the linker lengths, except the shortest 10Å length, did not significantly affect linked inhibitor potency.

As RAF dimerization is predicted to increase the thermal stability of the protein, we performed a thermal stability assay of $BRAF^{V600E}$ with and without inhibitors as a readout for $BRAF^{V600E}$ dimerization. We carried out these studies by measuring the fluorescence of the reporter molecule sypro orange as it binds hydrophobic residues of BRAF, which becomes exposed as thermal denaturation occurs (R. Zhang & Monsma, 2010). These studies reveal that while unlinked PLX increased the melting temperature of $BRAF^{V600E}$ by about 18 ^{o}C, the linked vemurafenib compounds produce a significant but

more modest 2-9 ºC increase in melting temperature (**Figure 17c**). These results are consistent with a model whereby the linked vemurafenib compounds change the conformation of the two $BRAF^{V600E}$ molecules relative to the conformation of the active dimer conformation.

To evaluate the cellular activity of the linked vemurafenib compounds, we treated melanoma cells that harbored $BRAF^{V600E}$ (Mel1617) or $BRAF^{WT}$ (WM3918) with unlinked or linked vemurafenib compounds. Consistent with the *in vitro* studies, the unlinked and linked (Vem-3-Vem and Vem-6-Vem) vemurafenib compounds showed comparable inhibitory activity on cell viability in $BRAF^{V600E}$- mutant melanoma cells, but showed no significant inhibitory activity in $BRAF^{WT}$-melanoma cells (**Figure 17d**). These results also demonstrate that the linked vemurafenib compounds are able to enter cells and exhibit on-target activity.

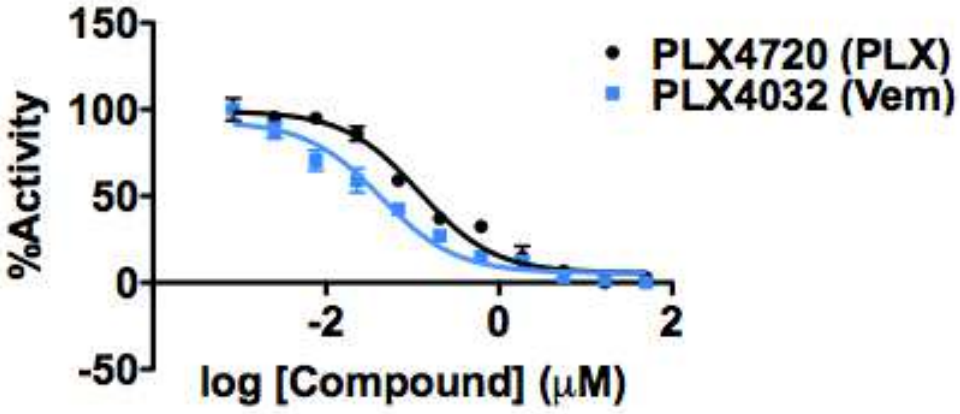

Figure 16 PLX4720 (PLX) vs PLX4032 (Vem)

$BRAF^{V600E}$ was assayed against Vem and PLX using the previously described ELISA assay. IC_{50} values were 119 nM for PLX and 42.8 nM Vem. Assay performed in duplicate, +/- SEM shown.

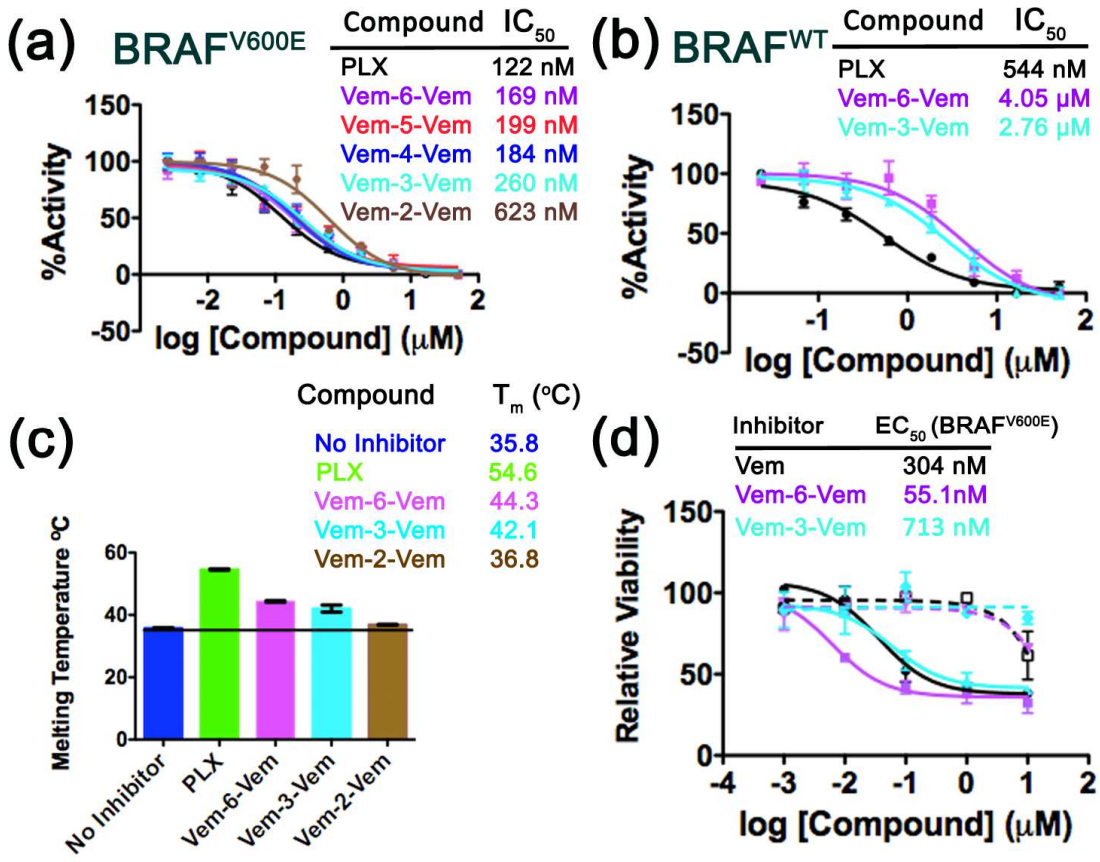

Figure 17 Potency of first generation linked vemurafenib inhibitors.

(a) Dose response curves of the Vem-Vem class of linked inhibitors against $BRAF^{V600E}$ with unlinked PLX4720 (PLX) as a control. Calculated IC_{50} values are indicated. The data is the average of two separate experiments, each performed in duplicate with +/- SEM shown. 95% Confidence Intervals are: PLX (75.8 nM to 195 nM), Vem-6-Vem (97.8 nM to 291 nM), Vem-5-Vem (111 nM to 356 nM), Vem-4-Vem (114 nM to 295 nM), Vem-3-Vem (186 nM to 364 nM), and Vem-2-Vem (391 nM to 994 nM). (b) Dose response curves of Vem-6-Vem and Vem-3-Vem against $BRAF^{WT}$ with PLX as a control, carried out in triplicate for PLX and Vem-6-Vem and in duplicate for Vem-3-Vem with +/- SEM

(from previous page) shown. The 95% Confidence Intervals are: PLX (335 nM to 883 nM), Vem-6-Vem (1.87 μM to 8.75 μM) and Vem-3-Vem (1.69 μM to 4.50 μM).

(c) Thermal shift assay measurements of melting temperature for $BRAF^{V600E}$ with no inhibitor, and with 50 μM of Vem-6-Vem, Vem-3-Vem, Vem-2-Vem, and PLX as a control, with calculated melting temperatures listed (n=6) with +/- SEM shown. 95% Confidence Intervals are as follows: DMSO Control (35.4 ºC to 36.2 ºC), PLX (54.0 ºC to 55.1 ºC), Vem-6-Vem (43.7 ºC to 45.0 ºC), Vem-3-Vem (39.1 ºC to 45.0 ºC), and Vem-2-Vem (36.5 ºC to 37.1 ºC). (d)$BRAF^{V600E}$ (Mel1617 cell line, solid line) and $BRAF^{WT}$ (WM3918, dashed line) cell lines were treated with the indicated doses of Vem-6-Vem or Vem-3-Vem for 72h. Cell viability was determined by MTT assays and calculated relative to DMSO-treated cells, Average cell viability taken from 3 separate experiments (n=7) and averaged together with +/- SEM shown.

2.2.2 Crystal structures of Vem-6-Vem and Vem-3-Vem demonstrate that linked vemurafenib inhibitors force $BRAF^{V600E}$ subunits into a face-to-face inactive dimer conformation

To determine the molecular basis for $BRAF^{V600E}$ inhibition by the linked vemurafenib compounds, we determined the crystal structure of the $BRAF^{V600E}$ kinase domain bound to Vem-6-Vem. The crystals formed in the space group $P2_1$ with two $BRAF^{V600E}$ molecules in the asymmetric unit, and the structure was determined by molecular replacement using 4WO5 as a search model and was refined to 2.3 Å resolution with good geometry and refinement statistics (**Table 1**). As expected, the refined

Crystal	$BRAF^{V600E}$/ Vem-6-Vem	$BRAF^{V600E}$/ Vem-3-Vem	$BRAF^{V600E}$/ Vem-BisAmide-2
Resolution Range (Å)	29.21-2.29 (2.34-2.29)	138.00-2.19 (2.24-2.19)	50-2.70 (2.75-2.70)
Space Group	$P2_1$	$P2_12_12_1$	$P2_12_12_1$
Unit Cell (a, b, c, α, β, γ)	56.84, 67.75, 67.88 90, 90.32, 90	64.61, 68.26, 276.01 90, 90, 90	65.10, 68.44, 275.60 90, 90, 90
Total Reflections	59,386	82,6367	192,419
Unique Reflections	22,352	63,307	34,634
Redundancy	2.7(2.7)	12.9 (12.100)	5.5 (5.8)
Completeness (%)	95.31 (90.21)	98.94 (96.12)	99.72 (99.50)
Mean I/sigma (I)	13.19 (2.76)	15.64 (1.37)	16.23 (2.62)
Wilson B Factor	32.72	51.44	57.32
R-merge	0.097 (0.521)	0.104 (2.323)	0.110 (0.862)
R-work	0.1947	0.2072	0.2122
R-free	0.2538	0.2597	0.2729
RMS (bonds)	0.008	0.009	0.009
RMS (angles)	1.18	1.19	1.28
Ramachandran Favored (%)	95	96	96
Ramachandran Outliers (%)	0.41	0.39	0.42
Clashscore	9.50	6.31	6.22
Average B Factor	27.20	50.10	41.10

Table 1. Summary of crystallographic statistics

$BRAF^{V600E}$/Vem-6-Vem structure shows a vemurafenib molecule bound in each enzyme active site, although electron density is not observed for the PEG linker, which was presumably disordered in the crystal structure (**Figure 18a**). Indeed, the last resolvable atom closest to the PEG linker, a carbon attached to the first oxygen in the linker portion, has a B factor of 34 $Å^2$, while the average B factor of the structure is 24 $Å^2$. As expected from the solution studies, the $BRAF^{V600E}$/Vem-6-Vem structure did not adopt the active RAF dimer conformation typically seen in RAF crystal structures, where the active sites are facing away from each other (**Figure 15a**). Instead, the $BRAF^{V600E}$/Vem-6-Vem dimer structure reveals that one protein subunit of the dimer is flipped about 180° relative to its position in the active RAF dimer such that the active sites are facing towards each other (**Figure 18a). Figure 18b** shows one subunit of the Vem-6-Vem structure superimposed with one subunit of the 1UWH biologically relevant dimer, demonstrating the different positions of the associated protein pair and αC-Helix, highlighted in orange, in both structural configurations. As a consequence of the altered configuration of the $BRAF^{V600E}$/Vem-6-Vem structure, key elements of the active RAF dimer are absent. Notably, R509 is surface exposed and thus does not participate in dimer interactions. Significantly, both BRAF molecules in the $BRAF^{V600E}$/Vem-6-Vem dimer structure are in an inactive dimer conformation as characterized by a shift of the C-helix to a more open configuration and an ordering of the activation segment into a helical conformation, referred to as AS-H1 (Thevakumaran et al., 2014) (**Figure 18c**). A similar inactive kinase conformation was noted in a recently reported BRAF monomer bound to vemurafenib (accession code 4WO5) (Thevakumaran et al., 2014) (**Figure 18c**). Notably, while the same inactive kinase configuration is observed between $BRAF^{V600E}$/Vem-6-Vem and

4WO5, the contact areas between both subunits in the asymmetric unit are different, despite being crystallized under similar conditions (details found in the methods section). This observation suggests that the crystallographically observed inactive kinase conformation results from a destabilization of the active BRAF dimer by Vem-6-Vem rather than by crystal contacts.

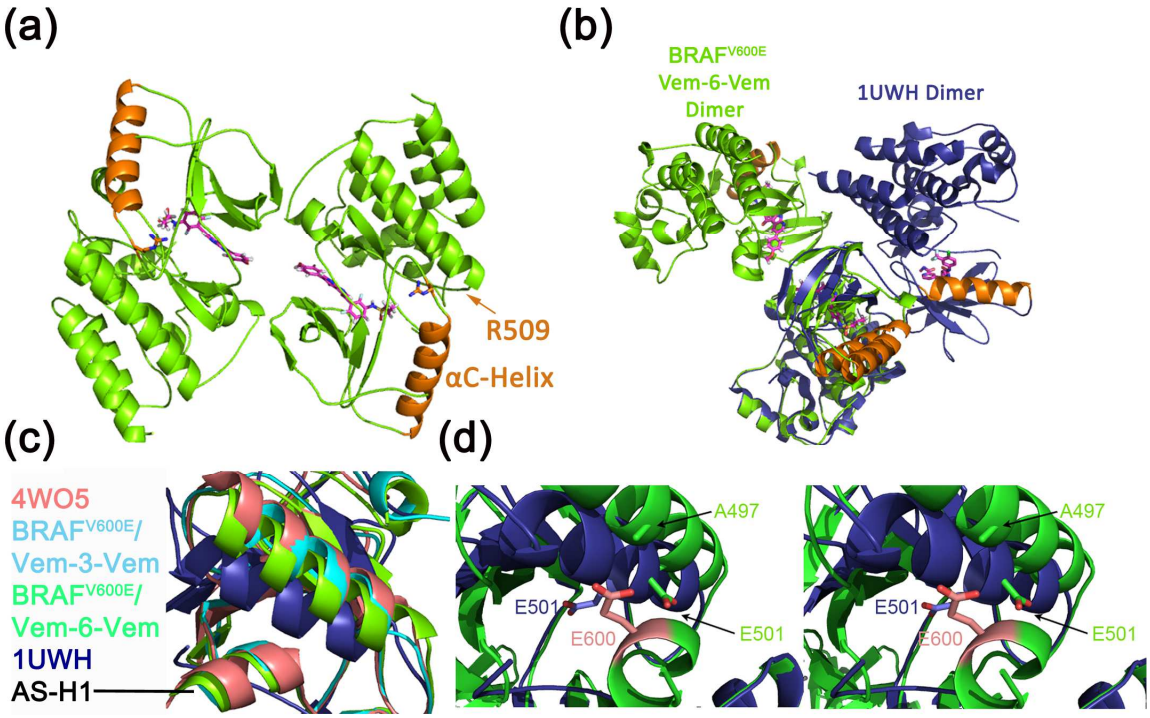

Figure 18 Structure of BRAF^{V600E}/Vem-6-Vem complex.

(a) Structure of BRAF^{V600E} bound to Vem-6-Vem. The αC-helix and R509 residues are highlighted in orange. (b) Overlay of one subunit of the BRAF^{V600E}/Vem-6-Vem dimer with an active dimer conformation (accession code 1UWH). (c) Superposition of BRAF^{V600E}/inhibitor structures (indicated by color-code) highlighting the position of the αC-helix and presence or absence of the AS-H1 helix. (d) Comparison of the αC-helix in active and inactive conformations highlighting the disposition of key residues, shown as a stereoimage.

Based on previous crystallographic and solution studies demonstrating that the $BRAF^{V600E}$ kinase domain favors a dimeric state, while $BRAF^{WT}$ favors a monomeric state, as well as analogies with other kinases, it was proposed that the AS-H1 helix is a driver of the inactive monomeric $BRAF^{WT}$ conformation (Thevakumaran et al., 2014). Based on this model, interactions between the AS-H1 helix and the C-helix are proposed to force the C-helix into an inactive conformation. $BRAF^{WT}$ activation loop phosphorylation or $BRAF^{V600E}$ mutation is proposed to destabilize interactions between the AS-H1 helix and the C-helix, causing the C-helix to shift into the active and dimeric form. The $BRAF^{V600E}$/Vem-6-Vem structure reveals that the AS-H1 helix is formed, even with the glutamate present in the $BRAF^{V600E}$ mutant. While the glutamate is within close contact to Ala497 (3.5 Å) (**Figure 18d**), the inactive conformation is still favored, and present in both BRAF molecules in the asymmetric unit. Alignment of the $BRAF^{V600E}$/Vem-6-Vem complex with 1UWH in **Figure 18d** reveals that the $BRAF^{V600E}$ mutation is still able to facilitate formation of AS-H1 helix and the inactive kinase conformation because Glu501 shifts away from Glu600, thus avoiding potentially destabilizing interactions. These observations argue against the AS-H1 helix being a driver of $BRAF^{V600E}$ activation and instead for the inherent ability of the linked Vem-6-Vem inhibitor to drive formation of the inactive $BRAF^{V600E}$ kinase conformation.

To determine if the inactive kinase conformation observed in the $BRAF^{V600E}$/Vem-6-Vem structure was dependent on the linker length between the vemurafenib molecules and to

potentially capture the path of the linker, we prepared crystals of $BRAF^{V600E}$ bound to Vem-3-Vem. Vem-3-Vem is estimated to have a linker length of ~15 Å, compared to the estimated linker length of ~30 Å, for the Vem-6-Vem compound. Crystallization of the $BRAF^{V600E}$/Vem-3-Vem complex under the conditions that produced the $BRAF^{V600E}$/Vem-6-Vem structure was unsuccessful, and we hypothesize that the lack of a highly dynamic linker altered crystal contacts. We were able to crystallize the $BRAF^{V600E}$/Vem-3-Vem complex in the $P2_12_12_1$ space group containing four BRAF protomers (two inhibitor-linked dimers) in the asymmetric unit cell. The structure was determined by molecular replacement using the $BRAF^{V600E}$/Vem-6-Vem structure and refined to 2.19 Å with good geometry and refinement statistics (**Table 1**). Despite the fact that the $BRAF^{V600E}$/Vem-3-Vem complex was in a different crystal environment than the $BRAF^{V600E}$/Vem-6-Vem complex, the two $BRAF^{V600E}$/Vem-3-Vem complexes in the asymmetric unit show the same face-to-face and inactive kinase conformation as $BRAF^{V600E}$/Vem-6-Vem (RMSD of 1.98 $Å^2$ for all common atoms) (**Figure 19a**). In particular, the $BRAF^{V600E}$/Vem-3-Vem complex shows the same C-helix shift and presence of the AS-H1 segment characteristic of the inactive kinase conformation (**Figure 18c**). This observation further supports the conclusion that the inactive kinase conformations observed in the $BRAF^{V600E}$ crystal structures bound to the chemically linked vemurafenib inhibitors are promoted by the linked inhibitors themselves and not crystal packing forces.

2.2.3 Functionalization of the linker can increase the potency of chemically linked vemurafenib over unlinked PLX

Unlike the ~30 Å, linker of the Vem-6-Vem compound in the BRAF^{V600E}/Vem-6-Vem structure, which was disordered, the shorter ~15 Å, linker of the Vem-3-Vem compound could be reliably traced into the electron density map (**Figure 19b**).

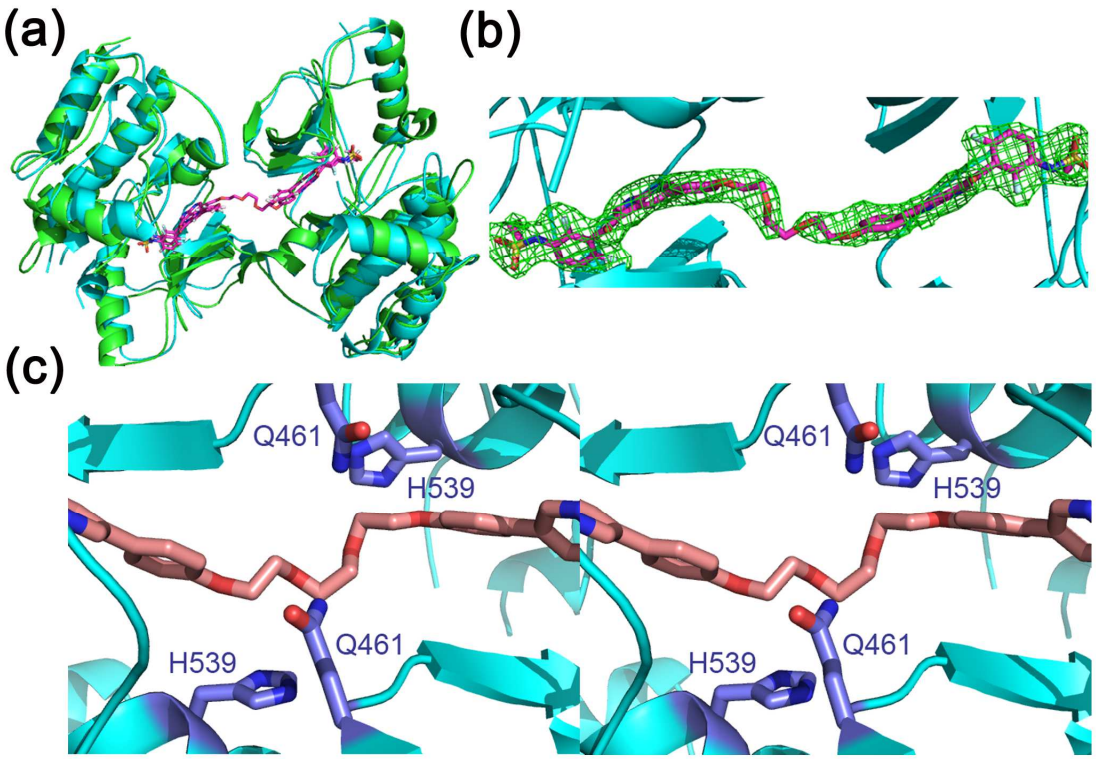

Figure 19 Structure of BRAF^{V600E}/Vem-3-Vem complex.

(a) Overlay of BRAF^{V600E}/Vem-6-Vem (green) and BRAF^{V600E}/Vem-3-Vem (cyan) structures. (b) Close-up of Vem-3-Vem inhibitor (magenta) and the simulated annealing omit map in green contoured at 2.5 sigma. (c) Close up of BRAF^{V600E} residues Q461 and H539 (purple) highlighting their proximity to the Vem-3-Vem linker (pink), shown as a stereo image.

Interestingly, the linker region is in proximity to residues Gln461 and His539 of both $BRAF^{V600E}$ subunits of the dimer (**Figure 19c**). We reasoned that functionalization of the linker region to introduce hydrogen bond acceptors and/or donors could introduce stabilizing protein-linker interactions to increase the potency of the linked vemurafenib inhibitors for $BRAF^{V600E}$. With this in mind, we designed a set of second-generation inhibitors, in which the linker region was functionalized. We reasoned that adding amide functional groups within the linker would add the hydrogen bond acceptors and/or donors with which Gln461 and His539 could interact, potentially strengthening the interaction of the inhibitor and, in turn, further stabilizing the forced inactive $BRAF^{V600E}$ conformation. We prepared three new diglycolic diamide linked-dimers, in which the number of methylenes between the diglycolic amide nitrogens and the phenyl ring of the vemurafenib core was varied. The three analogs synthesized consisted of an n-aryl diamide, as well as n-benzylic, and n-homobenzylic diamide linkers (**Figure 21a**). These compounds allowed us to examine the effect of linker length, in addition to increasing electronic density of the carbonyl functions due to amide resonance. We reasoned that this effect would facilitate increased interaction of the dimers with Gln461 and His539, relative to the analogous ketone linkers.

We assayed the inhibitory activity of the three bis amide-linked vemurafenib compounds against $BRAF^{V600E}$ and $BRAF^{WT}$ *in vitro* using the ELISA assay used for first generation inhibitors and found that all three amide-linked vemurafenib compounds lacked potency against $BRAF^{WT}$, as expected (**Figure 20**). However the ability of the compounds to inhibit $BRAF^{V600E}$ varied significantly (**Figure 21b**). Vem-BisAmide-1 inhibited $BRAF^{V600E}$ poorly compared to PLX, with an IC_{50} of ~3.62 μM compared to 115 nM for

PLX measured under identical conditions, and Vem-BisAmide-3 demonstrated an IC_{50} value of 195 nM, mimicking Vem-3-Vem and Vem-6-Vem. Vem-BisAmide-2 showed the greatest potency of the bis amide-linked vemurafenib compounds for $BRAF^{V600E}$, with an IC_{50} of 33.5 nM, about 3-5 fold higher than PLX and the PEG-linked vemurafenib inhibitors, but comparable to vemurafenib alone (**Figure 16**). We hypothesized that the geometry of Vem-BisAmide-2 is most optimal for inhibiting the inactive $BRAF^{V600E}$ dimer conformation, through more restricted movement of the linker and interactions with residues Gln461 and/or His539 of $BRAF^{V600E}$. Consistent with the findings of the activity assay, a thermal stability assay demonstrated that Vem-BisAmide-2 increases the thermal stability of $BRAF^{V600E}$ more than Vem-6-Vem and on the same level as unlinked PLX (**Figure 21c**). These results demonstrate that judicious functionalization of the linker can significantly increase $BRAF^{V600E}$ inhibitor potency.

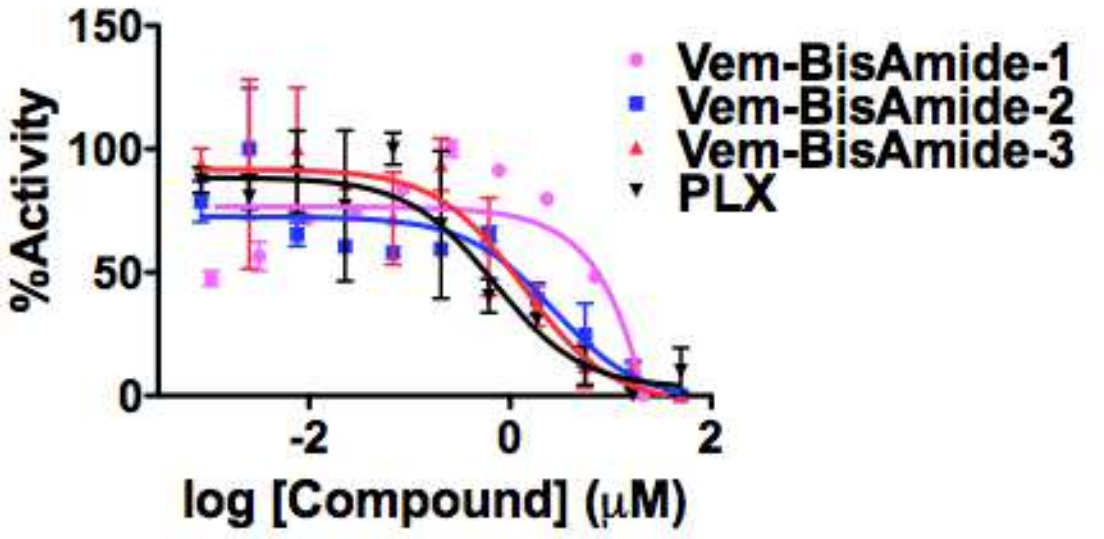

Figure 20 Vem-BisAmide inhibitors against $BRAF^{WT}$.

$BRAF^{WT}$ was assayed against Vem-BisAmide-1, Vem-BisAmide-2, Vem-BisAmide-3, and PLX using the previously described ELISA assay. IC_{50} values were 2.68 μM for Vem-

BisAmide-2, 1.35 μM for Vem-BisAmide-3, 697 nM for Vem, and N/A for Vem-BisAmide-1. Assay performed in duplicate, +/- SEM shown

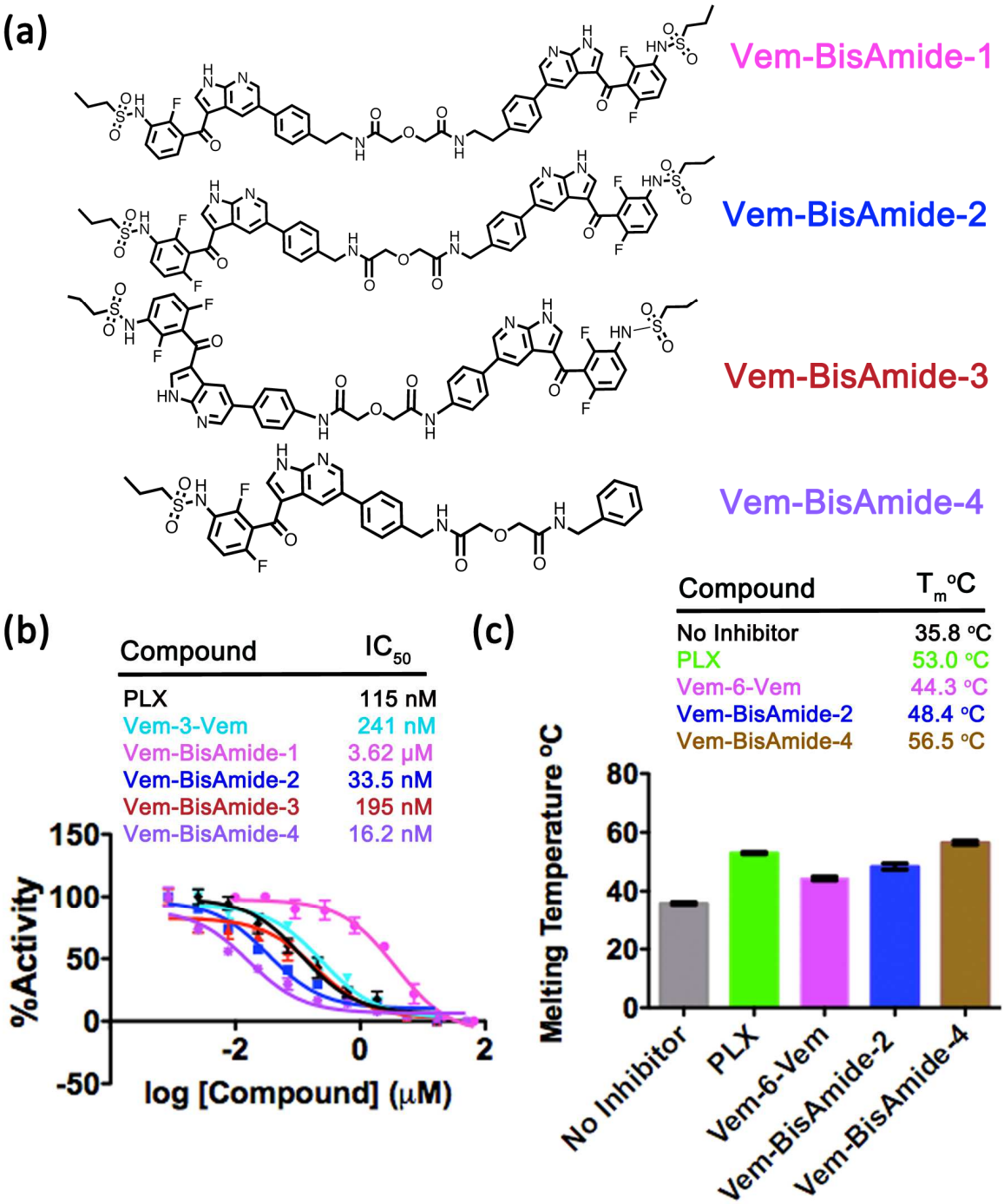

(from previous page)

Figure 21 Development of second generation linked vemurafenib inhibitors.

(a) Second generation linked vemurafenib inhibitors utilizing bis-amide linkers. (b) Dose response curves of second generation inhibitors against $BRAF^{V600E}$ with unlinked PLX4720 (PLX) as a control. Calculated IC_{50} values are indicated. The data is the average of two separate experiments, each performed in duplicate with +/- SEM shown. 95% Confidence Intervals are: PLX (70.0 nM to 191 nM), Vem-BisAmide-1 (2.28 μM to 5.75 μM), Vem-BisAmide-2 (23.7 nM to 47.5 nM), Vem-BisAmide-3 (114 nM to 332 nM), and Vem-3-Vem (165 nM to 352 nM) (c) Thermal stability assay of linked vemurafenib inhibitors with calculated melting temperatures listed (n=6) with +/- SEM shown. 95% Confidence Intervals are as follows: DMSO Control (35.5 ºC to 36.3 ºC), PLX (54.0 ºC to 55.1 ºC), Vem-6-Vem (43.7 ºC to 45.0 ºC), and Vem-BisAmide-2 (52.0 ºC to 53.3 ºC),

2.2.4 Crystal structure of $BRAF^{V600E}$/Vem-BisAmide-2 complex reveals the molecular basis for inhibition of $BRAF^{V600E}$ dimers

We were able to successfully crystallize Vem-BisAmide-2 bound to $BRAF^{V600E}$. The crystals were isomorphous to the $BRAF^{V600E}$/Vem-3-Vem structure and thus contained four BRAF protomers (two inhibitor-linked dimers) in the asymmetric unit. The structure was determined by molecular replacement using the $BRAF^{V600E}$ monomer from the $BRAF^{V600E}$/Vem-3-Vem structure and refined to 2.70 Å resolution with good geometry and refinement statistics (**Table 1**). As predicted, each enzyme active site was occupied by a vemurafenib molecule and the C-helix and the AS-H1 helix mimicked the conformation shown in the other structures with inactive conformations. The Vem-BisAmide-2 linker density was more pronounced than that of Vem-3-Vem despite the more limited resolution,

consistent with a more rigid linker. The linker region of Vem-BisAmide-2 shows that the amide carbonyls are making interactions with Gln461 and His539 residues. While the His539 residues make van der Waals contact to methyl groups in the linker, Gln461 residues hydrogen bond to the amide carbonyl groups of the linkers, with the nitrogen of the amide groups of the glutamine within close proximity of the carbonyl groups of the inhibitor's amide linker (**Figure 23a**). In the two $BRAF^{V600E}$ dimers in the asymmetric unit, the electron density for Gln461 is weak or unclear for one of the two dimer subunits (**Figure 22**). This observation suggests that stabilization of one Gln461-linker interaction does not synergistically nucleate the second Gln461-linker interaction and thus the interactions are independent. Nonetheless, the biochemical data argues for the importance of the Gln461-linker interaction in increasing inhibitor activity of the linked vemurafenib molecules, and we therefore hypothesize that only one Gln461/linker interaction contributes to formation of the protein/inhibitor complex.

To evaluate the contribution of the second vemurafenib molecule of the Vem BisAmide-2 compound on inhibitor potency and promotion of the inactive dimeric $BRAF^{V600E}$ conformation, a control inhibitor (Vem-BisAmide-4, **Figure 21a**) containing the BisAmide-2 linker but only one vemurafenib molecule was synthesized and tested against $BRAF^{V600E}$ and $BRAF^{WT}$ in activity and thermal stability assays. These data revealed comparable potency to PLX and Vem-BisAmide-2 (**Figure 21b**), but a thermal melting temperature closer to PLX than Vem-BisAmide-2 (**Figure 21c**). These data suggest that PLX and Vem-BisAmide-4 are promoting comparable $BRAF^{V600E}$ configurations that are distinct from the $BRAF^{V600E}$ complex with Vem-BisAmide-2, and consistent with the conclusion that the second vemurafenib molecule in the bivalent Vem-

BisAmide-2 inhibitor plays a key role in promotion of the inactive dimeric $BRAF^{V600E}$ conformation.

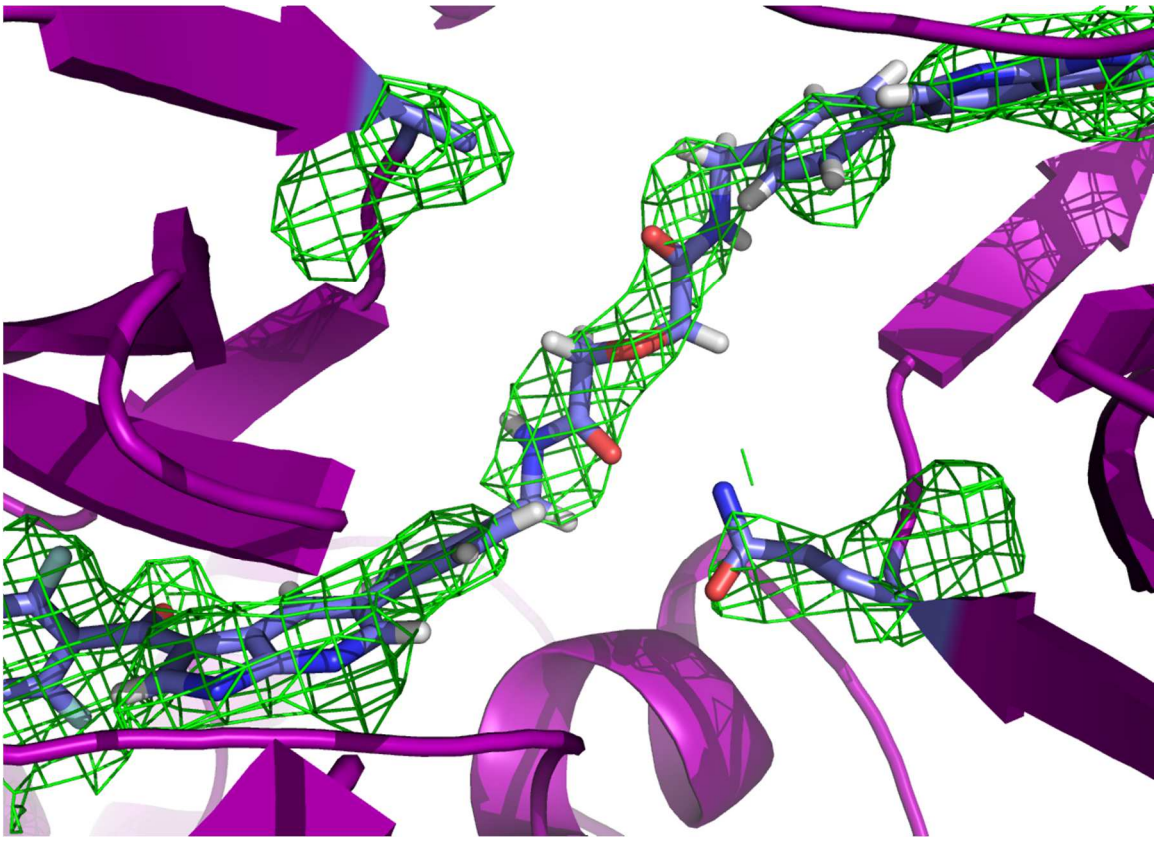

Figure 22 Simulated annealing omit map of Vem-BisAmide-2 and Q461.

Simulated annealing omit map of the $BRAF^{V600E}$/Vem-BisAmide-2 co-crystal with the omit map in green contoured at 2.0 sigma. Density for one Q461 residue within the off-state dimer is observable, however the other is not.

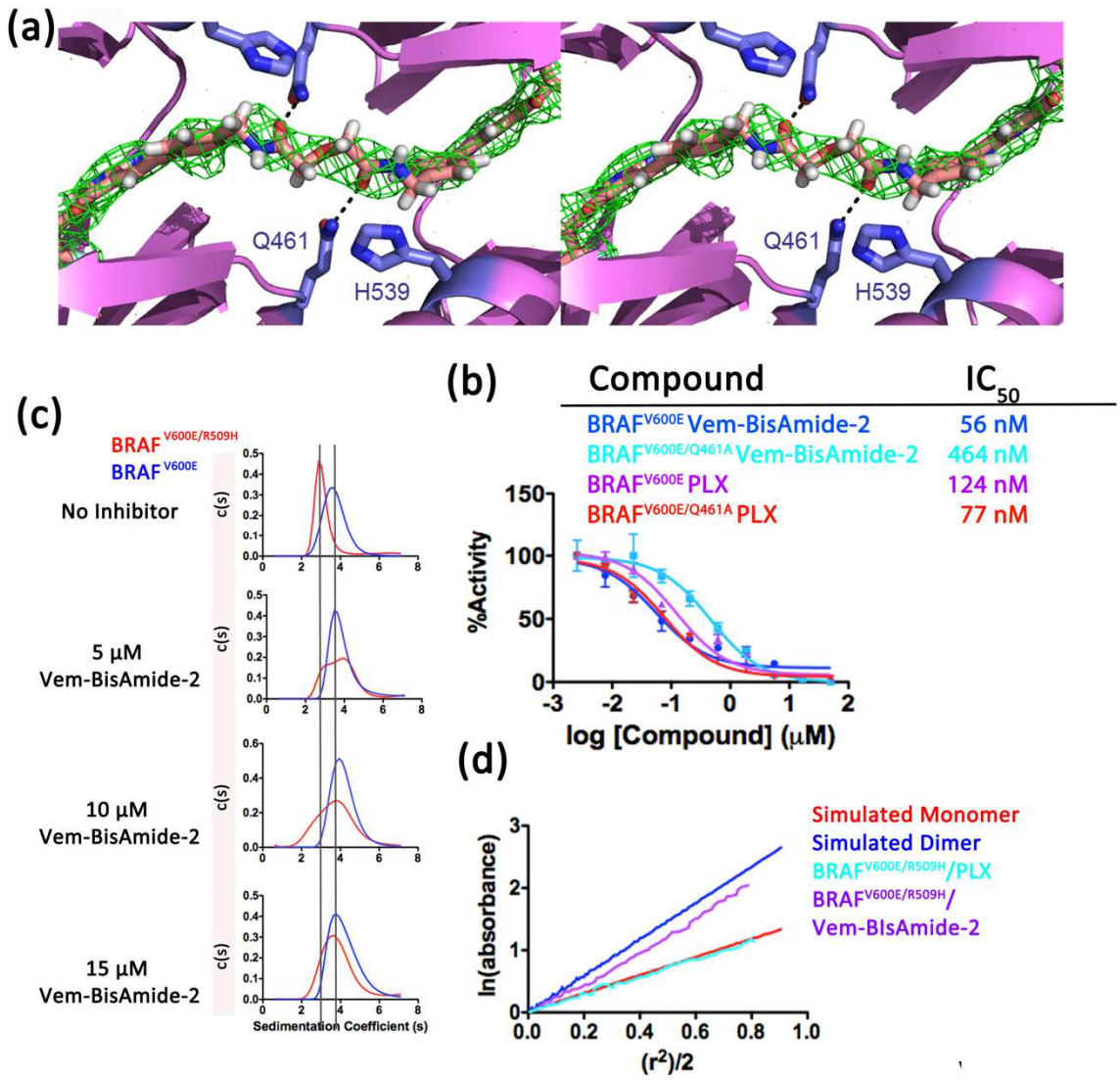

Figure 23 Structure of BRAFV600E/Vem-BisAmide-2 complex and functional characterization of Vem-BisAmide-2.

(a) Structure of $BRAF^{V600E}$ (violet) bound to Vem-BisAmide-2 (pink) with a simulated annealing omit map in green contoured at 2.5 sigma, highlighting close proximity between the carbonyls of the linker amide and Q461, shown as a stereo image (b) Dose response curves of Vem-BisAmide-2 against $BRAF^{V600E}$ (blue) and $BRAF^{V600E/Q461A}$ (cyan) with PLX4720 (PLX) against both proteins as a control. Calculated IC_{50} values from duplicate measurements are indicated with+/- SEM shown. 95% Confidence Intervals are as

(continued from previous page) follows: $BRAF^{V600E}$/Vem-BisAmide-2 (29.8 nM to 106 nM), $BRAF^{V600E/Q461A}$/Vem-BisAmide-2 (286 nM to 755 nM), $BRAF^{V600E}$/PLX (83.8 nM to 184 nM), and $BRAF^{V600E/Q461A}$/PLX (54.7 nM to 108 nM). (c) Sedimentation Velocity of $BRAF^{V600E}$ (blue) and $BRAF^{V600E/R509H}$ (red) as a function of added Vem-BisAmide-2. (d) Log plots of Sedimentation Equilibrium experiments showing theoretical monomer (red) and theoretical dimer (blue) slopes compared to $BRAF^{V600E/R509H}$ with equimolar concentrations of protein and Vem-BisAmide-2 (purple) and PLX (cyan).

Mutagenesis studies were performed to probe the importance of Gln461 for $BRAF^{V600E}$ inhibition by Vem-BisAmide-2. We prepared the $BRAF^{V600E/Q461A}$ mutant and assessed its ability to be inhibited by Vem-BisAmide-2 relative to $BRAF^{V600E/Q461A}$. IC_{50} curves of Vem-BisAmide-2 against $BRAF^{V600E}$ and $BRAF^{V600E/Q461A}$ demonstrated that the Gln461A mutation shifts the IC_{50} from ~56 nM to ~464 nM, respectively, an almost 10 fold difference (**Figure 23b**). In contrast PLX shows a comparable IC_{50} of ~80-130 nM for both $BRAF^{V600E}$ and $BRAF^{V600E/Q461A}$ (**Figure 23b**). These studies highlight the importance of the role of BRAF Gln461 for inhibition by Vem-BisAmide-2.

2.2.5 Vem-BisAmide-2 can promote the formation of $BRAF^{V600E}$ dimers in solution

In order to validate that Vem-BisAmide-2 can mediate an inactive $BRAF^{V600E}$ dimer in solution as was observed in the crystal structures, we performed analytical ultracentrifugation experiments with and without Vem-BisAmide-2. For these experiments, we utilized an R509H point mutation, previously shown to disrupt the active $BRAF^{V600E}$ dimer (Rajakulendran et al., 2009). Control sedimentation velocity

experiments demonstrated that while 10 μM $BRAF^{V600E}$ sediments as a dimer, $BRAF^{V600E/R509H}$ sediments as a monomer. However, the addition of 5 μM of Vem-BisAmide-2 to $BRAF^{V600E/R509H}$ shifts the sedimentation coefficient of $BRAF^{V600E/R509H}$ to two distinct populations, matching both a monomer and a dimer (**Figure 23c**). Vem-BisAmide-2 concentrations of 10 μM and 15 μM were also tested, and increasing concentrations of inhibitor were correlated with more dimer formation for $BRAF^{V600E/R509H}$ while $BRAF^{V600E}$ consistently sediments as a dimer, regardless of whether Vem-BisAmide-2 is added or not. To further quantify the sedimentation velocity experiments, sedimentation equilibrium experiments were performed. Log plots of the data are shown in **Figure 23d**, where the slope of the line is proportional to the estimated molecular weight of the species in solution. $BRAF^{V600E/R50H}$ with no inhibitor bound gives a single species with an estimated molecular weight of 40kD, where the predicted molecular weight of the monomer is ~35kD, indicative of predominantly monomer formation. This species also has a slope that corresponds to that of the predicted line of an ideal monomer. However, when Vem-BisAmide-2 is added, the single species molecular weight is ~70kD, precisely the predicted molecular weight of a BRAF dimer. When $BRAF^{V600E/R509H}$ is incubated with PLX, the ideal fit molecular weight is 40kD, demonstrating that the presence of the unlinked inhibitor is not able to alter the monomeric state of the kinase. These studies validate the promotion of $BRAF^{V600E}$ dimer formation by Vem-BisAmide-2, consistent with the crystallographic data demonstrating that it promotes the formation of $BRAF^{V600E}$ dimers in the inactive conformation. We also performed sedimentation velocity experiments with $BRAF^{V600E/R509H}$ and Vem-BisAmide-4, which contains a single vemurafenib moiety, and demonstrated that the $BRAF^{V600E/R509H}$/Vem-BisAmide-4

complex adopts a monomeric configuration (**Figure 24**) supporting our conclusion that the second vemurafenib molecule in the bivalent Vem-BisAmide-2 inhibitor plays a key role in promotion of the inactive dimeric $BRAF^{V600E}$ conformation.

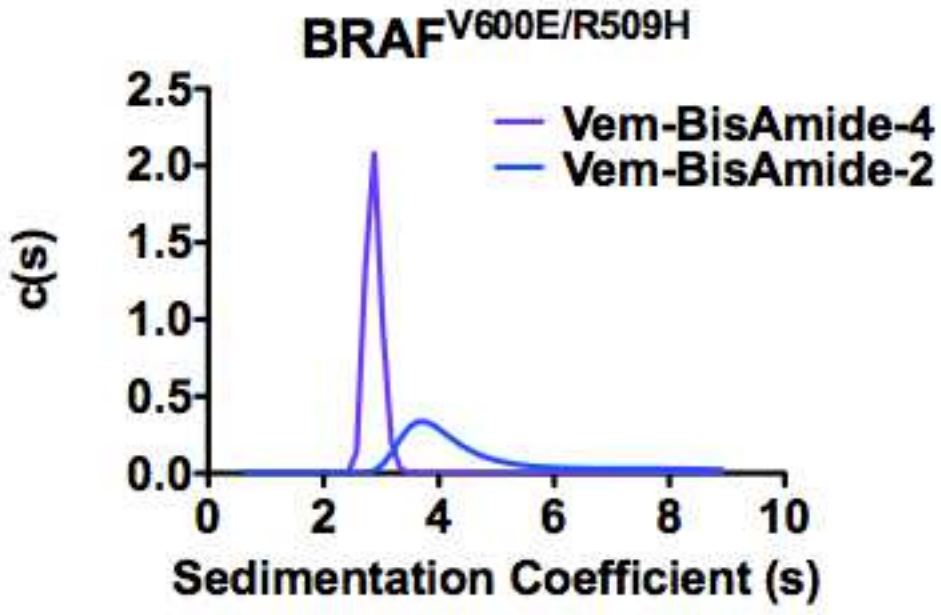

Figure 24 AUC sedimentation velocity of Vem-BisAmide-4 vs. Vem-BisAmide-2 complexed with $BRAF^{V600E/R509H}$.

Sedimentation Velocity experiment shows a difference in Sedimentation Coefficient (s) for $BRAF^{V600E/R509H}$ complexed with Vem-BisAmide-4 and Vem-BisAmide-2.

2.2.6 Vem-BisAmide-2 is able to enter melanoma cells to selectively target $BRAF^{V600E}$ over $BRAF^{WT}$

To determine if Vem-BisAmide-2 can selectively inhibit $BRAF^{V600E}$ in cells, we treated $BRAF^{V600E}$ (WM983B) or $BRAF^{WT}$ (WM3000) melanoma cells with Vem-BisAmide-2, vemurafenib and other selected linked vemurafenib inhibitors. We observed that each of the inhibitors tested showed comparable dose-response inhibition of cell growth (**Figures**

25a and 25b) in cells harboring mutant BRAF^{V600E} (WM983B) but not in cells harboring BRAF^{WT} (WM3000). Furthermore, we found that the linked compounds blunted MAPK signaling (assessed by pERK and pMEK levels) (**Figure 25c, top**), but less potently than the unlinked PLX or the MEK inhibitor PD901. Of note, none of the RAF inhibitors tested blocked MAPK signaling in BRAF^{WT} cells (**Figure 25c, bottom**). These studies demonstrate that Vem-BisAmide-2 can enter cells to selectively inhibit BRAF^{V600E}. The fact that BRAF^{V600E} homodimer species are unlikely to exist in BRAF^{V600E} –mutant melanoma cells (Hu et al., 2013) is consistent with the observation that unlinked and linked-vemurafenib inhibitors show comparable BRAF^{V600E} inhibitory potency in cells.

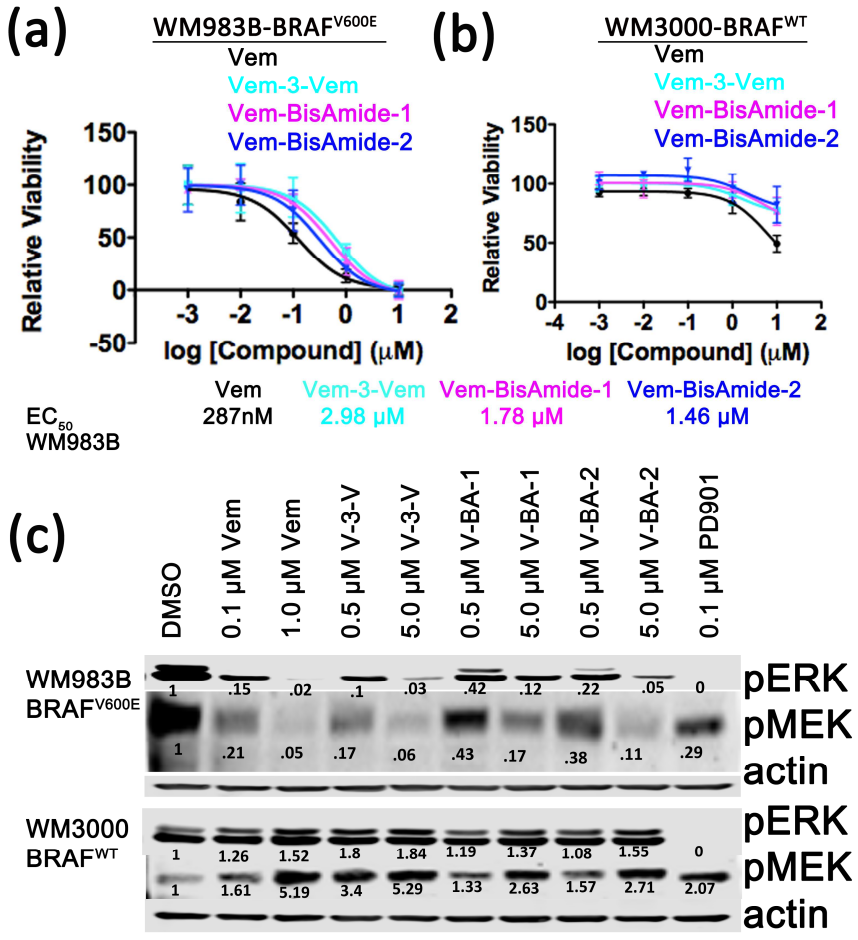

Figure 25 Activity of Vem-BisAmide-2 against melanoma cell lines.

(from previous page)(a-b) Effect of Vem-3-Vem (cyan), Vem (black), Vem-BisAmide-2 (blue) and Vem-BisAmide-1 (pink) on viability of $BRAF^{V600E}$ (WM983B; a) and $BRAF^{WT}$ (WM3000; b) melanoma cell lines treated as in figure 2. Average cell viability taken from 3 separate experiments (n=7) and averaged together with +/- SEM is shown. (c) WM983B (top) and WM3000 (bottom) melanoma cells were treated with the indicated compounds for 18 hr. Total protein lysates were analyzed by immunoblotting using antibodies against phospho-ERK and phospho-MEK. Actin was used as a loading control. Quantification of bands were performed using Odyssey software (Licor) and normalized to the DMSO treatment band.

2.3 Discussion

In summary, we demonstrate that appropriately covalently linking two vemurafenib molecules produces an inhibitor with enhanced potency and selectivity for targeting $BRAF^{V600E}$ over $BRAF^{WT}$, and most significantly, a shift from an active to inactive $BRAF^{V600E}$ conformation, which is trapped in a dimeric state that cannot undergo paradoxical activation. To our knowledge, this is the first inhibitor shown to promote such an inactive $BRAF^{V600E}$ dimeric conformation. While other sulfonamide inhibitors have been shown to favor an inactive monomeric state of $BRAF^{WT}$, the same is not true for $BRAF^{V600E}$, where sulfonamide inhibitors such as vemurabenib can promote an active dimeric conformation. In addition, recently reported "paradox breaker" inhibitors, such as PLX7904, PLX7922 and PLX5568, were shown to disfavor dimerization (C. Zhang et al., 2015). However, crystal structures of these inhibitors bound to $BRAF^{V600E}$ (4XV1 and 4XV3) and $BRAF^{WT}$ (4XV9) still demonstrate packing in a biologically relevant dimer in

the active conformation, characterized by the active conformation of the C-helix and the absence of the AS-H1 helix (C. Zhang et al., 2015). The two $BRAF^{V600E}$ co-crystal structures also have only one inhibitor molecule bound per dimer pair, with the second protomer binding site inhibitor-free and in the active conformation, suggesting that these inhibited dimers may be susceptible to paradoxical activation.

The studies reported here have important implications for developing analogous linked inhibitors to target $BRAF^{V600E}/RAF^{WT}$ heterodimers through the substitution of a pan RAF inhibitor for one of the vemurafenib molecules and appropriate alterations of the linker properties. Such inhibitors would be useful as molecular probes to study the biological importance of RAF dimerization in MAPK signaling and have the potential as novel molecules to target $BRAF^{V600E}$ resistant melanomas. Targeting heterodimers with a linked inhibitor rather than combinations of inhibitors has the potential to demonstrate more selectivity, leading to lower doses and potentially a more prolonged response.

The linked kinase inhibitor strategy described herein also has the potential to be extended to other kinase systems that utilize dimeric forms for signaling and allosteric regulation, such as RTKs, or two different interacting kinases such as RAF and MEK. This strategy could enhance inhibitor synergy or dosing issues that usually come with combination therapies (Flaherty et al., 2012; Greger et al., 2012; Johnson et al., 2014; Villanueva et al., 2013). While these dimeric structures are larger than 500 Da (1067 Da for Vem-BisAmide-2) and therefore do not follow the Lipinski rules (Lipinski, C.A.; Lombardo, F.; Dominy, B.W.; Feeney, 1997), our studies demonstrate that such molecules have good uptake into cells, can engage their substrates and show potent cellular activity. In another example of successfully employing linked inhibitors, Illendula *et. al.* recently

reported on PEG-linked inhibitor of the dimeric transcription factor CBFβ-SMMHC fusion protein to delay leukemia in mice (Illendula et al., 2015).

Taken together, the studies reported here demonstrate that chemically linked RAF inhibitors hold promise for eliciting a prolonged response to $BRAF^{V600E}$-driven melanoma, either administered alone or in combination with immunotherapy, and have implications for targeting other kinase dimers for therapy (Hu-Lieskovan et al., 2015).

2.4 Methods

2.4.1 Plasmids

DNA encoding the BRAF kinase domain residues 448-723 containing 16 solubilizing mutations (Tsai et al., 2008) (I543A, I544S, I551K, Q562R, L588N, K630S, F667E, Y673S, A688R, L706S, Q709R, S713E, L716E, S720E, P722S, and K723G) permitting kinase domain overexpression in bacteria was ordered from Epoch Biolabs and cloned into a Pet28a(+) vector encoding an N-terminal His tag and a thrombin cleavage site between the protein and His tag. This construct was used as a template to create His-tagged $BRAF^{V600E\text{-}16M}$, $BRAF^{R509H\text{-}16M}$ and $BRAF^{V600E/R509H\text{-}16M}$ mutants. These proteins were used in Analytical Ultracentrifugation Sedimentation Velocity and Sedimentation Equilibrium experiments, and Thermal Stability assays. DNA encoding the $BRAF^{V600E\text{-}16M}$ construct was sub-cloned into a PRSF vector containing a TEV protease-cleavable GST-tag and used for crystallization.

DNA encoding the BRAF kinase domain residues 442-724 was used as a template to prepare $BRAF^{WT}$, $BRAF^{V600E}$ and $BRAF^{V600E/Q461A}$ were cloned into a Pfastbac dual vector with mouse $p50^{cdc37}$ full length as an expression chaperone for protein expression in

baculovirus infected Sf9 insect cells and used for *in vitro* kinase assays. Full length human MEK1 with an N-terminal GST fusion tag and a C-terminal His tag in a pGex-3t vector was provided by Dr. Michael Olson (Beatson Institute for Cancer Research, Glasgow, UK) and was used for our *in vitro* kinase assays.

2.4.2. Protein Purification

His-tagged $BRAF^{-16M}$ proteins were expressed in Rosetta2 BL21 bacterial expression cells at 37 ºC and induced with 1mM IPTG overnight at 18ºC, spun down the next day and lysed in Lysis Buffer (50 mM Potassium Phosphate, pH 7.0, 250 mM NaCl, 5 mM Imidazole) and 1 mM PMSF. The lysate was then spun down at 19000 r.p.m. and the supernatant was added to 5 mL TALON metal affinity resin (Takara) and left to incubate at 4ºC for 1 hour. The supernatant was then eluted, the column washed with 1L of Lysis Buffer and the $BRAF^{-16M}$ proteins eluted with Lysis Buffer supplemented with 250mM Imidazole. Protein were then dialyzed into Lysis Buffer without imidazole but with 5 mM EDTA and NaCl adjusted to 5 mM NaCl, prior to application on a 5 mL SP Sepherose anion exchange column, followed by washing in the same buffer and elution in lysis buffer with 0 mM NaCl to 1 M NaCl gradient. Peak fractions were pooled, concentrated, and applied to a Superdex S200 gel filtration column in a final buffer of 20 mM HEPES pH 7.0, 150 mM NaCl, 10 mM Dithiothreitol and 5% glycerol. Protein was flash frozen in liquid nitrogen and stored for future use.

GST-tagged $BRAF^{V600E-16M}$ protein was expressed in bacteria as described for the His-tagged proteins, lysed Lysis Buffer 2 (50 mM KPi pH 7.0 and 250 mM NaCl) and incubated

on Glutathione Resin at 4 ºC for 1 hr. The protein on resin was then washed and left on the resin and cleaved with TEV protease overnight and eluted the next morning in Lysis Buffer 2 with 25 mM NaCl, run over both SP Sepharose and Q Sepharose ion exchange columns in tandem and the flow through collected. The protein was then concentrated using a 10kDalton cutoff centrifugal filter unit (Millipore) and chromatographed on a Superdex S200 gel filtration column in a final buffer of 20 mM HEPES pH 7.0, 150 mM NaCl, 10 mM Dithiothreitol and 5% glycerol. Protein eluted as a mix of dimer and monomer and both species were pooled together, concentrated to 10mg/mL (~320 μM) and used immediately for crystallization.

$BRAF^{WT}$, $BRAF^{V600E}$, and $BRAF^{V600E/Q461A}$ were overproduced as N-terminally His-tagged proteins in insect cells essentially as previously described (Qin et al., 2012). Briefly, protein constructs were coexpressed with $p50^{cdc37}$, pelleted, suspended in Lysis Buffer 3 (25 mM Tris 8.0, 250 mM NaCl, 5 mM Imidazole, and 10% glycerol) treated with Complete EDTA-free protease inhibitor cocktail tablets (Roche) and DNAseI, lysed, centrifuged at 19,000 r.p.m and added to TALON metal affinity resin and incubated for 1 hr at 4 ºC. The protein on the resin was then washed extensively with Lysis Buffer 3 and then eluted with 25 mM Tris pH 7.5, 250 mM NaCl, 250 mM Imidazole, and 10% Glycerol. The protein was then diluted in low salt buffer containing 1 mM EDTA and 1 mM Dithiothreitol and run on an SP Sepharose column, eluted with a salt gradient from 0 mM NaCl to 1 M NaCl. Peak fractions were pooled and run on a Superdex S200 gel filtration column and stored in a final buffer of 25 mM Tris 8.0, 300 mM NaCl, 1 mM Dithiothreitol

and 10% glycerol. Protein was concentrated to ~0.5mg/mL and flash frozen in liquid nitrogen and stored for later use for ELISA kinase assays.

GST-MEK1 fusion protein used as substrate in ELISA assays was prepared essentially as previously described (Qin et al., 2012). Briefly, protein was expressed in BL21 (Gold) cells at 37 ºC and induced with 0.5 mM IPTG at 15 ºC overnight. The cells were then harvested and resuspended in Lysis Buffer 4 (20 mM Hepes pH 7.5, 500 mM NaCl, 10 mM BME, 10 mM Imidazole, 5% Glycerol) supplemented with 1 mM PMSF and DNAseI. The lysate was sonicated and spun down, and the supernatant was added to Ni-NTA resin and incubated for 1 hr at 4 ºC. The resin was then washed extensively with Lysis Buffer 4 and eluted with Lysis Buffer 4 supplemented with 250mM Imidazole. Peak fractions were then concentrated as described above and loaded onto a Superdex S200 gel filtration column in a final buffer of 20 mM HEPES pH 7.0, 150 mM NaCl, 10 mM BME, and 5% glycerol. The protein eluted off the sizing column in two separate populations, and the second peak corresponding to a GST-MEK dimer was collected, concentrated to ~20mg/mL, and flash frozen in liquid nitrogen and stored for later use.

2.4.3 Crystallization, Data Collection, and Structural Analysis

$BRAF^{V600E\text{-}16M}$ at 10 mg/mL was mixed with a 10 mM (in 100% DMSO) stock solution of inhibitor (Vem-6-Vem, Vem-3-Vem, and Vem-BisAmide-2, respectively) to a final inhibitor concentration of 500 μM and trays were set up screening around a crystallization condition of 100 mM Tris pH 8.5, 14% PEG Monomethyl Ether 2000, and 200 mM Trimethyl Amine N-oxide Dihydrate for Vem-6-Vem and a condition of 100 mM Tris 8.5,

5% ethanol, and 2% Benzamidine HCl for Vem-3-Vem and Vem-BisAmide-2 using the hanging-drop vapor diffusion method at 4ºC. Crystals were flash frozen in cryo-protected mother liquor containing 20% glycerol. X-ray diffraction data were collected at a wavelength of 0.98 Å at the Advanced Photon Source (beamline 24-ID-E) for $BRAF^{V600E-16M}$ inhibitor crystals with Vem-6-Vem and Vem-3-Vem, and with Vem-BisAmide-2 was collected in house using the Rigaku MicroMax-007HF with a mar CCD 165mm detector. The $BRAF^{V600E-16M}$ inhibitor crystal with Vem-6-Vem was processed using HKL-2000 (Otwinowski & Minor, 1997), Vem-3-Vem was processed using XDS (Kabsch, 2010) and Vem-BisAmide-2 was processed using HKL-2000 (Otwinowski & Minor, 1997).

All three co-crystal structures were determined by molecular replacement in PHENIX using phaser (Adams et al., 2010; McCoy et al., 2007). The $BRAF^{V600E-16M}$/Vem-6-Vem structure was determined using PDB 4WO5 (Thevakumaran et al., 2014) as a search model in Phaser and the $BRAF^{V600E-16M}$/Vem-3-Vem and $BRAF^{V600E-16M}$/Vem-BisAmide-2 structures were determined using the $BRAF^{V600E-16M}$/Vem-6-Vem structure as a search model. Molecular Replacement search models had the inhibitor removed from them, and for the structure determination of $BRAF^{V600E-16M}$/Vem-6-Vem, the C-helix was removed from the search model. For the structure determinations of $BRAF^{V600E-16M}$ with Vem-3-Vem and Vem-BisAmide-2, the C-helix was included in the molecular replacement model but deleted during refinement and rebuilt manually after PHENIX refinement. Model building and refinement were performed using Coot and PHENIX (Afonine et al., 2012; Emsley, Lohkamp, Scott, & Cowtan, 2010). For all three structures, NCS was used, as multiple BRAF monomers were present in the asymmetric unit. Simulated Annealing omit maps were generated by taking the fully built model, deleting the inhibitor, and

running through PHENIX refine using simulated annealing in the refinement. The coordinates for the Vem-6-Vem inhibitor were generated by downloading the PDB file for Vemurafenib, editing it using the REEL program in PHENIX to edit the molecule, and then running through ELBOW (Moriarty, Grosse-Kunstleve, & Adams, 2009). The coordinates for the inhibitors Vem-3-Vem and Vem-BisAmide-2 were generated using ChemDraw, saving as a pdb file and running through ELBOW to generate a cif file. Table 1 statistics were generated using PHENIX validation tools (V. B. Chen et al., 2010). The two sets of "dimers" in the asymmetric unit of the $BRAF^{V600E\text{-}16M}$/Vem-3-Vem and $BRAF^{V600E\text{-}16M}$/Vem-BisAmide-2 structures are also making interactions with one another, with a Benzamidine molecule buried within the protein-protein interface. Benzamidine Hydrochloride was a crystal additive, and we reason that it facilitated crystallization by stabilizing crystal contacts in this crystal form.

2.4.4. In Vitro Kinase Assay

Compound inhibition of $BRAF^{WT}$ and $BRAF^{V600E}$ were assessed using an ELISA assay performed essentially as previously described (Qin et al., 2012). Briefly, GST-MEK fusion protein was diluted 3:1000 in Tris-Buffered Saline treated with 0.05% Tween-20 (TBST) and diluted MEK was added to a glutathione-coated 96 well plate (Pierce #15240) and incubated at room temperature for 1 hour with shaking. BRAF was diluted from 0.5 mg/mL frozen stocks 1:1000 in 50 mM Hepes pH 7.0 and 50 mM NaCl and treated with inhibitor at various concentrations and incubated with GST-MEK. Glutathione plates were washed extensively, and the protein-inhibitor mixture was then added to the plate with 100 μM final concentration of ATP in a buffer containing 50mM HEPES pH 7.0, 200 mM NaCl,

and 10 mM $MgCl_2$. The plate was then incubated at 37ºC for 30 minutes, the reaction was then discarded, and the plate was washed with TBST extensively and a 1:8000 dilution of primary antibody (p-MEK1/2 (S217/S221) Rabbit Antibody (Cell signaling)) was added to the plate and incubated for 1 hour. The plate was then treated with stringent TBST washes and then incubated with a 1:10000 dilution of secondary antibody (Goat Anti-Rabbit IgG (H+L)-HRP (BioRad)) for 1 hour. The plate was then washed and Supersignal ELISA Pico Chemiluminescent Substrate (Pierce #37069) was added and the plate read on a Perkin Elmer EnVision. Each curve was repeated in duplicate or triplicate, normalized using GraphPad Prism by selecting the largest value as the maximum and the lowest value as the minimum, and used to calculate IC_{50} values by using a log (inhibitor) vs. response fit on Prism 5.0 (GraphPad). IC_{50} values of PLX monomer, first generation Vem-linked inhibitors, and Vem-BisAmide-2 against $BRAF^{V600E}$ were calculated using data from two separate experiments, each performed in duplicate. Error bars are indicative of the SEM of each point, and 95% confidence intervals of the IC_{50} values are listed in the figure legend, as calculated using GraphPad Prism.

2.4.5. Thermal Stability Assays

Frozen aliquots of $BRAF^{V600E-16M}$ proteins were thawed and diluted in Thermal Stability Buffer (25 mM Hepes pH 7.0, 150 mM NaCl) to a final concentration of 5 μM (0.2 mg/mL) and 15 μL were added to the selected wells of a MicroAmp Optical 384 well plate (Applied Biosystems). Sypro Orange (5000X stock, ThermoFisher Scientific) was diluted 1:300 and 4 μL of that diluted stock was added to each well. 1 μL of inhibitor in 100% DMSO was added to each well to a final concentration of 50 μM and the plate was spun down and

heated from 20 ºC to 95 ºC using a qPCR (ABI 7900 RealTime PCR) with a 2% ramp rate. Fluorescent readings were recorded every 2 minutes. Melting curves were generated from this data and analyzed by taking the first derivative of the curve. Data were analyzed and plotted using GraphPad, with error bars indicating as SEM of each sample and 95% confidence intervals of the T_m values listed in the figure legend, both metrics were calculated using GraphPad Prism with an n=6.

2.4.6. Analytical Ultracentrifugation (AUC)

Sedimentation Velocity AUC was performed with a Beckman Optima XL-I at 42,000 r.p.m. Data were obtained over ~8 hours of centrifugation at 20 ºC by monitoring absorbance. Concentrations of $BRAF^{V600E/R509H\text{-}16M}$ and $BRAF^{V600E\text{-}16M}$ were at 10 μM while inhibitor concentration ranged from 5 μM to 15 μM in AUC buffer (25 mM Tris pH 7.5, 150 mM NaCl). Data was analyzed using SEDFIT to calculate a continuous c(s) distribution and data was graphed using GraphPad.

Sedimentation Equilibrium AUC was performed with the same Beckman Optima XL-I at three speeds (12,000 r.p.m, 18000 r.p.m., and 26000 r.p.m.) at three different concentrations (15 μM, 10 μM, and 5 μM) of $BRAF^{V600E/R509H\text{-}16M}$ supplemented with a 1:1 molar ratio of inhibitor at either concentration. AUC buffer from sedimentation velocity experiments was used for equilibrium experiments. Data was analyzed using Heteroanalysis to calculate an Ideal fit molecular weight of the species in each cell and log plots of the data were subsequently graphed using GraphPad Prism. Ideal monomer and dimer fits were calculated using Heteroanalysis.

2.4.7.Cell Viability Assays

The protocol is not included in this text, but is listed in (Grasso et al., 2016). These assays were performed by Minu Samanta in the Villanueva lab.

2.4.8 Small Molecule Inhibitors

Inhibitors were purchased from Selleck Chem: BRAF inhibitor PLX4720 (cat# S1152), and MEK inhibitor PD0325901 (cat#S1036). BRAF inhibitor PLX4032 was purchased from Santa Cruz Biotechnology (cat# sc-364643). EC50 calculation: The EC_{50} (the concentration of a drug that gives half-maximal response) values for BisAmide inhibitors are calculated from relative viability data from three separate experiments with seven replicates each. The EC_{50} values for Vem-x-Vem dimers are calculated from relative viability data from one experiment with seven replicates each. EC_{50} values for Mel1617 cell line ($BRAF^{V600E}$ melanoma cell line) are shown in Figure S8 and was calculated from relative viability data from three separate experiments with seven replicates each. Relative viability values were input in GraphPad and calculated using log (inhibitor) vs normalized response curve.

2.4.9. Western Blotting

The protocol is not included in this text, but is listed in (Grasso et al., 2016). These assays were performed by Minu Samanta in the Villanueva lab.

2.4.10 Inhibitor Synthesis

The protocol is not included in this text, but is listed in (Grasso et al., 2016). Inhibitor synthesis and purification analysis was performed by Michelle Estrada in the Winkler lab.

Chapter 3- TAK632 promotes inhibition of BRAF through the induction of inhibited dimers

This research was performed in collaboration with Dr. Michelle Estrada, and Kiara Berrios of the University of Pennsylvania. Dr. Estrada performed the synthesis of inhibitors, Kiara Berrios performed initial sedimentation velocity experiments of vemurafenib against $BRAF^{WT}$ and $BRAF^{V600E}$. Repeated with permission from Grasso, M., Estrada, M. A., Berrios, K. N., Winkler, J. D., Marmorstein, R. (2018) N-(7-Cyano-6-(4-fluoro-3-(2-(3-(trifluoromethyl)phenyl)acetamido)phenoxy)benzo[d]thiazol-2-yl) cyclopropanecarboxamide (TAK632) Promotes Inhibition of BRAF through the Induction of Inhibited Dimers. *J. Med. Chem.* DOI: 10.1021/acs.jmedchem.8b00499. Copyright 2018 American Chemical Society.

3.1 Introduction

Due to inhibitor resistance via transactivation in patients with BRAF-mutant melanoma, it is important to understand different BRAF inhibitor binding modes and their effects on BRAF dimerization and activation. A prior study characterized several RAF kinase inhibitors that can induce dimerization *in vitro* and in cells, and correlated this to the stabilization of a closed conformation of N and C lobes of the kinase (H Lavoie et al., 2013). A more recent study comparing eight diverse RAF inhibitors led to their classification according to their ability to promote an active or inactive αC-helix conformation, αC-in versus αC-out, respectively (Karoulia et al., 2016). The authors determined that the more BRAF mutant specific αC-out inhibitors (such as vemurafenib) are correlated with inhibitor resistance due to negative allostery, whereas the less BRAF mutant selective pan-RAF αC-in inhibitors can occupy both active sites of a BRAF dimer and are therefore less correlated with drug resistance during treatment (Karoulia et al., 2016).

We previously reported on the development of bivalent vemurafenib (Type-I) inhibitors as a novel approach to potently inhibit active $BRAF^{V600E}$ dimers (Grasso et al., 2016). We found that these inhibitors promote an inactive $BRAF^{V600E}/BRAF^{V600E}$ homodimeric conformation with both protomers in αC-out conformations and with improved vemurafenib potency and selectivity for $BRAF^{V600E}$ *in vitro* (Grasso et al., 2016). To evaluate the BRAF dimerization and inhibition properties of bivalent inhibitors that contain a monovalent compound that promotes an αC-in conformation, we employed the type-II αC-in inhibitor TAK632 (Okaniwa et al., 2013). We hypothesized that a bivalent TAK inhibitor would further stabilize an inactive dimeric BRAF

conformation and be more useful in a cellular environment due to resistance involving $BRAF^{WT}$ and $CRAF^{WT}$ as well as $BRAF^{V600E}$. Surprisingly, we found that while monovalent TAK632 promotes dimerization and potently inhibits BRAF dimers *in vitro*, bivalent TAK inhibitors cannot induce dimers, and concomitantly reduce inhibitor potency. This study indicates that the promotion of an αC-in/αC-in BRAF dimer conformation is integral to the ability of TAK632, and likely other Type-II BRAF kinase inhibitors, to inhibit RAF kinases. These studies have implications for the more effective targeting of BRAF dimers with bivalent BRAF inhibitors to target paradoxical activation for more durable treatment of melanoma.

3.2 Results

3.2.1. Bivalent TAK inhibitors have reduced potency relative to monovalent TAK in vitro

The pan-RAF inhibitor TAK632 targets wild-type or mutant BRAF and CRAF with IC_{50} values in the low nanomolar range (Okaniwa et al., 2013). We used the crystal structure of $BRAF^{WT}$ complexed with TAK632 (accession code 4KSP) to determine where to link the two TAK632 molecules without compromising TAK632 potency. The TAK632 inhibitor binds both subunits of a BRAF dimer with the αC-helix of both protomers in the αC-in conformation. While the trifluoromethylphenyl moiety of TAK632 is located near the hydrophobic pocket of the binding site, the cyclopropyl amide makes minimal protein contacts, i.e., no interaction between the cyclopropane ring and the protein surface is observed, although there is an interaction between the amide N-H and Cys532 (**Figures 26a and 26b**). The amide moiety is exposed to solvent, suggesting it would be an appropriate place to link the monomers, with the caveat that the amide N-H bond is retained

in the bivalent molecule (**Figure 26a**). We therefore prepared a series of PEGylated amide dimers, where n equals the number of PEG units present in the oxydiacetic acid linker of the dimeric structure (**Figure 26c**). Superposition of the $BRAF^{WT}$/TAK632 structure with $BRAF^{V600E}$/Vem-BisAmide-2, ($BRAF^{V600E}$ bound to a bivalent vemurafenib inhibitor, accession code 5JT2), suggests that the amide-linking site on TAK632 would produce bivalent TAK inhibitors with similar topology as Vem-BisAmide-2 and related compounds (**Figure 26d**). The distance between the two TAK632 molecules within a BRAF dimer of the $BRAF^{V600E}$/Vem-BisAmide-2 structure would be predicted to be about 10Å. Based on this docking exercise, we synthesized a series of bivalent TAK-n-TAK molecules where

n=0, 2, 3, 4, and 6 to account for various possible protein dimer orientations (**Figure 26e**).

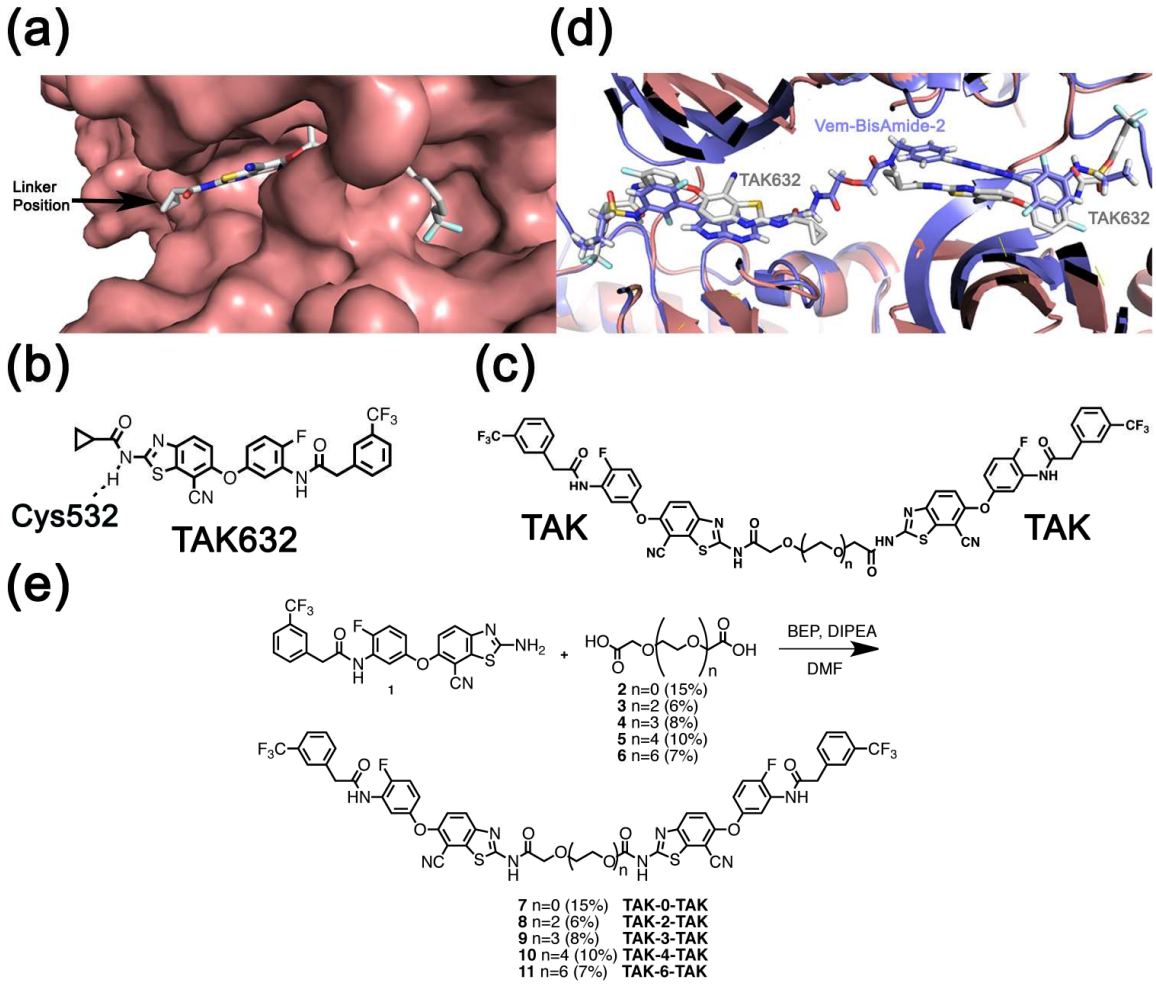

Figure 26 Structure of TAK632 bound BRAF and rationale for linked TAK inhibitors. ***(from previous page)*** (a) Structure of $BRAF^{WT}$/TAK632 (accession code 4KSP), highlighting the exposed cyclopropane ring. (b) Structure of monovalent TAK632, and where it interacts with residue Cys532 of BRAF (c) Initial scaffold for bivalent TAK inhibitors where n equals the number of ethylene glycol moiety groups present. (d) Alignment of $BRAF^{WT}$/TAK632 (pink and grey) with $BRAF^{V600E}$/Vem-BisAmide-2 structure (blue) (5JT2). (e). Preparation of bivalent TAK-n-TAK structures

The requisite dimers were prepared by reaction of the known TAK aminobenzothiazole **1** with the requisite oxydiacetic acids **2-6** in the presence of BEP and DIPEA in DMF, in which the tether length was increased by incremental addition of ethylene glycol moieties to generate the TAK-n-TAK series, in which n represents the number of ethylene glycol moieties in the linker between the two TAK ligands. The inhibitor potency of each molecule was then evaluated *in vitro* against both $BRAF^{WT}$ and $BRAF^{V600E}$ using an ELISA assay that measures the level of phosphorylation of GST-tagged MEK by purified BRAF kinase domain. While all inhibitors showed comparable potency against $BRAF^{WT}$ and $BRAF^{V600E}$, their inhibitory potencies were 15- to 400- fold reduced relative to monovalent TAK632 (**Figure 27a and 27b**). Compounds TAK-2-TAK and TAK-4-TAK showed the greatest potencies of the bivalent inhibitors, with IC_{50} values of 132 nM and 90.2 nM, respectively, against $BRAF^{WT}$ and 73.9 nM and 73.8 nM, respectively, against $BRAF^{V600E}$. The other bivalent TAK inhibitors (TAK-0-TAK, TAK-3-TAK and TAK-6-TAK) had IC_{50} values ranging from 168 nM to 732 nM. In comparison, monovalent TAK632 had IC_{50} values of 3.23 nM and 4.46 nM against $BRAF^{WT}$ and $BRAF^{V600E}$, respectively. These experiments reveal that although the bivalent TAK inhibitors show some dependency on linker length, they are considerably less potent than monovalent TAK632 and therefore likely binding BRAF in a different mode than bivalent Vem-BisAmide-2 and related compounds.

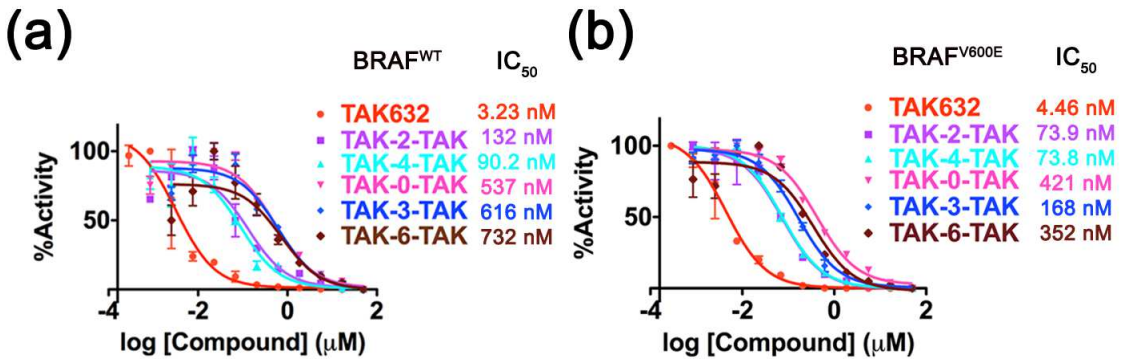

Figure 27 Potency of first generation bivalent TAK inhibitors.

(a) Dose response curves of bivalent TAK inhibitors against $BRAF^{WT}$ with TAK632 as a control. Calculated IC_{50} values are indicated. The experiments were performed in triplicate with +/- SEM shown. 95% confidence intervals are: TAK632 (1.47 nM to 7.47 nM), TAK-2-TAK (69.6 nM to 249 nM), TAK-4-TAK (48.4 nM to 168 nM), TAK-0-TAK (347 nM to 832 nM), TAK-3-TAK (351 nM to 1.08 μM), and TAK-6-TAK (277 nM to 1.94 μM). (b) Dose response curves of bivalent TAK inhibitors against $BRAF^{V600E}$ with TAK632 as a control, carried out in triplicate with +/- SEM shown. The 95% confidence intervals are: TAK632 (2.67 nM to 7.45 nM), TAK-2-TAK (47.5 nM to 115 nM), TAK-4-TAK (59.7 nM to 91.1 nM), TAK-0-TAK (323 nM to 549 nM), TAK-3-TAK (128 nM to 219 nM), and TAK-6-TAK (199 nM to 621nM).

3.2.2 Monovalent TAK inhibitors promote BRAF dimers while bivalent TAK inhibitors do not

Our previous studies revealed that bivalent vemurafenib inhibitors promoted an inactive "face-to-face" αC-out/αC-out BRAF dimer configuration that differed significantly from the "side-to-side" active αC-in/αC-out BRAF dimer configuration as

bound to monovalent vemurafenib or αC-in/αC-in BRAF dimer configuration not bound to inhibitor (Grasso et al., 2016). To determine if bivalent TAK inhibitors also promoted BRAF dimers, we performed analytical ultracentrifugation (AUC) sedimentation velocity experiments to compare the oligomeric state of BRAF as a function of added TAK inhibitors. We first utilized an R509H BRAF mutant protein that disrupts the side-to-side active dimer interface to promote the formation of BRAF monomers (Rajakulendran et al., 2009). As expected, unliganded $BRAF^{R509H}$ migrated with a sedimentation coefficient of ~ 3 corresponding to an apparent protein monomer (**Figure 28a**). Surprisingly, however, the addition of a molar excess of bivalent TAK inhibitors did not alter the apparent monomer migration position of $BRAF^{R509H}$, irrespective of linker length (**Figures 28a – 28c**). The bivalent TAK inhibitors were therefore unable to shift BRAF into an inactive dimeric configuration as anticipated. This differed from chemically linked Vemurafenib inhibitors such as Vem-BisAmide-2, which were able to shift $BRAF^{V600E/R509H}$ into a dimeric configuration in solution (**Figure 29**).

In contrast to the effect of adding bivalent TAK inhibitors to $BRAF^{R509H}$, the addition of a molar excess of monovalent TAK632 to $BRAF^{R509H}$ led to the formation of an apparent $BRAF^{R509H}$ dimeric species (sedimentation coefficient of ~ 4**, Figure 28a – 28c**). While the literature demonstrates that TAK632 can induce dimers at lower concentrations than vemurafenib (Nakamura et al., 2013), the fact that TAK632 can induce dimers *in vitro* despite a R509H point mutation that is known to disrupt dimers was unexpected. These studies demonstrate that monovalent TAK632 actively promotes the formation of BRAF dimers.

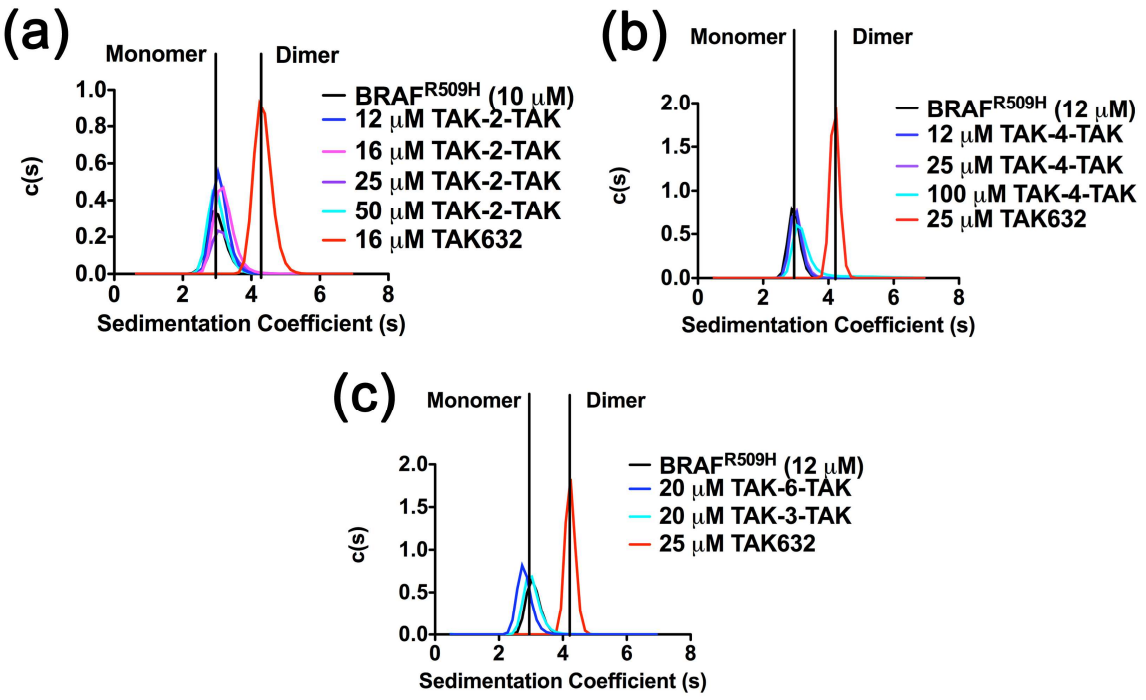

Figure 28 Sedimentation velocity experiments of bivalent TAK inhibitors.

(a) BRAF^{R509H} (10 μM) in the absence and presence of TAK632 and TAK-2-TAK inhibitor at different concentrations. (b) BRAF^{R509H} (12 μM) in the absence and presence of TAK632 and TAK-4-TAK inhibitor at different concentrations. (c) BRAF^{R509H} (12 μM) in the absence and presence of TAK632, TAK-3-TAK and TAK-6-TAK inhibitors at 20 μM.

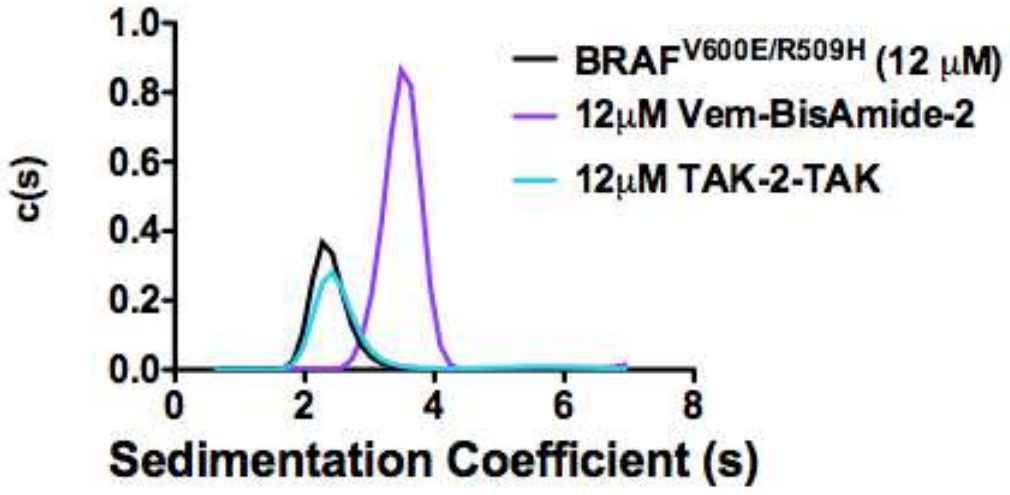

Figure 29 Bivalent TAK inhibitors versus bivalent vemurafenib inhibitors.
Sedimentation velocity curves for 12 μM $BRAF^{V600E/R509H}$ either in the presence of 12 μM Vem-BisAmide-2, 12 μM TAK-2-TAK, or no inhibitor. These curves demonstrate Vem-BisAmide-2 can induce inactive dimers while TAK-2-TAK cannot.

To determine whether higher concentrations of the bivalent TAK inhibitors are able to shift $BRAF^{R509H}$ into a dimeric configuration, we titrated 20 μM protein with 25 – 200 μM TAK-4-TAK and found that even the highest concentration of bivalent inhibitor was unable to fully shift the protein into a dimeric configuration, although at the highest concentration of TAK-4-TAK (200 μM), $BRAF^{R509H}$ gives a more broad sedimentation curve, indicating that at these high concentrations the protein/inhibitor complex begins to shift towards a dimeric species (**Figure 30a**). Consistent with the results above, we also demonstrated that $BRAF^{WT}$ and $BRAF^{V600E}$ form dimeric species in the presence of

monovalent TAK632 and form either monomers or mixed monomer/dimer populations in the presence of bivalent TAK inhibitors (**Figures 30b and 30c**). To confirm these findings, we ran sedimentation equilibrium experiments of $BRAF^{R509H}$ in the absence and presence of monovalent TAK632 and bivalent TAK inhibitors. Log plots of the data are shown in **Figure 30d**, where the slope of the line is proportional to the estimated molecular weight of the species in solution. $BRAF^{R509H}$/TAK632 gave an ideal molecular weight fit of ~69 kDa, aligning with the simulated dimer of ~70 kDa. In contrast, $BRAF^{R509H}$/TAK-4-TAK gave an ideal molecular weight fit of ~40kDa, aligning with the simulated monomer of ~35 kDa. $BRAF^{R509H}$ without inhibitor also aligns with the simulated monomer, giving an ideal molecular weight fit of ~36 kDa. Taken together, the observation that monovalent TAK632 inhibitors promote the formation of BRAF dimers and that the bivalent TAK inhibitors cannot, coupled with our earlier findings that monovalent TAK632 is much more potent than bivalent TAK for BRAF inhibition (**Figure 27**), leads to the conclusion that TAK632 promotes inhibition of BRAF through the induction of inhibited dimers.

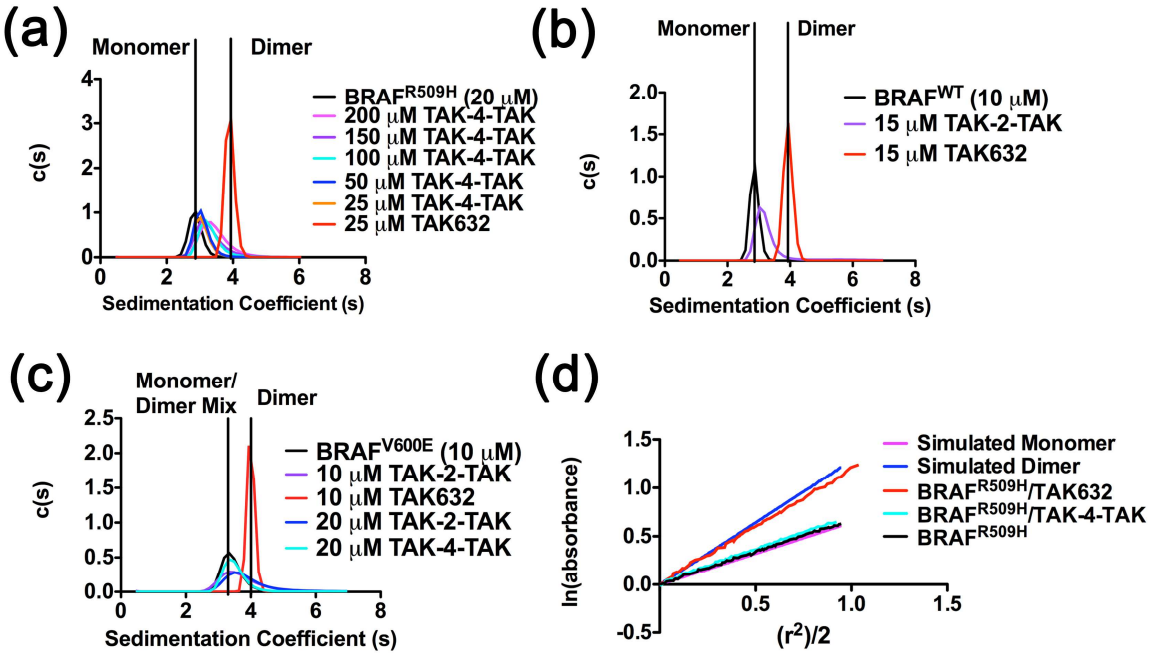

Figure 30 Sedimentation velocity and sedimentation equilibrium experiments of bivalent TAK inhibitors.

(a) $BRAF^{R509H}$ (20 μM) in the absence and presence of TAK632 and TAK-4-TAK inhibitor at different concentrations. (b) $BRAF^{WT}$ (10 μM) in the absence and presence of TAK632 and TAK-2-TAK. (c) $BRAF^{V600E}$ (10 μM) in the absence and presence of TAK632 and TAK-2-TAK and TAK-4-TAK inhibitors at different concentrations. (d) Log plots of sedimentation equilibrium experiments showing theoretical monomer (purple) and theoretical dimer (blue) slopes of BRAF compared to $BRAF^{R509H}$ in the absence and presence of TAK632 and bivalent TAK-4-TAK at a 2:1 molar ratio of inhibitor to protein.

3.2.3 The bivalent nature of the linked TAK inhibitors is required to reduce inhibitor potency and to promote BRAF monomers

To determine whether the two TAK632 ligands or the glycol linker was responsible for promoting the formation of the BRAF monomers, we prepared two compounds with the linker intact and only one TAK632 molecule (TAK-L and TAK-L-C, **Figure 31a**). TAK-L, included the PEG portion of the linker, while TAK-L-C included the PEG and the 1,3-thiazole-2-amide moiety of the second TAK632 molecule as a cap. Coupling of the TAK molecule **1** (**Figure 26e**) with commercially available 2-(2-methoxyethoxy)acetic acid **12** led to the formation of **13 TAK-L**. The TAK-L-C **14** was prepared from 3,6,9-trioxaundecandioic acid **3**, first by anhydride formation with DCC, followed by ring opening with 2-aminothiazole, and coupling of the TAK molecule **1** with the resulting monoacid intermediate to give **14 (TAK-L-C)**. Both molecules were evaluated in ELISA kinase activity assays and sedimentation velocity experiments to assess the effect of these two linker regions on TAK potency and the ability to promote BRAF dimers, respectively. Dose response kinase inhibition experiments demonstrated that TAK-L had similar inhibitor potency to TAK632, with IC_{50} value of 5.75 nM and 7.11 nM, respectively, and TAK-L-C showed only about a 4-fold reduced potency (20.3 nM) relative to TAK632 (**Figure 31b**). In contrast, the bivalent TAK inhibitors, TAK-2-TAK and TAK-4-TAK, showed about a 12-fold reduction in potency (> 85 nM) relative to TAK632 (**Figure 31b**). These data demonstrate that the second TAK632 ligand in the bivalent TAK inhibitor plays a significant role in the reduced potency of the bivalent TAK inhibitors relative to monovalent TAK632. These results also indicate that linker placement does not

significantly hinder the ability of the bivalent inhibitors to inhibit BRAF relative to monovalent TAK632.

Sedimentation velocity experiments with $BRAF^{R509H}$ in the presence of monovalent TAK-L and TAK-L-C or the bivalent TAK-2-TAK, reveal that the TAK inhibitors containing linkers and a single TAK632 ligand promoted the formation of protein dimers, while TAK-2-TAK could not alter the oligomerization state upon binding (**Figure 31c**), as previously shown (**Figure 28a**). These data demonstrate that the second TAK632 ligand in the bivalent TAK inhibitor plays a driving role in preventing the formation of inhibited BRAF dimers, which appears to be correlated with the reduced potency of the bivalent TAK inhibitors relative to monovalent TAK632.

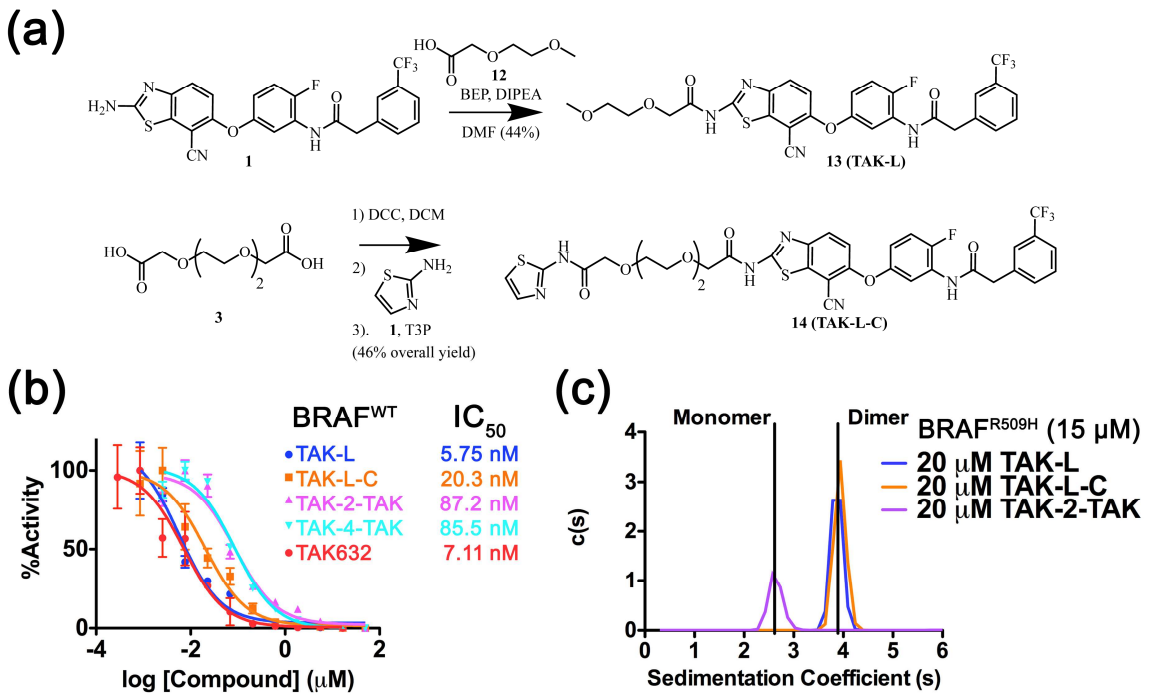

Figure 31 Biochemical and biophysical properties of TAK-linker compounds.

(a) Preparation of monomeric TAK control compounds, TAK-L (TAK with linker) and TAK-L-C (TAK with linker and cap). (b). Dose response curves of TAK control compounds along with bivalent TAK-2-TAK and TAK-4-TAK and TAK632 against $BRAF^{WT}$. Calculated IC_{50} values are indicated. The experiments are performed in duplicate with +/- SEM shown. 95% confidence intervals are: TAK-L (3.33 nM to 9.91 nM), TAK-L-C (10.3 nM to 40.2 nM), TAK-2-TAK (50.2 nM to 151 nM), TAK-4-TAK (56.7 nM to 129 nM), and TAK632 (3.32 nM to 15.2 nM). (c). Sedimentation velocity experiments with $BRAF^{R509H}$ (15 μM) in the presence of TAK-L, TAK-L-C, and TAK-2-TAK at 20 μM.

3.2.4 Bivalent TAK inhibitors display distinct BRAF properties

To further explore the mechanism by which bivalent TAK inhibitors bind BRAF, we performed a limited proteolysis experiment in which trypsin was added to $BRAF^{WT}$ in the presence and absence of TAK632, TAK-2-TAK, TAK-L-C, and vemurafenib (**Figure 32a**). When no ligand is present (lane 1), the major digested band (species A), is very close in size to undigested BRAF, with the appearance of two smaller minor bands (species B and C). In the presence of TAK632 and TAK-L-C (lanes 2 and 3 respectively), $BRAF^{WT}$ species A becomes a minor band, while species B and C become major bands. In contrast, in the presence of TAK-2-TAK (lane 4), $BRAF^{WT}$ had a digestion pattern resembling that of unliganded $BRAF^{WT}$, producing $BRAF^{WT}$ species A as a major band but with slightly larger amounts of species B and C. In the presence of vemurafenib (lane 5), $BRAF^{WT}$ produces species A as the major band, with negligible amounts of species B and C. These results demonstrate that in the presence of the bivalent TAK-2-TAK, BRAF has a digestion pattern that is somewhere in between $BRAF^{WT}$ alone and monomeric TAK632/TAK-L-C. These observations indicate that bivalent TAK inhibitors cannot fully promote a conformation allowing for degradation to species B and C, whereas monovalent TAK molecules can.

To further dissect the mode of bivalent TAK inhibitor binding to BRAF, we performed Differential Scanning Calorimetry (DSC) experiments in which $BRAF^{WT}$ protein (37 μM) was heated in the presence and absence of ligands to determine melting temperatures (**Figure 32b**). When no ligand is present (black), we observe a single melting temperature of 37.84 ºC, which we interpret as melting of a $BRAF^{WT}$ monomer. In the presence of TAK632 or TAK-L-C (125 μM) (violet and cyan, respectively), we observe

single melting temperatures of 68.74 ºC and 63.29 ºC, respectively, which we interpret as melting of $BRAF^{WT}$ dimers bound to monovalent TAK inhibitors. In contrast, in the presence of TAK-2-TAK (125 µM) (pink), two broad melting temperatures are observed of 38.72 ºC and 59.6 ºC, and titration of TAK-2-TAK between 75-250 µM produces more of the higher melting temperature species at the expense of the lower melting temperature species. We interpret this observation to indicate that while bivalent TAK inhibitors do have a capacity to promote BRAF dimers at high concentration of bivalent inhibitor, they do so significantly more poorly than monovalent TAK632. Taken together, both the limited proteolysis (**Figure 32a**) and DSC (**Figure 32b**) studies reveal that bivalent TAK inhibitors promote BRAF species in solution that act as a combination of both unbound BRAF and BRAF bound to monovalent TAK, indicating that the bivalent TAK inhibitors cannot fully stabilize the dimeric TAK632-mediated BRAF configuration.

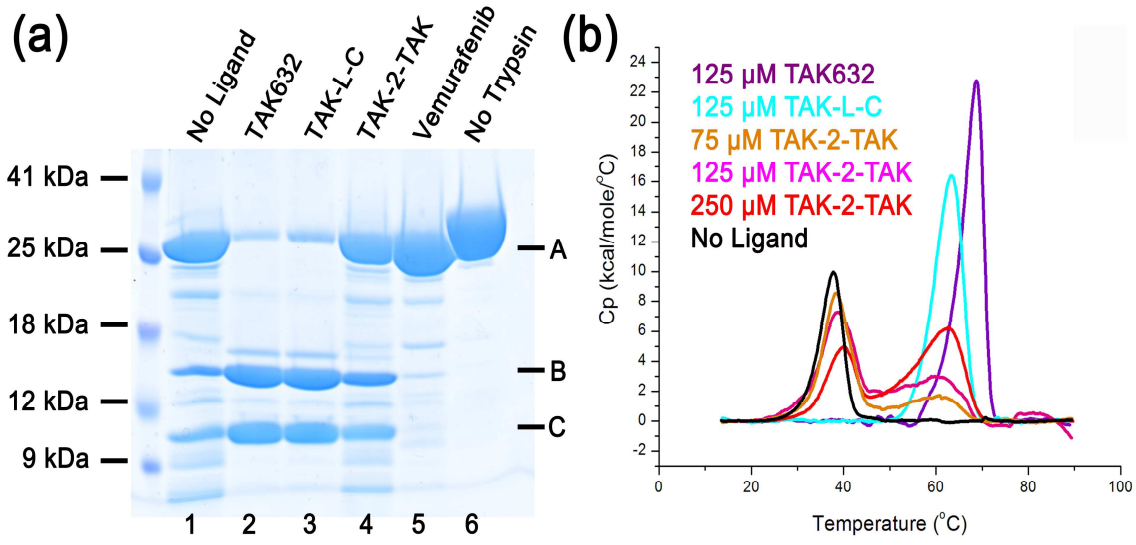

Figure 32 Determination of bivalent TAK inhibitor binding modes to BRAF.

(from previous page) (a) Limited proteolysis experiment of $BRAF^{WT}$ in the presence and absence of 200 μM inhibitors after exposure to trypsin for 30 minutes (lanes 1-5) and lane 6 shows $BRAF^{WT}$ without ligand or trypsin. (b) Differential Scanning Calorimetry (DSC) experiments in which $BRAF^{WT}$ is heated in the presence and absence of inhibitors ranging in concentration from 25 μM to 250 μM. Melting temperatures are as follows: 125 μM TAK632-68.7 ºC; 125 μM TAK-L-C- 63.3 ºC; 75 μM TAK-2-TAK- 38.4 ºC, 58.7 ºC; 125 μM TAK-2-TAK- 38.7 ºC, 59.6 ºC; 250 μM TAK-2-TAK- 40.1 ºC, 62.6 ºC; No ligand- 37.8 ºC.

3.2.5 Trp450, Arg506 and the αC-helix play a significant role in dimer formation via TAK binding

Given our surprising finding that the monovalent TAK632 inhibitor promotes formation of αC-in/αC-in BRAF dimers, even in the presence of the R509H dimerization defective mutant, we set out to better understand the nature of the BRAF dimer that is stabilized by monovalent TAK632. R509 is able to stabilize the active "side-to-side" αC-in/αC-in configuration by making hydrogen bond interactions with backbone carbonyls of T508 and R506 (Grasso et al., 2016; Rajakulendran et al., 2009). To assess what additional changes are necessary to facilitate TAK632-induced dimerization, we superimposed different subunits of the $BRAF^{WT}$/TAK632 (accession code 4KSP) (Okaniwa et al., 2013), $BRAF^{V600E}$/AZ628 (accession code 4G9R) (Wenglowsky et al., 2012), and $BRAF^{R509H}$/AZ628 (accession code 4RZW) (Karoulia et al., 2016) crystal structures.

AZ628 is another Type-II, αC-in inhibitor, and was also shown to be able to induce dimerization in the presence of an R509H mutation, however at a higher concentration (Karoulia et al., 2016). This superposition revealed that the inhibitor complexes with $BRAF^{WT}$ and $BRAF^{V600E}$ contain highly super imposable αC-in/αC-in configurations (RMSD of 0.596 $Å^2$ for $BRAF^{WT}$/TAK αC segments and 0.463 $Å^2$ for $BRAF^{V600E}$/AZ628 αC segments), while the $BRAF^{R509H}$/AZ628 structure contains more variable αC-in configurations (RMSD of 1.713 $Å^2$ for corresponding αC segments) where one of the αC segments orients further away from the αC-out configuration while the other moves closer towards the αC-out configuration (as seen in the $BRAF^{V600E}$/Vem complex, **Figure 33a).** This observation suggests that while the R509H mutation destabilizes the active αC-in/αC-in dimer and favors an inactive, αC-out configuration, Type-II inhibitor binding is able to compensate for the destabilizing R509H mutation to further strengthen the dimer by biasing the kinase towards an αC-in/αC-in dimer configuration.

In comparing the three crystal structures described above, we noted that W450 participates in van der Waals interactions with the aliphatic region of R509 but that W450 adopts a distinct conformation in one of the protomers of the $BRAF^{R509H}$/AZ628 structure, which appears to be facilitated by a pi-stacking interaction with the R509H mutation of the other protomer (**Figures 33b and 33c**), and accompanied by a movement of D448 to hydrogen bond to W450 of the opposing subunit (**Figure 33d**). Reinforcing the importance of W450 for active BRAF dimer formation, a W450A mutation was previously demonstrated to impair transactivation in cells. (Hu et al., 2013; Jambrina et al., 2016)

These results indicate that W450 plays a critical role in the ability of TAK632 (and possibly other Type-II αC-in inhibitors such as AZ628) to induce dimerization.

R506 is another residue previously noted to play a significant role in inhibitor-induced dimerization based on the unique conformations that it adopts in co-crystal structures of BRAF bound to αC-in (ie. AZ628) and αC-out (ie. vemurafenib) inhibitors (Karoulia et al., 2016). Specifically, R506 adopts an "in" position in the $BRAF^{R509H}$/AZ628 structure, but adopts an "out" position in $BRAF^{V600E}$/Vemurafenib (Vem) (3OG7, yellow) structures (**Figure 33e**). R506 lies close to W450, and the distinct W450 shift present in the one $BRAF^{R509H}$/AZ628 protomer that shifts closer to the R506 "out" conformation, further supporting the role of R506 in dimerization (**Figure 33f**).

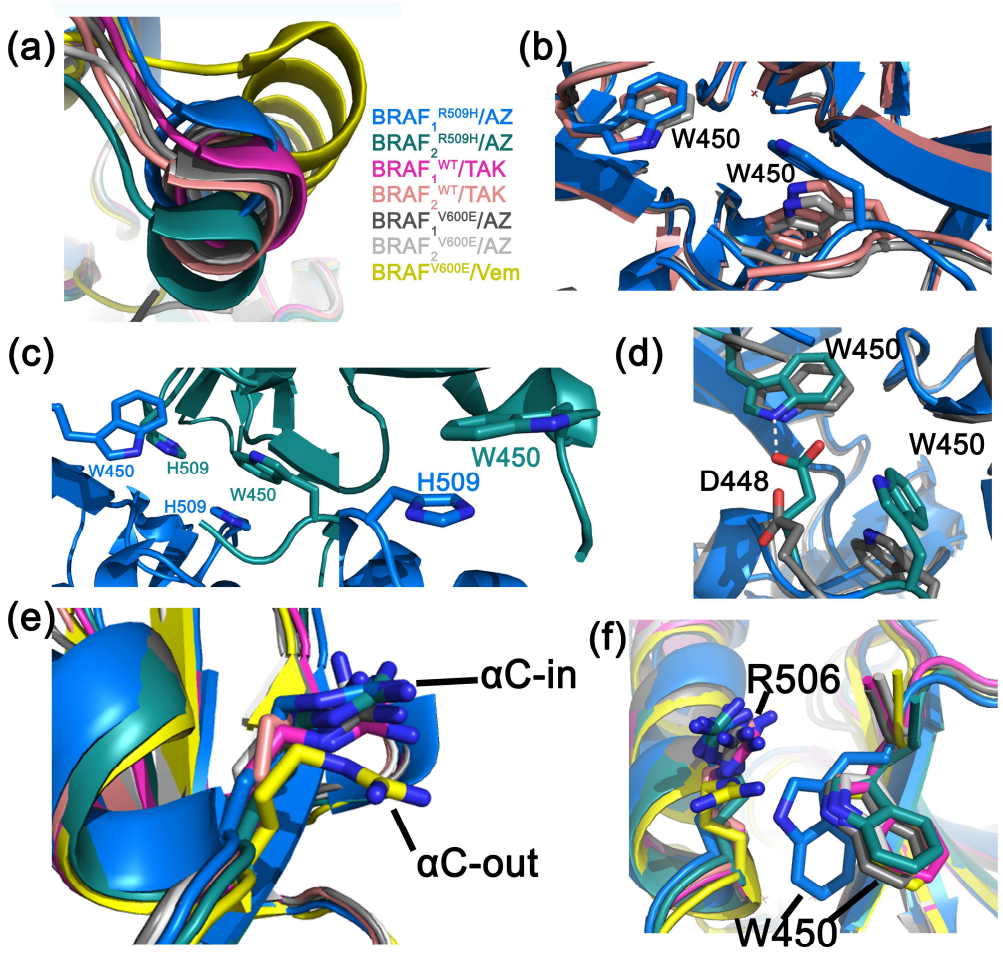

Figure 33 BRAF^{R509H} dimer interface via TAK632 binding.

(a) Overlay of BRAF^{WT}/TAK632 (light pink and magenta), BRAF^{V600E}/AZ628 (light grey and dark grey), BRAF^{R509H}/AZ628 (blue and teal), and BRAF^{V600E}/Vemurafenib (yellow) structures, highlighting the shift within the aC-in position. Different subunits of the crystal structures are denoted with subscript 1 and 2, respectively. (b) Overlay of BRAF^{WT}/TAK632 (light pink, PDB ID: 4KSP), BRAF^{V600E}/AZ628 (grey, PDB ID: 4G9R), and BRAF^{R509H}/AZ628 (blue, PDB ID: 4RZW) highlighting a shift in the W450 residue in the BRAF^{R509H} structure. (c). Crystal structure of BRAF^{R509H} bound to AZ628 demonstrates that W450 forms pi- stacking interactions with His509. (d) Residue D448

(continued from last page) accompanies the shift in the W450 residue, hydrogen bonding with the other static W450. (e) R506 residues in both subunits of $BRAF^{WT}$/TAK632 (light pink and magenta), $BRAF^{V600E}$/AZ628 (light grey and dark grey), and $BRAF^{R509H}$/AZ628 (blue and teal) aligned with one subunit of $BRAF^{V600E}$/Vemurafenib (yellow) demonstrating "in" and "out" positions of R506. (f). W450 lies within close proximity of R506, and the W450 in $BRAF^{R509H}$/AZ628 shifts closer to R506.

To evaluate the effect of W450 and R506 on TAK-induced dimerization, we performed sedimentation velocity experiments with $BRAF^{W450A}$, $BRAF^{R506A}$, $BRAF^{W450A/R509H}$, $BRAF^{R506A/R509H}$, and $BRAF^{R506A/W450A/R509H}$ mutants alone and in the presence of TAK632 **(Figure 34a-34b**). We found that TAK632 promotes the complete dimerization of $BRAF^{R506A}$ and $BRAF^{W450A}$, but TAK632 with the double mutants of $BRAF^{R509H/W450A}$ and $BRAF^{R506A/R509H}$ showed a peak that is in between that of a monomer and a dimer. The peaks also appear to be slightly broader than those of species that sediment as complete monomers or dimers. We hypothesize that these mutants are able to disrupt TAK632-induced dimerization, however not completely, thus giving a mixed monomer/dimer peak. The triple mutant $BRAF^{R509H/R506A/W450A}$ in the presence of TAK632 sediments less broadly and more closely to that of a monomer peak, indicating that the combination of all three mutations disrupts TAK632 induced dimerization more than any of the individual mutations. We confirmed these results with sedimentation equilibrium measurements (**Figure 34c**), where $BRAF^{R509H/R506A}$ gives an estimated ideal molecular weight of 58,000 kDa while $BRAF^{R509H/W450A}$ gives an estimated molecular weight of 57,000 kDa. $BRAF^{R509H/R506A/W450A}$ leads to the smallest molecular weight of the mutants,

47,000 kDa, indicating that while TAK632 binding does still induce dimerization slightly, the ability to do so is dramatically decreased due to mutation of the residues that mediate dimerization. These mutants also all show gel filtration curves similar to that of the wild type protein, indicating that they are properly folded and not aggregated (not shown). While each of these mutants alone is not enough to prevent TAK632-induced dimerization, combining them causes conformational changes in the active dimer and combining all three prevents the majority of molecules in solution from forming dimers. Taken together, these studies indicate that R509, W450 and R506 play important roles in facilitating the active αC-in/αC-in BRAF dimer as well as TAK632-induced dimerization. The observation that TAK632 still efficiently promotes dimers of the single $BRAF^{W450A}$, $BRAF^{R506A}$, and $BRAF^{R509H}$ mutants but not the $BRAF^{R509H/R506A/W450A}$ mutant suggests that all three residues play a coordinated role in "side-to-side" αC-in/αC-in configuration dimerization, which is further reinforced by TAK632 binding.

3.2.6 Type II αC-in and Type I αC-out inhibitors promote BRAF dimers and monomers, respectively

To assess whether other Type II αC-in inhibitors are able to induce BRAF dimerization in solution, we performed sedimentation velocity experiments with sorafenib, another well-known Type II, αC-in inhibitor (Karoulia et al., 2016; Wan et al., 2004). As shown in **Figure 34d,** sorafenib behaves similarly to TAK632, promoting dimerization despite the R509H mutation, further reinforcing the finding that Type II αC-in inhibitors function by stabilizing the active "side-to-side" αC-in/αC-in BRAF dimer configuration. To explore the effects of a Type I αC-out inhibitor, we used vemurafenib as a model αC-

out inhibitor. We found that $BRAF^{WT}$ monomers were stabilized and $BRAF^{V600E}$ dimers were disrupted upon addition of vemurafenib (**Figure 34e**). Taken together, Type II αC-in inhibitors appear to promote BRAF dimerization, while Type I αC-out inhibitors such as vemurafenib promote a disruption of the BRAF dimer. TAK632 therefore relies on its ability to induce dimerization for effective inhibition, unlike αC-out inhibitors such as vemurafenib.

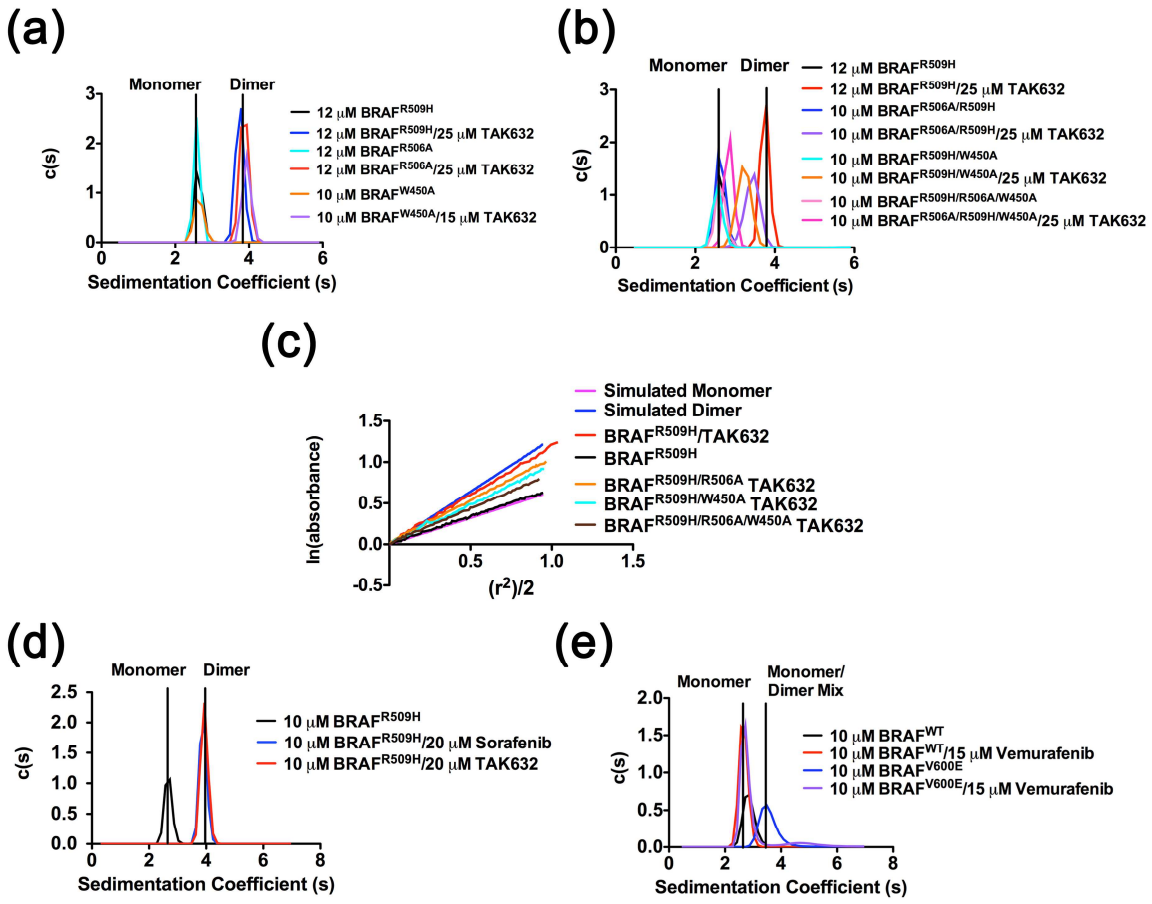

Figure 34 Sedimentation velocity experiments of dimerization mutants and αC-in/αC-out inhibitors.

(a) Sedimentation velocity experiments of $BRAF^{R509H}$, $BRAF^{R506A}$, and $BRAF^{W450A}$ in the absence and presence of TAK632 at 15-25 μM. (b) Sedimentation velocity experiments of $BRAF^{R509H}$, $BRAF^{R506A/R509H}$, $BRAF^{W450A/R509H}$ and $BRAF^{R506A/W450A/R509H}$ in the absence and presence of TAK at 25 μM. (c) Sedimentation velocity experiments of $BRAF^{R509H}$ without inhibitor and with 20 μM of both TAK632 and sorafenib. (d) Sedimentation velocity experiments of $BRAF^{WT}$ and $BRAF^{V600E}$ with 15 μM vemurafenib.

3.3 Discussion

In this study, we demonstrate that TAK632 promotes inhibition of BRAF by inducing dimerization with an αC-in/αC-in configuration. The mutational and analytical ultracentrifugation analyses further highlight the importance of R509, W450, R506, and likely also D448 in mediating this dimeric BRAF conformation. The analysis that we present here with the other Type II αC-in inhibitors AZ628 and sorafenib suggests that these findings extend to the broader family of αC-in inhibitors. Coupled with the potent BRAF inhibitory activity and absence of paradoxical activation activity of such inhibitors, these findings support the conclusion that TAK632 and related inhibitors promote inhibition of BRAF through the induction of inhibited dimers.

While previous studies have highlighted the importance of R509 in stabilizing αC-in/αC-in BRAF dimers, in this study we have extended the analysis of the molecular basis of stabilization of this dimeric BRAF configuration, concomitant with positioning the C-helix in the αC-in configuration. We demonstrate that W450, R506 and likely also D448 play important roles in this activity. Other studies have also proposed the importance of R506 in mediating BRAF dimer formation, and we have demonstrated that it plays a similar role in inhibitor-induced dimerization as W450 (Karoulia et al., 2016).

In contrast to monovalent TAK632, the less potent bivalent TAK inhibitors appear unable to promote the αC-in/αC-in dimeric configuration. This leads to BRAF monomers being the predominant species, while monovalent TAK632 is able to induce dimerization upon binding. Comparison of the BRAF activities and multimerization states of BRAF complexes with bivalent TAK inhibitors and monovalent TAK632 inhibitors with attached

linkers reveals that the second TAK632 molecule of the bivalent TAK inhibitors plays a particularly important role in the reduced BRAF kinase activity and promotion of the monomeric BRAF state. The control inhibitors TAK-L and TAK-L-C also demonstrate that linker placement does not affect active site binding, indicating a more complex mechanism. Although our data imply that the reduced inhibitor activity of the bivalent TAK inhibitors is correlated with their inability to promote BRAF dimers, the molecular basis for how the second TAK632 ligand of the bivalent TAK inhibitor destabilizes the BRAF dimer configuration that is promoted by TAK632 is unclear. Limited proteolysis and DSC experiments suggest that while bivalent TAK inhibitors can mediate a BRAF configuration that is similar to that of TAK632-bound BRAF, their affinities for these sites are notably decreased. We propose that bivalent TAK inhibitors have significantly reduced affinities for BRAF because they are unable to assume stable dimeric BRAF configurations.

In previous studies, we demonstrated that bivalent vemurafenib inhibitors promote inactive $BRAF^{V600E}$/$BRAF^{V600E}$ homodimeric conformations with both protomers containing αC-out conformations and with improved potency and selectivity for $BRAF^{V600E}$ *in vitro* relative to vemurafenib (Grasso et al., 2016). Interestingly, we found that bivalent vemurafenib inhibitors were able to induce the same face-to-face αC-out/αC-out BRAF dimeric configurations, independent of linker length. This was not the case with bivalent TAK inhibitors in this study, in which we found that the bivalent TAK inhibitors cannot promote BRAF dimers, resulting in reduced potency relative to monovalent TAK632. To understand the molecular basis for why bivalent TAK inhibitors are unable to induce the same dimer face-to-face αC-out/αC-out BRAF dimeric configuration

promoted by bivalent vemurafenib inhibitors, we overlayed individual BRAF molecules bound to TAK632 with the "face-to-face" conformation of BRAF bound to the bivalent Vem-BisAmide-2 inhibitor (**Figure 35a**). Although this modeling exercise does not reveal any steric clashes between the BRAF molecules in the modeled TAK632-bound inactive dimeric configuration, we observe different configurations of the Vem-BisAmide-2 and TAK632-bound BRAF proteins that could destabilize TAK632-bound BRAF dimers in this BRAF dimer configuration (**Figure 35b**).

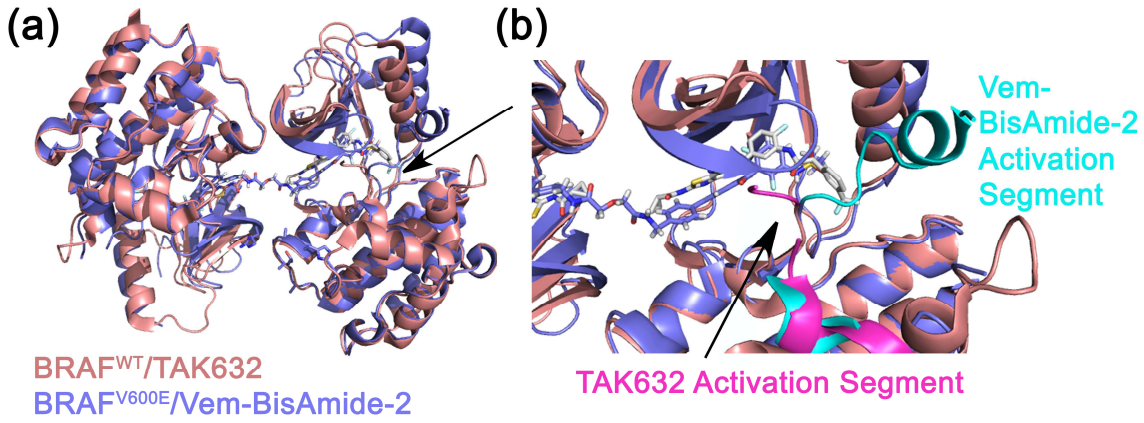

Figure 35 Superposition of BRAF^{V600E}/Vem-BisAmide-2 with BRAF^{WT}/TAK632.

(a) Overlay of BRAF^{WT} co-crystallized with TAK632 (PDB ID: 4KSP) overlayed with the αC-out/αC-out "face-to-face" dimer induced by Vem-BisAmide-2 (PDB ID: 5JT2). (b) Comparison of activation segment of BRAF^{V600E} bound to Vem-BisAmide-2 in an active conformation (cyan) and the activation segment of BRAF^{WT} bound to TAK632 in an inactive conformation (magenta), protruding into the other molecule of the "face-to-face" dimer.

Specifically, we note that while Vem-BisAmide-2 binding favors the activation segment to flip outwards into an active conformation (cyan), the activation segment of BRAF bound to TAK632 molecules favors an inactive, inward activation segment conformation (magenta). While the activation segment is mostly unresolved in the BRAF/TAK632 structure, this dynamic region could form steric clashes with the activation segment of another BRAF molecule, making the "face-to-face" dimeric conformation energetically unstable. We therefore propose that it is not possible for bivalent TAK inhibitors to induce an inactive, "off-state" BRAF dimer configuration, and this is likely true with other αC-in inhibitors such as sorafenib and AZ628. Instead, we hypothesize that pan-RAF inhibitors that favor the αC-out conformation will be more amenable to the preparation of bivalent inhibitors with improved BRAF potency and with the ability to counteract transactivation of RAF^{WT}/RAF^{WT} homodimers and $RAF^{WT}/BRAF^{V600E}$ heterodimers in melanoma and other BRAF-associated cancers. Interestingly, the pan-RAF inhibitors reported to date all appear to stabilize the active αC-in conformation. We propose that a solution to this is to prepare bivalent BRAF inhibitors with highly potent $BRAF^{V600E}$-specific αC-out promoting inhibitors that still retain appreciable affinity for $BRAF^{WT}$. Such inhibitors could be molecules such as Dabrafenib and BI 882370, which inhibit $BRAF^{WT}$ and $CRAF^{WT}$ with potencies similar to pan RAF inhibitors such as TAK632 (Waizenegger et al., 2016). Another possibility is a purinylpyridinylamino-based BRAF inhibitor that is $BRAF^{V600E}$-specific, but binds two molecules of a $BRAF^{WT}$ side-to-side dimer with two αC-out configurations (Liu et al., 2016). Taken together, these studies highlight the importance of understanding the impact of BRAF inhibitors on kinase dimerization to effectively target RAF^{WT}/RAF^{WT} homodimers and $RAF^{WT}/BRAF^{V600E}$ heterodimers with

bivalent pan-RAF inhibitors to target paradoxical activation for more durable treatment of melanoma.

3.4 Methods

3.4.1. Plasmids

Proteins used for analytical ultracentrifugation sedimentation velocity experiments. DNA encoding the BRAF kinase domain residues 448-723 containing 16 solubilizing mutations (I543A, I544S, I551K, Q562R, L588N, K630S, F667E, Y673S, A688R, L706S, Q709R, S713E, L716E, S720E, P722S, and K723G) was ordered from Epoch Biolabs and cloned into a Pet28a(+) vector encoding an N-terminal 6XHis Tag and a thrombin cleavage site between the protein and the tag. This construct was used as a template to create His-tagged $BRAF^{V600E}$, $BRAF^{R509H}$, $BRAF^{R506A}$, $BRAF^{W450A}$, $BRAF^{W450A/R509H}$, $BRAF^{R506A,R509H}$, and $BRAF^{R506A,R509H,W450A}$ mutants (each harboring the 16 stabilizing mutations noted above). These proteins were used in analytical ultracentrifugation sedimentation velocity experiments.

Proteins used for kinase inhibition assays. DNA encoding the BRAF kinase domain residues 442-724 was used as a template and cloned into a Pfastbac dual vector with mouse $p50^{cdc37}$ full length as an expression chaperone for protein expression in baculovirus infected Sf9 insect cells. An N-terminal 6X-His tag was inserted into the plasmid, and this plasmid was used as a template to create mutant $BRAF^{V600E}$. Full length human MEK1 with an N-terminal GST fusion tag and a C-terminal His tag in a pGex-3t vector was provided by Dr. Michael Olson (Beatson Institute for Cancer Research, Glasgow, UK) and was used as the substrate for the *in vitro* kinase assays.

3.4.2 Protein Purification

Proteins used for analytical ultracentrifugation sedimentation velocity, limited proteolysis, and differential scanning calorimetry experiments. His-tagged BRAF proteins were produced as previously described (Grasso et al., 2016). In brief, proteins were expressed in (DE3)RIL bacterial expression cells at 37 ^{o}C and induced with 1mM IPTG overnight at 18 ^{o}C, spun down the next day, and lysed in lysis buffer (50mM potassium phosphate pH 7.0, 250mM NaCl) with 1mM PMSF and DNaseI. The lysate was spun down at 19000 rpm for 20 minutes, and the supernatant was added to 7mL of TALON metal affinity resin (Takara) and left to incubate at 4 ^{o}C for 1 hr. The supernatant was eluted via gravity column, and the resin was washed with 1 L of lysis buffer with 10 mM imidazole. The BRAF proteins were eluted with lysis buffer supplemented with 250 mM Imidazole. Protein was dialyzed into dialysis buffer (50 mM potassium phosphate pH 7.0, 5 mM EDTA pH 7.5, 1mM DTT (Dithiothreitol)) overnight and then applied to a 5 mL SP Sepherose cation exchange column followed by washing in dialysis buffer and elution in 50 mM potassium phosphate pH 7.0, 1 M NaCl, and 1 mM DTT. Peak fractions were run on an SDS-PAGE gel, pooled, concentrated, and applied to a Superdex S200 gel filtration column in a final buffer of 20 mM HEPES pH 7.0, 150 mM NaCl, 5% Glycerol and 10 mM DTT. Protein was concentrated to 5-10 mg/mL, flash frozen in liquid nitrogen, and stored in -80 ^{o}C freezer for future use.

Proteins used for kinase inhibition assays. $BRAF^{WT}$ and $BRAF^{V600E}$ were overproduced as N-terminally His-tagged proteins in insect cells essentially as previously described (Grasso et al., 2016). Briefly, protein constructs were co-expressed with $p50^{cdc37}$, pelleted, suspended in lysis buffer 2 (25 mM Tris pH 8.0, 250 mM NaCl, 5 mM Imidazole and 10%

glycerol) treated with Complete EDTA-free protease inhibitor cocktail tablets (Roche) and DNaseI, lysed, centrifuged at 19,000 rpm for 30 minutes, and added to TALON metal affinity resin and incubated for 1 hour at 4 ºC. The protein on the resin was washed extensively with 1 L of lysis buffer 2 and eluted with 25 mM Tris pH 7.5, 250 mM NaCl, 250 mM imidazole, and 10% Glycerol. The protein was diluted into a low salt buffer containing 25mM Tris pH 8.0, 1 mM EDTA and 1 mM DTT and run on an SP Sepharose cation exchange column, and eluted with a salt gradient from 50 mM NaCl to 1 M NaCl. Peak fractions were run on an SDS-PAGE gel and fractions containing protein were pooled, concentrated, and applied to a Superdex S200 gel filtration column and stored in a final buffer of 25 mM Tris pH 8.0, 300 mM NaCl, 1 mM DTT, and 10% glycerol. Protein was concentrated to ~0.5 mg/mL and flash frozen in liquid nitrogen and stored for later use in a -80 ºC freezer.

GST-MEK1 fusion protein used as a substrate in ELISA assays was prepared essentially as described previously.[19] Briefly, the protein was expressed in (DE3) RIL cells at 37 ºC and induced with 0.5 mM IPTG at 15 ºC overnight. The cells were harvested and resuspended in lysis buffer 3 (20 mM HEPES at pH 7.0, 500 mM NaCl, 10 mM BME, 10 mM imidazole and 5% glycerol) supplemented with 1mM PMSF and DNaseI. The lysate was sonicated and spun down at 19,000 rpm for 30 minutes and the supernatant was added to Ni-NTA resin and incubated for 1 hr at 4 ºC. The resin was washed extensively with lysis buffer 3 with 20 mM Imidazole instead of 10 mM and eluted with lysis buffer 3 supplemented with 250 mM imidazole. Eluted protein was concentrated and loaded onto a Superdex S200 16/60 gel filtration column into a final buffer of 20 mM HEPES pH 7.0,

150 mM NaCl, 10 mM BME and 5% glycerol. The protein eluted off the sizing column in two separate populations, and the second peak was collected, concentrated to ~20 mg/mL, and flash frozen in liquid nitrogen and stored in -80 ºC freezer for future use.

3.4.3. In Vitro Kinase Assay

Compound inhibition of $BRAF^{WT}$ and $BRAF^{V600E}$ were performed using an ELISA assay described previously (Grasso et al., 2016). Briefly, GST-MEK fusion protein was diluted 3:1000 in Tris-buffered saline (25 mM Tris pH 7.5, 140 mM NaCl) treated with 0.05% Tween-20 (TBST), and diluted MEK was added to each well of a glutathione coated 96-well plate (Pierce #15240) and incubated at room temp for 1 hr with shaking. BRAF was diluted from frozen stocks (1:500 dilution for $BRAF^{WT}$ and 1:1000 dilution for $BRAF^{V600E}$) in 50 mM HEPES pH 7.0 and 50 mM NaCl. 2 µL of desired concentration of inhibitor was added to 100 µL of diluted BRAF in a 96 well "V" bottom plate (Corning #2897) and the inhibitor/protein mixture was incubated for 1 hr at room temp. Glutathione plates were washed extensively with TBST and the protein-inhibitor mixture was added to the plate with a 100 µM final concentration of ATP in a buffer containing 50 mM HEPES pH 7.0, 200 mM NaCl, and 20 mM $MgCl_2$. The plate was incubated at 37 ºC for 30 minutes. The reaction was washed from the plate and the plate was again washed with TBST. A 1:8000 dilution of primary antibody (p-MEK1/2 (S217/S221) rabbit antibody (cell signaling)) in TBST treated with 0.5% BSA was added to the plate and incubated for 1 hr with shaking. The plate was then treated with multiple TBST washes and then incubated with a 1:10,000 dilution of secondary antibody (goat anti-rabbit IgG (H+L)-HRP (BioRad)) in TBST treated with 0.5% BSA for 1 hr with shaking. The plate was washed extensively with

TBST and Supersignal ELISA Pico Chemiluminescent Substrate (Pierce #37069) was added. The plate was read on a Promega GloMAX 96 Microplate Luminometer. Each curve was repeated in duplicate or triplicate, normalized using GraphPad Prism by selecting the largest value as the maximum and the lowest value as the minimum, and used to calculate IC_{50} values by using a log (inhibitor) vs response fit on Prism 5.0 (GraphPad). Error bars are indicative of the SEM of each point, and 95% confidence intervals are listed in the figure legends as calculated by GraphPad Prism.

3.4.4. Analytical Ultracentrifugation (AUC)

Sedimentation velocity AUC was performed with a Beckman Optima XL-I at 42,000 rpm. Data were obtained over a period of ~15 hours of centrifugation at 20 ^{o}C by monitoring absorbance. Previously frozen stocks of BRAF and all corresponding mutations (R509H, V600E, R506A, W450A, R506A/R509H. R509H/W450A, and R506A/R509H/W450A) were thawed and diluted to ~10-20 μM depending on the experiment in AUC buffer (25 mM Tris pH 7.5, 150 mM NaCl) and inhibitor was added to the desired final concentration by adding 20 μL of stock concentration of inhibitor in 100% DMSO to 430 μL of protein to give a final DMSO concentration of 4.44%. Samples run without inhibitor had 20 μL of DMSO added to give the same 4.44% DMSO concentration as a control. Data were analyzed using SEDFIT to calculate a continuous c(s) distribution with a frictional coefficient set to 1.20, and data were graphed using GraphPad Prism.

Sedimentation Equilibrium AUC was performed with the same Beckman Optima XL-I at three speeds (9,000 rpm, 12,000 rpm, and 18,000 rpm) at three different concentrations (20

μM, 10 μM, and 5 μM) of $BRAF^{R509H}$ supplemented with a 2:1 molar ratio of inhibitor to protein at each concentration. AUC buffer from sedimentation velocity experiments were used in sedimentation equilibrium experiments. Data were analyzed using heteroanalysis to calculate an ideal fit molecular weight of the species, and log plots of the data were subsequently graphed using GraphPad Prism. Log plots were calculated using the 12,000 rpm data of each set. Ideal monomer and dimer fits were calculated using heteroanalysis.

3.4.5. Limited Proteolysis.

98 μL of 29 μM $BRAF^{WT}$ in LP Buffer (20 mM HEPES pH 7.0, 150 mM NaCl) were added to eppendorf tubes with 1 μL of 0.5 mg/mL trypsin (Sigma-Aldrich, T1426-50MG) and 2 μL of either DMSO or inhibitor dissolved in 100% DMSO to give a final inhibitor concentration of 200 μM. Inhibitors TAK632, TAK-4-TAK, TAK-L-C, and vemurafenib were tested, as well as a control in which no trypsin was added. After 30 min. of protease treatment, 20 μL of the reaction mixture was removed and added to 5 μL of 5X SDS loading buffer, boiled and run on a 13.5% Acrylimide gel using SDS-PAGE, followed by staining using Coomassie blue.

3.4.6. Differential Scanning Calorimetry (DSC)

$BRAF^{WT}$ was diluted to a final concentration of 37 μM in DSC Buffer (20 mM HEPES pH 7.0, 150 mM NaCl). 50 μL of either DMSO or inhibitor dissolved in 100% DMSO was added to 450 μL of $BRAF^{WT}$ and degassed for 3 minutes. The protein/inhibitor or protein/DMSO mixture was then added to a MicroCal VP-Capillary DSC (Malvern) and blanked with 450 μL of DSC Buffer and 50 μL of DMSO. The protein (sample) and buffer

(blank) were both heated from 10 ºC to 90 ºC with a scan rate of 60 ºC/hour and a filtering period of 10 seconds. The difference in heat required to raise the temperature of the sample as compared to the blank is measured as a function of temperature. The data was plotted using Origin 7.

3.4.7. Small Molecule Inhibitors

PLX4032 (Vemurafenib) was purchased from Santa Cruz Biotechnology (cat# sc-364643). Sorafenib was purchased from Santa Cruz Biotechnology (cat# sc-220125). TAK632 was purchased from BioVision Inc. (cat# 2473-5).

3.4.8. General Chemistry Information

Solvents used for extraction and purification were HPLC grade from Fisher. Unless otherwise indicated, all reactions were run under an inert atmosphere of argon. Anhydrous tetrahydrofuran, diethyl ether, and toluene were obtained via passage through an activated alumina column. Merck pre-coated silica gel plates (250 mm, 60 F254) were used for analytical TLC. Spots were visualized using 254 nm ultraviolet light, with either anisaldehyde or potassium permanganate stains as visualizing agents. Chromatographic purifications were performed on Sorbent Technologies silica gel (particle size 32-63 microns). ^{1}H and ^{13}C NMR spectra were recorded at 500 MHz and 125 MHz, or 360 MHz and 90 MHz, respectively, in $CDCl_3$, DMSO-d_6, or CD_3OD on a Bruker AM-500, a DRX-500, or a DMX-360 spectrometer. Chemical shifts are reported relative to internal chloroform (δ 7.26 for ^{1}H, δ 77.0 for ^{13}C), DMSO-d_6 (δ 2.50 for ^{1}H, δ 39.5 for ^{13}C), or CD_3OD (δ 3.31 for ^{1}H, δ 49.0 for ^{13}C). Infrared spectra were recorded on a NaCl plate using a Perkin-Elmer 1600 series Fourier transform spectrometer. High resolution mass

spectra were obtained by Dr. Rakesh Kohli at the University of Pennsylvania Mass Spectrometry Service Center on an Autospec high resolution double-focusing electrospray ionization/chemical ionization spectrometer with either DEC 11/73 or OPUS software data system. All compounds were chromatographically homogeneous materials that were determined to be >95% pure by ^{1}H and ^{13}C NMR, and where necessary, HPLC.

3.4.9. Synthesis of TAK-X-TAK dimers

To diacid **2-6** (Figure 1) (Wittmann, Takayama, Gong, Weitz-Schmidt, & Wong, 1998) (0.225 mmol), TAK aminobenzothiazole **1** (Figure) (Okaniwa et al., 2013) (0.472 mmol), and DIPEA (1.3 mmol) in DMF (0.3 M) was added BEP (0.582 mmol). The reaction was then stirred at 25 °C for 18 h. The reaction was then quenched with brine and extracted with 9:1 ethyl acetate: THF. The combined organic fractions were then washed with brine, dried over Na_2SO_4, filtered and concentrated to afford a crude solid. The crude mixture was purified by silica gel column chromatography (MeOH/DCM) and then purified by preparative thin layer chromatography (MeOH/DCM) to afford TAK-X-TAK dimers as thin films.

TAK-0-TAK

Thin Film; Yield=15%; ^{1}H NMR (500 MHz, Acetone-d_6) δ 9.35 (s, 1H), 8.17 (s, 2H), 7.99 (d, J = 9.0 Hz, 2H), 7.73 (s, 1H), 7.68 (d, J = 7.2 Hz, 2H), 7.63 – 7.52 (m, 3H), 7.31 – 7.24 (m, 2H), 7.14 (d, J = 8.9, 1.6 Hz, 2H), 6.93 (dd, J = 9.1, 3.7 Hz, 2H), 4.70 (s, 3H), 3.99 (s, 3H) ppm; ^{13}C NMR (126 MHz, $CDCl_3$) δ 170.03, 169.74, 157.46, 156.34, 151.64, 151.21, 149.30, 149.28, 144.81, 142.46, 139.03, 137.30, 136.30, 133.87, 129.68, 129.64,

129.43, 129.19, 127.97, 127.87, 127.18, 126.28, 126.25, 126.22, 126.20, 125.68, 123.76, 123.73, 123.52, 117.20, 117.11, 116.94, 115.65, 115.59, 114.71, 114.13, 95.83, 70.02, 42.36 ppm; FT-IR (neat) : 1703, 1663, 1625, 1595, 1545 cm^{-1}; HRMS (ESI) *m / z* calcd for $C_{50}H_{30}F_8N_8O_7S_2$ $(M + Na)^+$ 1093.1449; Found 1093.1472.

TAK-2-TAK

Thin Film; Yield = 6%; ^1H NMR (500 MHz, DMSO-d_6) δ 10.21 (s, 1H), 7.93 (d, *J* = 9.0 Hz, 1H), 7.83 (s, 0H), 7.67 (s, 1H), 7.59 (s, 3H), 7.57 – 7.49 (m, 1H), 7.41 – 7.30 (m, 1H), 7.02 (d, *J* = 9.0 Hz, 1H), 6.94 (d, *J* = 8.9 Hz, 1H), 4.34 (s, 2H), 3.88 (s, 2H), 3.79 – 3.72 (m, 3H), 3.69 – 3.62 (m, 3H) ppm; ^{13}C NMR (126 MHz, DMSO) δ 170.35, 169.34, 157.14, 155.72, 151.26, 151.24, 150.80, 148.87, 144.42, 136.92, 135.88, 133.48, 129.61, 129.29, 129.26, 129.04, 128.79, 128.54, 127.57, 127.46, 126.60, 125.90, 125.87, 125.84, 125.81, 125.30, 123.40, 123.37, 123.34, 123.31, 123.14, 120.97, 116.70, 116.62, 116.52, 115.20, 115.14, 114.28, 113.75, 113.63, 95.31, 70.38, 69.85, 69.32, 41.97 ppm; FT-IR (neat) : 1675, 1596, 1544, 1485, 1460 cm^{-1}; HRMS (ESI) *m / z* calcd for $C_{54}H_{38}F_8N_8O_9S_2$ $(M + Na)^+$ 1181.1973; Found 1181.1975

TAK-3-TAK

Thin Film; Yield = 8%; ^1H NMR (500 MHz, DMSO-d_6) δ 12.44 (s, 1H), 10.18 (s, 1H), 7.95 (dd, *J* = 9.1, 4.1 Hz, 1H), 7.83 (s, 1H), 7.66 (s, 1H), 7.63 – 7.49 (m, 3H), 7.38 – 7.30 (m, 1H), 7.04 (s, 1H), 6.98 – 6.90 (m, 1H), 4.32 (s, 2H), 3.86 (s, 2H), 3.72 – 3.65 (m, 2H), 3.60 (s, 4H) ppm; ^{13}C NMR (126 MHz, DMSO) δ 170.26, 169.38, 157.00, 155.83, 151.25, 150.80, 148.87, 144.43, 136.93, 135.87, 133.52, 129.33, 129.30, 129.26, 129.05, 128.80,

128.55, 127.60, 127.49, 126.75, 126.66, 125.92, 125.83, 125.33, 123.38, 123.16, 116.73, 116.66, 116.57, 115.24, 114.34, 113.80, 113.69, 95.35, 70.52, 69.75, 69.31, 41.98 ppm; FT-IR (neat) : 1690, 1596, 1537, 1458, 1431 cm^{-1}; HRMS (ESI) *m / z* calcd for $C_{56}H_{42}F_8N_8O_{10}S_2$ $(M + H)^+$ 1203.2416; Found 1203.2382.

TAK-4-TAK

Thin Film; Yield = 10%; ^1H NMR (500 MHz, Acetone-d_6) δ 9.34 (s, 1H), 8.12 (dd, *J* = 6.6, 3.1 Hz, 1H), 7.86 (d, *J* = 9.0 Hz, 1H), 7.71 (s, 1H), 7.65 (d, *J* = 7.9 Hz, 1H), 7.60 – 7.48 (m, 2H), 7.23 (dd, *J* = 10.7, 9.0 Hz, 1H), 7.03 (d, *J* = 9.0 Hz, 1H), 6.90 (ddd, *J* = 9.0, 3.9, 3.1 Hz, 1H), 4.32 (s, 2H), 3.96 (s, 2H), 3.87 – 3.80 (m, 4H), 3.79 – 3.70 (m, 4H) ppm; ^{13}C NMR (126 MHz, Acetone-d_6) δ 171.48, 170.01, 158.00, 157.26, 152.84, 152.82, 151.44, 149.52, 145.73, 137.75, 137.44, 134.37, 131.22, 130.97, 130.71, 130.46, 130.09, 129.09, 128.99, 127.38, 127.10, 127.06, 127.03, 127.00, 124.47, 124.45, 124.41, 124.38, 124.28, 117.50, 117.08, 116.90, 115.68, 115.62, 114.88, 114.02, 97.17, 72.52, 71.45, 71.11, 70.96, 70.54, 43.56 ppm; FT-IR (neat) : 1684, 1625, 1592, 1538, 11487 cm^{-1}; HRMS (ESI) *m / z* calcd for $C_{58}H_{46}F_8N_8O_{11}S_2$ $(M + Na)^+$ 1269.2497; Found 1269.2457.

TAK-6-TAK

Thin Film; Yield = 7%;^1H NMR (500 MHz, Chloroform-*d*) δ 10.67 (s, 1H), 8.11 (dd, *J* = 6.6, 3.1 Hz, 1H), 7.78 (d, *J* = 9.0 Hz, 1H), 7.62 – 7.44 (m, 5H), 7.06 (t, *J* = 10.4, 8.9 Hz, 1H), 6.94 (d, *J* = 9.0 Hz, 1H), 6.80 – 6.74 (m, 1H), 4.30 (s, 2H), 3.84 – 3.69 (m, 11H), 3.66 – 3.57 (m, 5H) ppm; ^{13}C NMR (126 MHz, $CDCl_3$) δ 169.48, 168.09, 159.11, 156.87, 156.62, 151.73, 149.96, 148.04, 144.53, 136.96, 134.64, 132.73, 131.33, 131.07, 129.41,

127.14, 127.05, 126.25, 126.09, 126.06, 124.85, 124.42, 124.40, 116.16, 115.71, 115.55, 115.09, 114.03, 112.80, 96.53, 71.56, 70.68, 70.43, 70.39, 70.36, 70.15, 69.90, 43.98 ppm; FT-IR (neat) : 1693, 1595, 1537, 1485, 1456 cm^{-1}; HRMS (ESI) *m / z* calcd for $C_{62}H_{54}F_8N_8O_{13}S_2$ $(M + H)^+$ 1335.3202; Found 1335.3214.

3.4.10. Synthesis of TAK-L

To a solution 2-(2-Methoxyethoxy)acetic acid **12** (Figure 5a; 57 μ L, 0.504 mmol), TAK benzotriazole **1** (Okaniwa et al., 2013) (Figure 5a; 0.232 mg, 0.458 mmol), and DIPEA (0.498 ml, 2.8 mmol) in DMF (1.5 mL) was added BEP (0.169 g, 0.620 mmol). The reaction was then stirred at 25 °C for 24 h. The reaction was then quenched with brine and extracted with 9:1 ethyl acetate: THF. The combined organic fractions were then washed with brine, dried over Na_2SO_4, filtered and concentrated to afford a crude foam. The crude product was purified by silica gel column chromatography (5% MeOH/DCM) and then purified by preparative thin layer chromatography (4% MeOH/DCM) to afford TAK-L **13** (Figure 5a) as a white foam.

Yield = 0.128 g (44% yield); ^{1}H NMR (500 MHz, Chloroform-*d*) δ 10.91 (s, 1H), 8.15 (dd, *J* = 6.4, 3.1 Hz, 1H), 7.84 (d, *J* = 9.0 Hz, 1H), 7.62 – 7.48 (m, 4H), 7.48 – 7.41 (m, 1H), 7.08 (t, *J* = 10.5, 8.9 Hz, 1H), 6.97 (d, *J* = 9.0 Hz, 1H), 6.79 (ddd, *J* = 8.9, 4.1, 2.9 Hz, 1H), 4.30 (s, 2H), 3.87 – 3.77 (m, 4H), 3.69 – 3.62 (m, 2H), 3.57 (s, 3H) ppm; ^{13}C NMR (126 MHz, $CDCl_3$) δ 170.31, 168.88, 168.81, 156.95, 156.41, 151.84, 150.45, 148.53, 144.90, 136.73, 136.50, 133.28, 130.24, 129.99, 129.73, 129.48, 129.04, 128.15, 128.05, 127.96, 127.56, 126.52, 126.00, 125.96, 123.40, 123.36, 116.62, 116.02, 115.85, 114.59, 114.53, 113.83, 113.06, 96.25, 71.46, 71.18, 69.58, 57.95, 42.56 ppm; FT-IR (neat) : 1686,

1533, 1486, 1458, 1429 cm^{-1}; HRMS (ESI) *m / z* calcd for $C_{28}H_{22}N_4O_5F_4S$ $(M + Na)^+$ 625.1145; Found 625.144.

3.4.11. Synthesis of TAK-L-C 14: 2-(2-(2-(2-oxo-2-(thiazol-2-ylamino)ethoxy)ethoxy)ethoxy)acetic acid.

To 3,6,9-Trioxaundecandioic acid **3** (2.5 g, 11.25 mmol) in DCM (50 mL) was added DCC (2.32 g, 11.25 mmol). The reaction was then stirred at 25 °C for 18 h. The resulting suspension was then filtered and rinsed with chilled DCM. The filtrate was concentrated to afford the crude anhydride, which was taken directly on to the next step. The anhydride was dissolved with dry THF and was then treated with 2-aminothiazole (1.12 g, 11.25 mmol). The reaction was stirred for 3 hrs at 25°C and volatiles then removed by evaporation under reduced pressure. The resulting solid was then suspended in Et_2O and filtered. The solid was then rinsed with chilled Et_2O. The crude solid was then purified by silica gel column chromatography (2-10% MeOH/DCM) to give 2-(2-(2-(2-oxo-2-(thiazol-2-ylamino)ethoxy)ethoxy)ethoxy)acetic acid.

Pale yellow solid; Yield = 1.57 g (46% yield); ^{1}H NMR (500 MHz, Methanol-d_4) δ 7.46 (d, J = 3.7 Hz, 1H), 7.14 (d, J = 3.7 Hz, 1H), 4.29 (s, 2H), 4.11 (d, J = 3.4 Hz, 2H), 3.81 – 3.71 (m, 8H).; ^{13}C NMR (126 MHz, DMSO) δ 171.68, 168.50, 157.37, 137.65, 113.68, 70.49, 69.81, 69.75, 69.60, 69.24, 67.59, 40.02, 39.86, 39.69, 39.52, 39.35, 39.19, 39.02.; IR (neat) : 3200, 1719, 1689, 1495, 1063 cm^{-1}; HRMS (ESI) *m / z* calcd for $C_{48}H_{41}N_6O_8F_4S_2$ $(M + H)^+$ 305.0822; Found 305.0807.

3.4.12 Synthesis of TAK-L-C.

To a solution of 2-(2-(2-(2-oxo-2-(thiazol-2-ylamino)ethoxy)ethoxy)ethoxy)acetic acid (0.159 mg, 0.524 mmol), TAK aminobenzothiazole[2] (0.085 mg, 0.174 mmol) and TEA (0.243 ml, 1.74 mmol) in DMF (0.587 mL) was added T3P (0.333 mL, 0.524 mmol) in DMF (1:1; v/v) dropwise. The reaction was then stirred at 25 °C for 18 h. The reaction was then quenched with brine and extracted with 9:1 ethyl acetate: THF. The combined organic fractions were then washed with brine, dried over Na_2SO_4, filtered and concentrated to afford a crude solid. The crude product was then purified by preparative thin layer chromatography (3% MeOH/chloroform) to afford TAK-control-2 as a thin film.

Thin Film; Yield = 0.135g (55% yield); ^{1}H NMR (500 MHz, Chloroform-*d*) δ 10.55 (s, 1H), 10.35 (s, 1H), 8.11 (dd, *J* = 6.5, 3.1 Hz, 1H), 7.72 (d, *J* = 9.0 Hz, 1H), 7.62 (d, *J* = 3.4 Hz, 1H), 7.60 – 7.45 (m, 4H), 7.37 (d, *J* = 3.7 Hz, 1H), 7.06 (t, *J* = 9.7 Hz, 1H), 6.95 – 6.86 (m, 2H), 6.76 (dt, *J* = 8.9, 3.5 Hz, 1H), 4.31 (s, 2H), 4.24 (s, 2H), 4.06 – 3.99 (m, 4H), 3.85 (dt, *J* = 4.2, 2.3 Hz, 4H), 3.80 (s, 2H) ppm; ^{13}C NMR (126 MHz, $CDCl_3$) δ 169.38, 168.05, 157.07, 156.82, 156.63, 151.76, 149.96, 148.04, 144.29, 137.57, 137.38, 136.91, 136.46, 134.69, 132.74, 131.31, 131.05, 130.80, 129.39, 127.16, 127.07, 126.11, 126.09, 126.06, 126.03, 124.87, 124.41, 124.38, 122.71, 116.19, 115.68, 115.51, 115.09, 115.02, 114.03, 113.76, 112.88, 96.47, 71.41, 71.33, 70.42, 69.77, 69.74, 43.97 ppm; FT-IR (neat) : 1692, 1595, 1533, 1484, 1455 cm^{-1}; HRMS (ESI) *m / z* calcd for $C_{34}H_{28}N_6O_7F_4S_2$ $(M + H)^+$ 773.1475; Found 773.1464.

Chapter 4- A High-Throughput Approach to Identifying Novel Small Molecule Inhibitors that Target BRAF/MEK Heterodimerization

This research was performed in collaboration with Kanupriya Whig, and Adam Olia of the University of Pennsylvania. Kanupriya Whig of the UPenn High Throughput Screening facility assisted the high-throughput screening. Adam Olia purified NF-κB.

4.1 Introduction

Finding BRAF inhibitors that can help bypass inhibitor resistance is crucial in the field of drug discovery due to the strong correlation of BRAF mutation in melanoma, as well as a variety of other cancers (Davies et al., 2002; Wellbrock et al., 2004). Exploring novel methods to inhibit the MAPK pathway to circumvent this resistance can offer insight into the underlying mechanisms behind transactivation, as well as lead to unique approaches in the field. While many kinase inhibitors exist that target the MAPK signaling pathway, most are Type I and II inhibitors, i.e. ATP-competitive inhibitors (Müller et al., 2015). There are some Type III kinase inhibitors that target an allosteric pocket somewhere on the enzyme, such as MEK inhibitor Trametinib, but Type I and II inhibitors are more common (Müller et al., 2015; Salama & Kim, 2013). Interestingly, MEK mutations have been documented in inhibitor resistant melanoma cell lines (Villanueva et al., 2013), and combination therapies of MEK and BRAF inhibitors have shown promise in the clinic (Flaherty et al., 2012; Greger et al., 2012; Johnson et al., 2014), although inhibitor resistance still ensues.

Type IV kinase inhibitors that bind the surface of a protein to block interactions with another protein or molecule have emerged as possible therapeutic targets in the MAPK signaling pathway. The small molecule Rigosertib has been discovered to bind to Ras Binding Domains (RBDs) of the RAF kinases, disrupting RAS-RAF interactions and, in turn, inhibiting the activation of ERK (Athuluri-Divakar et al., 2016). Another study has developed bivalent ERK inhibitors that utilize an ATP-competitive ERK inhibitor chemically linked to a surface binding inhibitor that blocks the "DRS" site on ERK, which is known to recognize and bind numerous ERK partners (Lechtenberg et al., 2017). This

emerging technique is also gaining more traction in other kinase systems, and the potential for more Type IV inhibitors within the MAPK signaling pathway could introduce a potent and selective mechanism for bypassing BRAF inhibitor resistance.

In 2014, the crystal structure of the BRAF/MEK complex was determined, and interestingly, the complex was found to have a dissociation constant (K_D) of ~43 nM, indicating a very strong interaction (Haling et al., 2014). We hypothesized that targeting BRAF-MEK dimerization would represent a potentially powerful strategy for MAPK pathway inhibition. Such molecules would also be useful probes for studying the MAPK signaling pathway and inhibitor resistance. Here, we report the development and optimization of a high throughput screen of more than 44,000 small molecules to discover novel inhibitors that disrupt the protein-protein interaction between BRAF and MEK. We identified 15 small molecules which inhibit BRAF-MEK dimerization and kinase activity in the low μM IC_{50} range.

4.2 Results

4.2.1 Mutations in the solubilized E. Coli construct of BRAF allows for restoration of MEK complex formation and kinase activity in vitro.

The crystal structure of the MEK/RAF complex demonstrates that BRAF forms its canonical dimer with itself, and each BRAF molecule binds MEK, forming a heterotetramer (**Figure 36a**). The RAF and MEK kinases also sit in a face to face conformation, with their active sites and inhibitor pockets facing one another (Haling et al., 2014). The tight interaction between the two kinases makes it a good target for small molecule screening, as relatively low concentrations would be able to produce a signal

indicating dimerization. Their face-to-face conformation also makes this a good target, as the chemical linking of vemurafenib to a small molecule inhibitor that binds to either the surface of BRAF or MEK would be feasible to add selectivity to this class of inhibitors. Before developing and optimizing a screen, we aimed to recapitulate complex formation using the *E. Coli* construct of the kinase domain of BRAF, as yield, purity, and accessibility make *E. Coli* purification much more applicable for high throughput screening quantities rather than SF9 protein expression, which was used in the crystal structure (Haling et al., 2014; Tsai et al., 2008a). The *E. Coli* construct of the BRAF kinase domain contains 16 point mutations on the surface of BRAF to allow for expression and solubility in *E. Coli*. Interestingly, this construct is not active, despite no mutations to key catalytic residues, and is still able to bind ATP (and inhibitors) (Tsai et al., 2008). None of the point mutations appear to be key contact residues listed in the literature. However, an alignment of the MEK/RAF complex and the *E. Coli* construct shows that one of the mutations, F667E, interrupts a key hydrophobic interaction between the BRA and MEK proteins that could lead to a charge-charge repulsion with D315 of MEK (**Figure 36b**). Indeed, leaving F667E in the *E. Coli* construct ablates complex formation between BRAF and MEK, whereas an E667F mutation in this construct allows BRAF-MEK complex formation to occur (**Figure 37a and b**). This key residue also restored activity in the *E. Coli* construct, indicating that tight complex formation is necessary for BRAF's activity to phosphorylate MEK *in vitro* (**Figure 37c**).

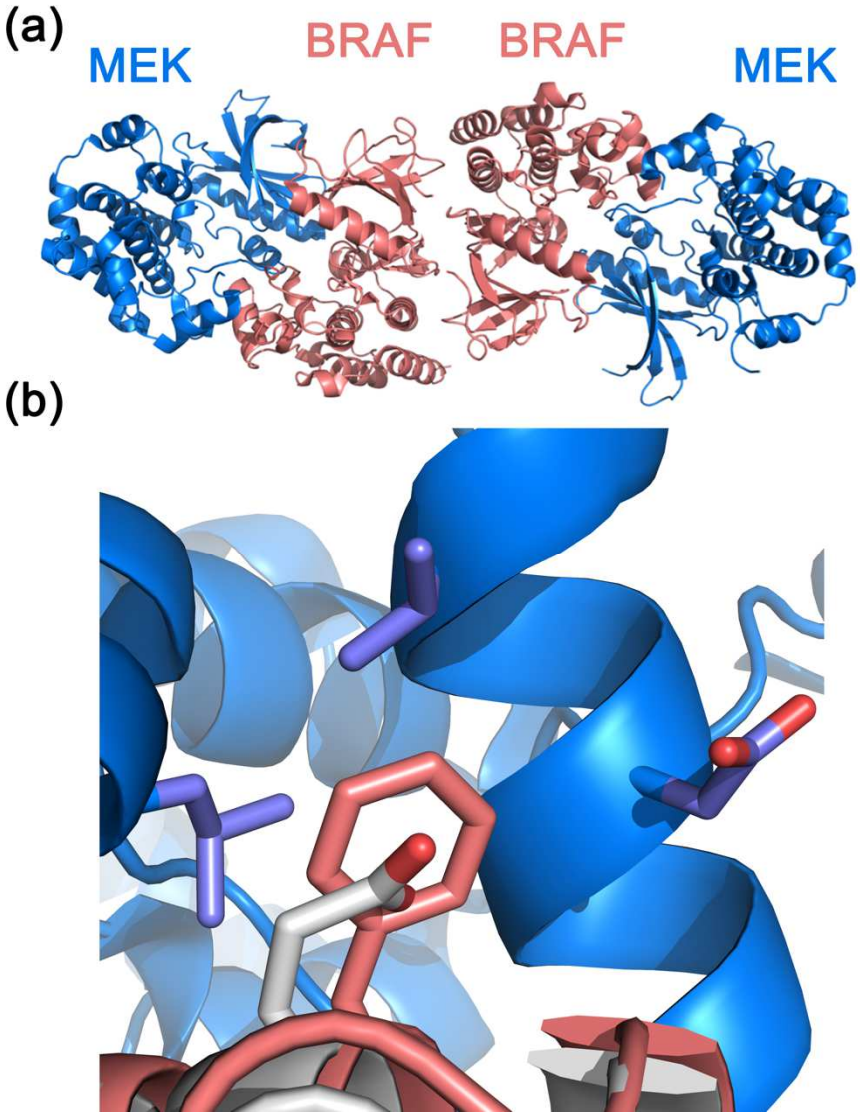

Figure 36 BRAF and MEK complexation in vitro.

(a) Crystal structure of BRAF (salmon) bound to MEK (blue), forming a heterotetrameric complex. (b) Overlay of the complex with the wildtype kinase domain of BRAF (salmon) and the e. coli expressed construct of BRAF harboring 16 point mutations (grey) shows F667E can disrupt a key hydrophobic patch that stabilizes the complex.

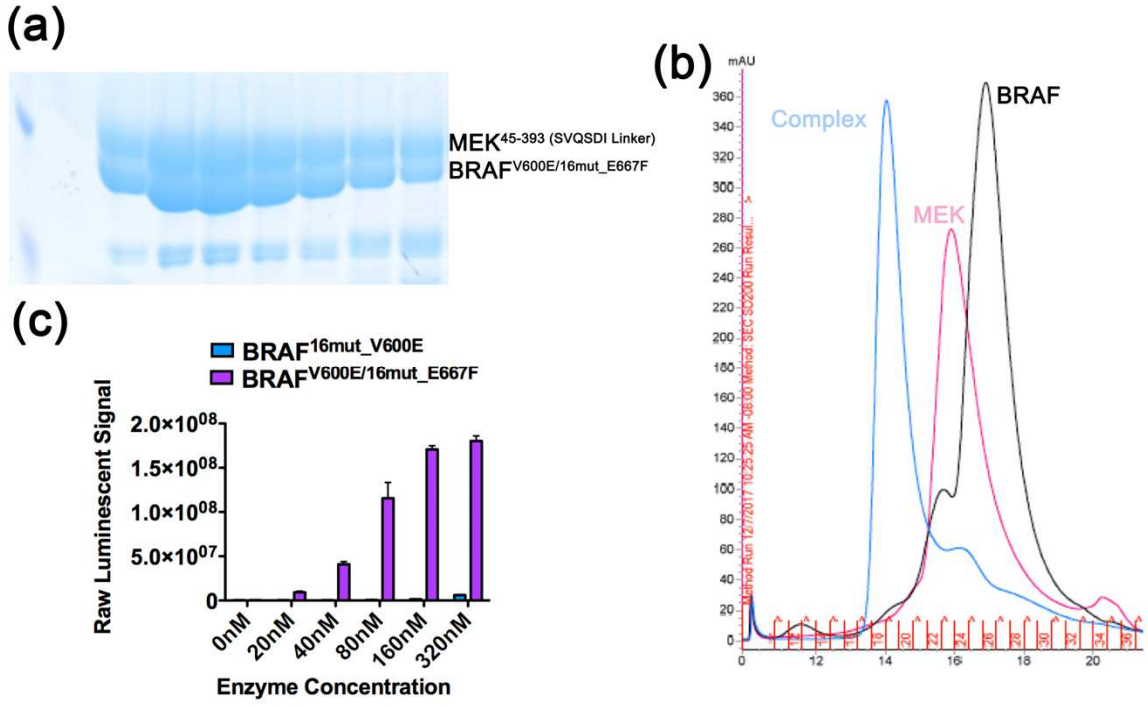

Figure 37 E667F mutation restores complexation and activity.

(a) SDS-PAGE gel of BRAF$^{V600E/16mut_E667F}$ complexed with MEK$^{45-393}$ (Δ264-307,replaced with SVQSDI linker) (b) Overlay of BRAF$^{V600E/16mut_E667F}$ alone (black), MEK$^{45-393}$ (Δ264-307,replaced with SVQSDI linker) alone (pink), and the complex (blue) on size exclusion chromatography, showing the two proteins co-elute when mixed together. (c) While BRAF^{V600E_16mut} has little kinase activity *in vitro*, mutating back to F667 restores kinase activity.

4.2.2. Development and optimization of a Time-Resolved Fluorescence Resonance Energy Transfer (TR-FRET) assay to identify small molecules disrupting a BRAF/MEK complex.

The High Throughput Screen (HTS) to identify novel small molecules disrupting the interaction between BRAF and MEK was designed as a Time-Resolved Fluorescence Resonance Energy Transfer (TR-FRET) assay. In this assay, both BRAF and MEK are expressed and purified with different affinity tags, in this case a 6X-Histidine tag for MEK and a FLAG-tag for BRAF (Hopp & Prickett, 1988). The MEK construct used was an N-terminally truncated version, encoding residues 63-393 (Ohren et al., 2004) and BRAF was the E. Coli mutated Kinase domain (residues 448-723) with mutation E667 mutated back to phenylalanine (E667F) (Tsai et al., 2008a). The assay was designed using Perkin Elmer's LANCE® TR-FRET assay (Ma, Deacon, & Horiuchi, 2008), in which a LANCE® Europium Chelate donor conjugated to an antibody or substrate is paired with an acceptor fluorophore such as a ULight™ Dye, also conjugated to an antibody or substrate, and when in close proximity, the donor and acceptor can generate a fluorescent signal. In this assay, we used Anti-His conjugated Europium (Eu) chelate (Cat # AD0110) to bind the His tagged MEK kinase, and ULight™ Dye conjugated with an Anti-FLAG antibody (Cat # TRF0059M) (**Figure 38a**). The assay allows for a fluorescent transfer when excited with 320nm light, and elicits a 665nm emission when the Eu chelate is within 10nm of the acceptor. When screening for small molecules, a loss in signal at 665nm indicates an ablation of interaction between MEK and BRAF proteins. While the readout of the fluorescence transfer occurs at 665nm, we use the emission at 620nm (fluorescence of Eu fluorophore alone) as a loading control to ensure the signal is due to the FRET signal and not an issue with Eu concentration, controlling for possible loading errors. To further elucidate if any hits were false positives due to non-specific interactions between the antibodies and the proteins, or signal quenching, a counter-screen was developed in which

$BRAF^{E667F}$ with a FLAG-tag and a 6XHis-tag only was used (**Figure 38b**), as any compounds that hit in this screen as well as the primary screen would likely be disrupting the assay components, rather than the RAF-MEK interaction.

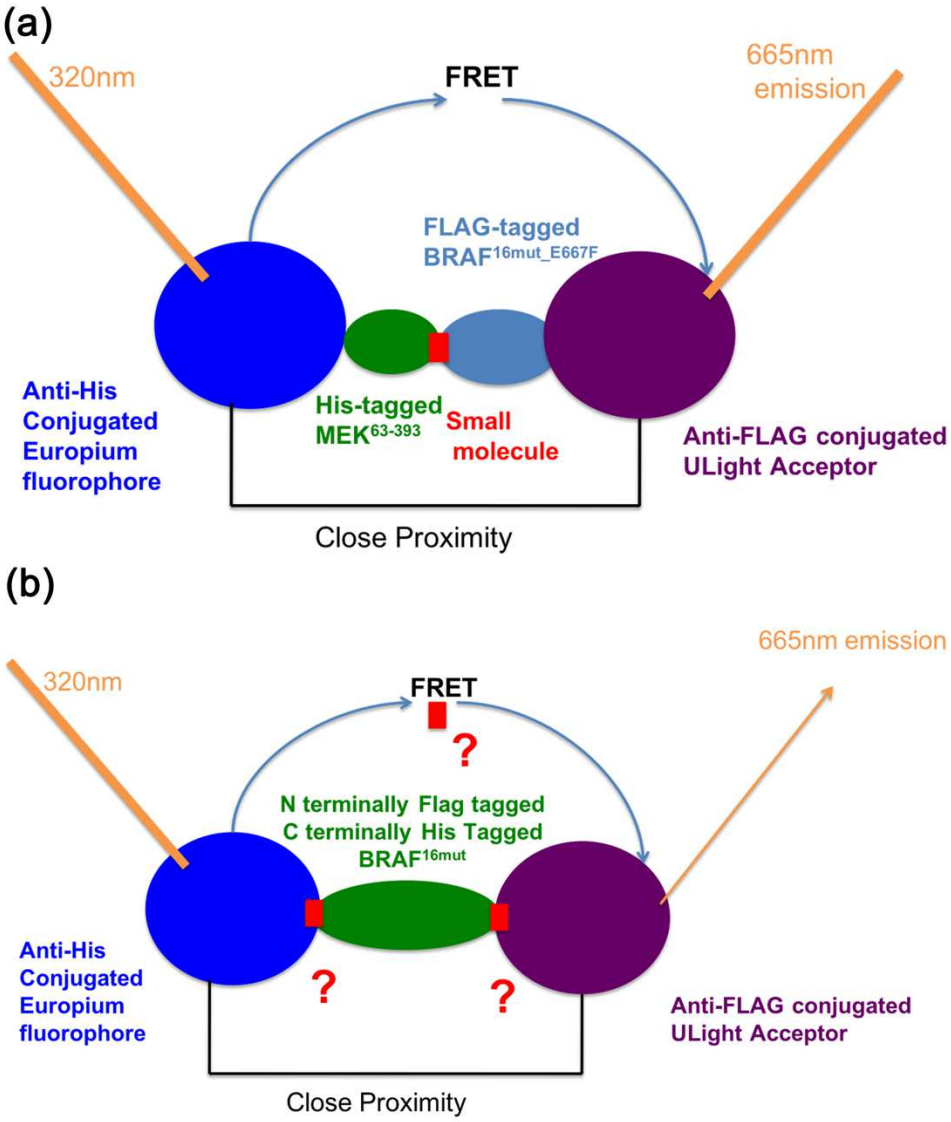

Figure 38 TR-FRET assay diagrams.

(a) primary assay screening for small molecules by disrupting FRET signal between MEK and BRAF bound to acceptor and donor conjugated antibodies (b) Counter-screen with dual-tagged BRAF to determine false positives.

To optimize screening conditions, we initially did a titration of both proteins to find optimal protein concentrations resulting in the highest signal. The assay is dependent on the "hooking effect," where saturating the acceptor and donor fluorophores past their binding capacities results in a decrease, or "hooking" of the signal, as protein unbound to fluorophore can begin to compete off bound protein. Our initial "hooking" experiment varied each protein from 30nM to 240nM (**Figure 39a**), and concentrations past 60nM of either protein decreased the signal appreciably, leading us to hypothesize the binding capacity is at or close to 60nM. We then chose to screen at 50nM and moved forward with screen optimization.

As no positive control small molecule inhibitors exist that completely ablate BRAF/MEK dimerization, we chose to use untagged $BRAF^{16mut\_E667F}$ to compete off the signal. As a negative control to show selectivity, we used untagged $BRAF^{16mut\_E667}$ to ensure signal (and loss of signal) is solely from BRAF/MEK dimerization. We performed a 50/50 plate experiment in which we added both proteins mixed with donor and acceptor fluorophore to a 384-well plate, and then added $BRAF^{16mut\_E667F}$ to one half of the plate and $BRAF^{16mut\_E667}$ to the other half to a final concentration of 2 μM for both in order to test our signal window (**Figure 39b**). The average signal of the negative control ($BRAF^{16mut}$) is 565.7, while our positive control ($BRAF^{16mut\_E667F}$) is 263.7. Despite the signal to noise ratio being just over 2, the screening window was ideal in regard to the Z factor (Z'). Z' is a statistical tool to measure effect size and can be used to assess how useful the assay will be in determining hits from the data. By using both the standard deviations and means of both the positive and negative controls, Z' can assess if the difference between the positive

and negative controls is statistically significant (J. Zhang, Chung, & Oldenburg, 1999). A Z' larger than 0.5 is considered an excellent assay for high throughput screening, and the 50/50 plate experiment gave us a Z' of 0.671 (n=192), indicating an ideal range for screening. We next established a window for the counter-screen. For a positive control, we used 6X-His tagged protein NF-κB-p65 subunit as this protein does not interact with BRAF and will be able to compete off the signal by binding the 6X-His Eu fluorophore. At a concentration of 30 μM, this protein was able to decrease the signal from 936.2 to 277, giving us a large window and a Z' of 0.841 (n=24) (**Figure 39c**).

Before moving to a larger screen, we performed a pilot screen using the Natural Product Collection from MicroSource, which contains 800 purified natural product compounds dissolved in DMSO. We screened at 25 μM final concentration of compounds. The screen consisted of three 384-well plates, with rows 1 and 23 representing a negative control (2 μM $BRAF^{16mut}$) and rows 2 and 24 representing a positive control (2 μM $BRAF^{E667F}$). The third plate was set up the same way, but half of the plate contained DMSO only, yielding 1152 wells but only 800 compounds screened (**Figure 39d**). We performed the pilot screen in full against both the primary screen and the counter-screen to rule out any false positives. Due to the counter-screen being able to rule out many false hits, our hit rate was 0.75%. We classified a "hit" as a compound that was able to have a normalized percent inhibition (NPI) above 25% in the primary screen but did not surpass 5% NPI in the counter-screen. **Table 2** lists the hits and their NPI values for both screens. We next verified these hits through reproducing the assay and validation with secondary assays.

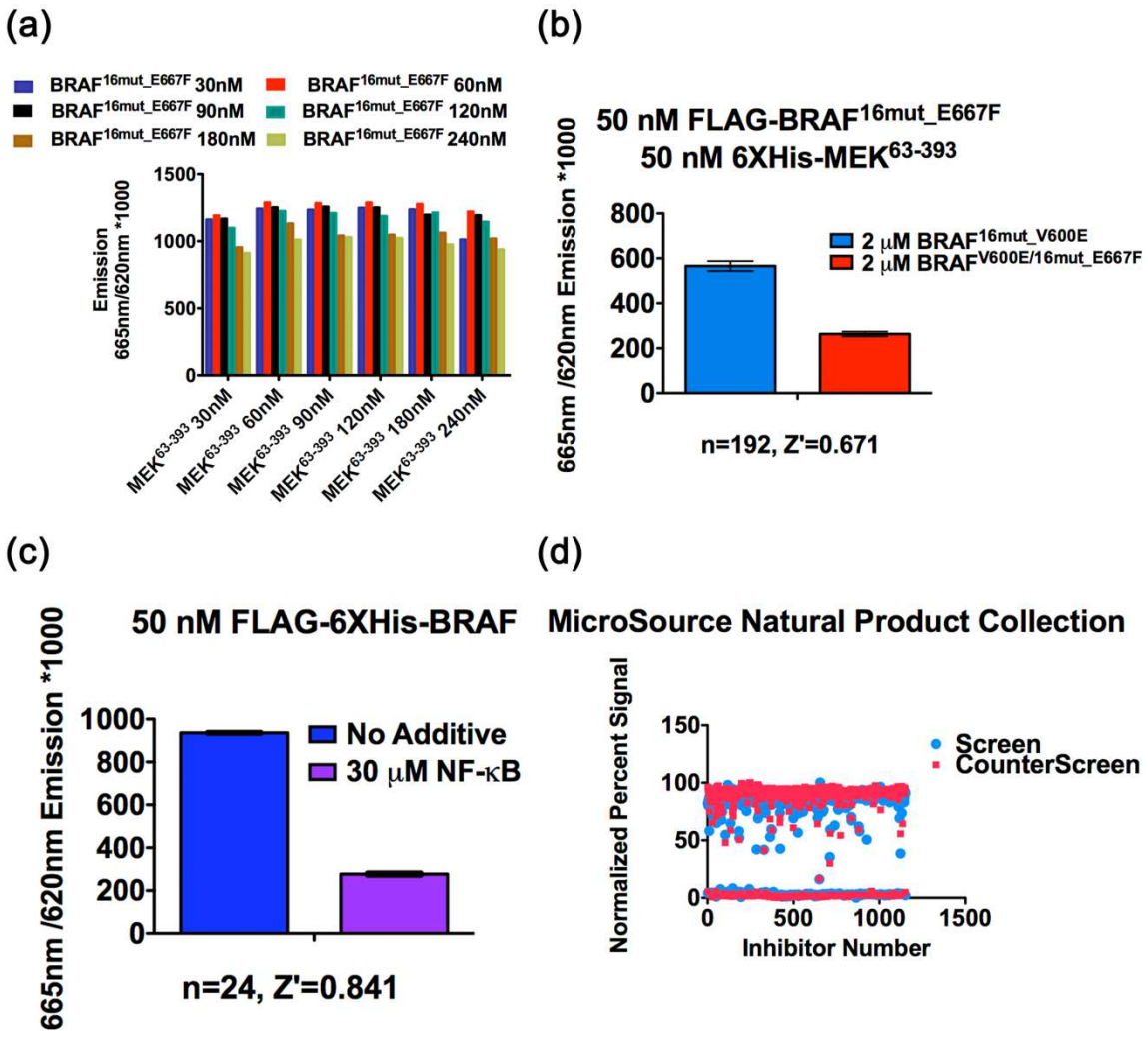

Figure 39 Optimization of high-throughput screen.

(a) Hooking Effect assay titrating different amounts of FLAG-BRAF^{16mut_E667F} and 6XHis-MEK$^{63-393}$ to determine ideal screening concentration. (b) 50/50 plate experiment demonstrating that signal can be selectively competed off with untagged BRAF$^{V600E/16mut_E667F}$ but not untagged BRAF^{V600E} and that the screening window is ideal for a high throughput format. (c) Test demonstrating counter-screen of FLAG-6XHis-BRAF^{16mut} can be competed off with 6XHis-NF-κB and also gives a good screening window. (d) Overlay of Natural Product (MicroSource) Pilot Screen for both primary and counter-screen.

Natural Product Pilot Screen	Primary screen	Counter screen
Compound Name	**NPI (%)**	**NPI (%)**
Plumbagin	56.6	3.71
Eseroline fumarate	45.9	4.78
4-methoxy-4-hydroxy-dalbergione	38.3	2.09
Erythromycin	38.2	4.37
4,4-dimethoxydalbergione	37.6	1.77
Thymoquinone	31.1	-0.540
Menadione	26.9	3.80

Table 2-Natural Product pilot screen results

A list of the small molecule compounds that hit against the primary screen with a normalized percent inhibition (NPI) at 25% or above and did not hit in the counter screen (NPI at 5% or below).

4.2.3 Plumbagin and thymoquinone can selectively disrupt a BRAF/MEK complex

Of the 7 hits from the pilot screen, four (plumbagin, eseroline fumarate, erythromycin, and thymoquinone) were commercially available. We repeated the TR-FRET assay, testing all four inhibitors purchased commercially against both the primary and counter screens in quadruplicate to test reproducibility (**Figure 40a**). Both plumbagin and thymoquinone were able to effectively inhibit at 25 μM (58.13% and 62.53% inhibition, respectively) and at 50 μM (69.27% and 63.81% inhibition, respectively), indicating reproducible inhibition. Erythromycin and eseroline fumarate inhibited dimerization marginally in comparison at 50 μM (15.07% in the primary screen and 8.65% in the counter screen for erythromycin and 22.03% in the primary screen and 11.08% in

the counter screen for eseroline fumarate), indicating these hits are either false positives or not as potent.

To further confirm these hits, we tested all four inhibitors in our ELISA-based kinase assay, as we have elucidated that BRAF dimerization with MEK is necessary for BRAF phosphorylation of MEK (**Figure 40b**). In corroboration with our TR-FRET assay, both plumbagin and thymoquine inhibited BRAF activity in the low μM range (1.94 μM and 2.52 μM, respectively). While eseroline fumarate did decrease the overall kinase activity of BRAF, it was not able to fully decrease activity even at the highest concentration of inhibitor (150 μM). Erythromycin did not decrease activity at all, indicating that this inhibitor was a false positive. Interestingly, plumbagin and thymoquinone have similar structures (**Figure 40c**), with thymoquinone being a 1,4-benzoquinone and plumbagin being a 1,4-napthoquinone.

To further elucidate how these compounds can disrupt the RAF/MEK complex, we performed thermal stability assays (Differential Scanning Fluorimetry or DSF) in which we heat the protein in the presence of fluorescent dye spyro orange, which binds hydrophobic residues and gives off a fluorescent signal as the protein unfolds (R. Zhang & Monsma, 2010). We hypothesized that compound binding would increase the thermal stability of the protein to which it binds. We performed these experiments with both $BRAF^{V600E/16mut\_E667F}$ and MEK^{63-393} in the absence and presence of plumbagin at different concentrations to determine if it can stabilize either protein (**Figure 41a-41b**). Interestingly, the melting temperature of BRAF shifts from ~33 ºC to ~44 ºC in the presence of 100-300 μM of plumbagin. MEK, meanwhile, stays at ~43 ºC despite the addition of 100-300 μM plumbagin, indicating that plumbagin is interacting with BRAF.

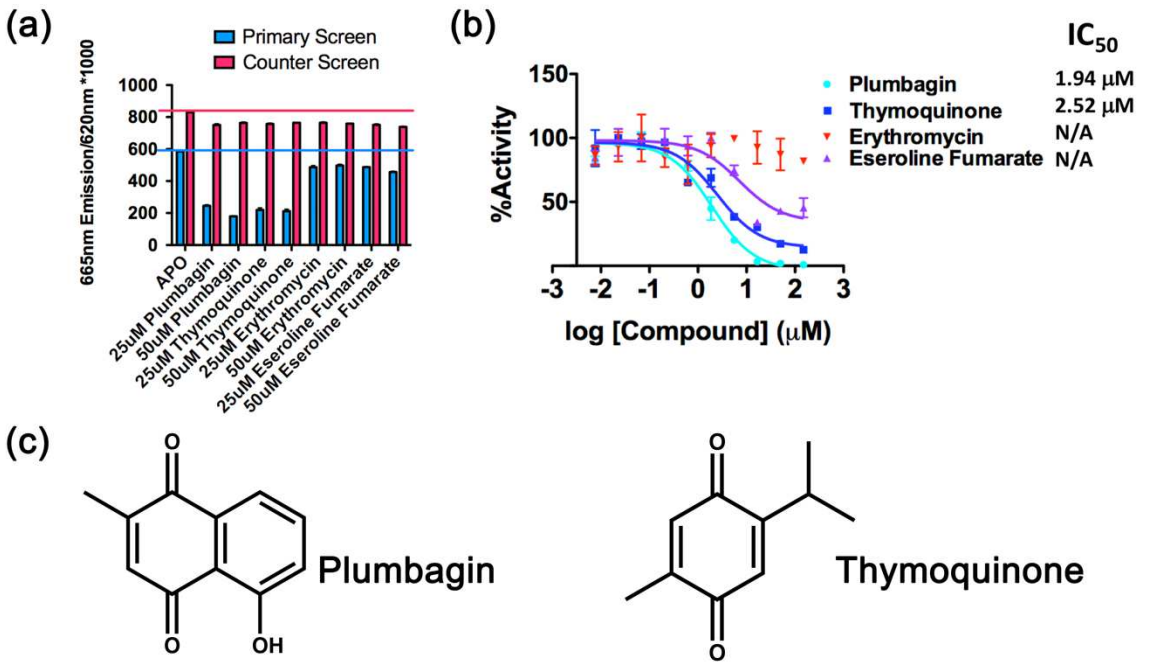

Figure 40 Confirmation of hits.

(a) TR-FRET experiments testing 4 hit compounds purchased commercially at 25 μM and 50 μM concentrations. (b) ELISA-based kinase assay testing 4 hit compounds against BRAF's ability to phosphorylate MEK. The experiments were performed in duplicate with +/- SEM shown. 95% confidence intervals are: Plumbagin (1.26 μM to 2.98 μM), and Thymoquinone (1.34 μM to 4.74 μM). (c) Chemical structures of plumbagin (left) and thymoquinone (right), indicating both have similar chemical structures.

To further validate the DSF results, we performed Differential Scanning Calorimetry (DSC) experiments (**Figure 41c**). While $BRAF^{16mut}$ without any inhibitor added has a melting temperature of 38.06 ^{o}C, adding 50-75 μM of plumbagin results in the addition of a second peak at ~49 ^{o}C, indicating plumbagin is able to bind and stabilize

BRAF. 100 μM of plumbagin is able to shift the majority of BRAF to the second, 49 ºC peak, but addition of higher concentrations of plumbagin (300-400 μM) distorts the peak with negative C_p values, indicating aggregation of the sample. While the addition of thymoquinone to $BRAF^{16mut}$ shifted the melting temperature from ~38 ºC to ~42 ºC (**Figure 41d**), the amplitude of the peak was severely diminished with the addition of small molecule, indicating that the molecule is crashing the protein out of solution. Because of the tendencies to aggregate protein, we did not pursue these inhibitors further, although plumbagin may warrant further investigation.

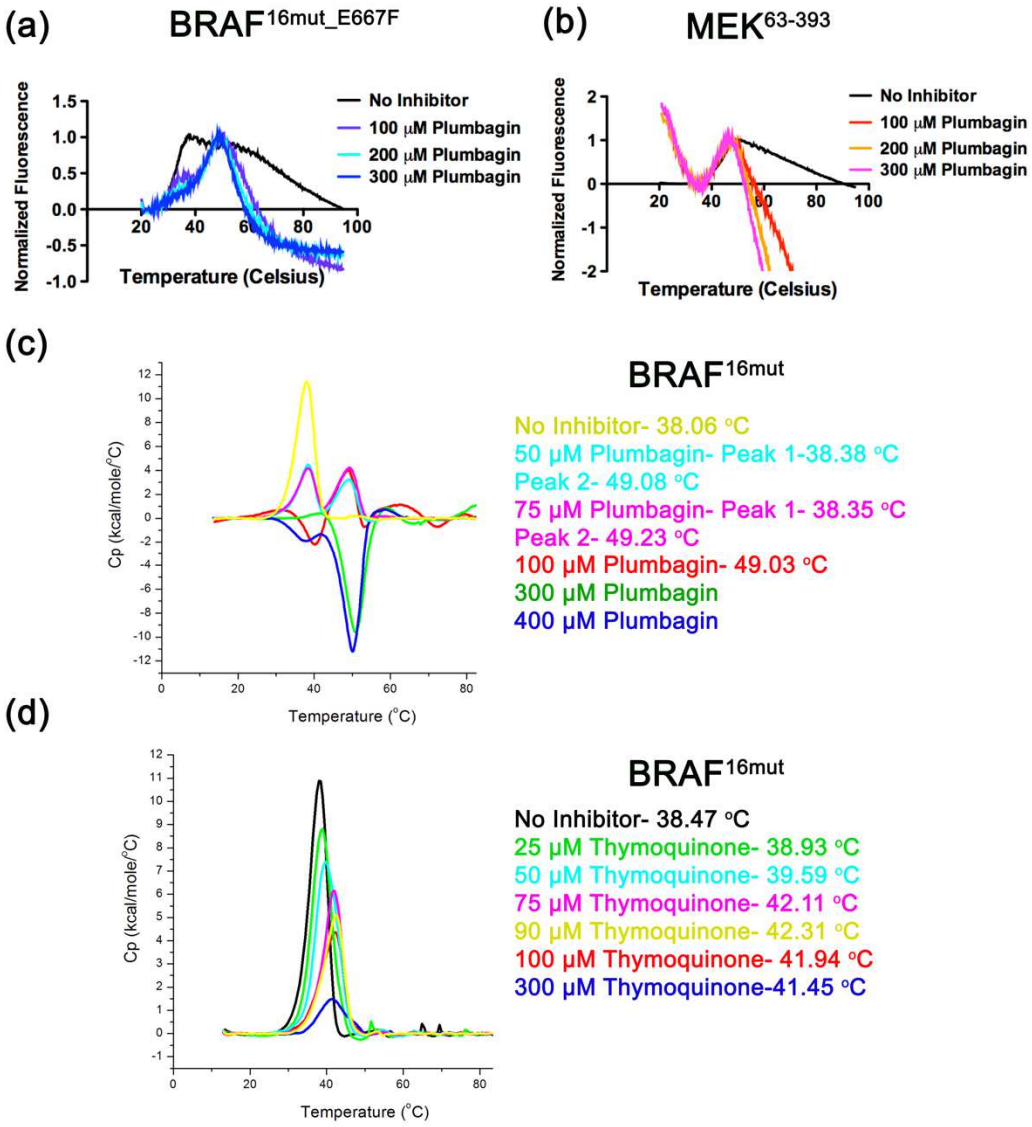

Figure 41 Confirmation of hits using DSF and DSC.

(a) DSF assay of $BRAF^{V600E/16mut\_E667F}$ in the presence and absence of plumbagin at concentrations ranging from 100-300 µM. (b) DSF assay of MEK^{63-393} in the presence and absence of plumbagin at concentrations ranging from 100-300 µM. (c) DSC assay of $BRAF^{WT}$ in the presence and absence of plumbagin at concentrations ranging from 50-400 µM. (d) DSC assay of $BRAF^{16mut}$ in the presence and absence of thymoquinone at concentrations ranging from 50-400 µM.

4.2.4 ChemDiv and ChemBridge 136 plate screen set up and analysis

With the success of the pilot screen, we decided to move forward with two larger screens: 12,000 compounds from ChemDiv's SMART library, and 32,000 compounds from ChemBridge, 20,000 from their CORE set and 12,000 from their ExpressPick set. In order to ensure similar results throughout the entire screen, we expressed and purified enough FLAG-BRAF^{16mut_E667F} and 6XHis-MEK$^{63-393}$ to be used for all 136 plates. Due to the large nature of the screen, we decided to cut down on donor and acceptor fluorophore concentrations (from 20 nM donor and 5 nM acceptor to 10 nM donor and 2.5 nM acceptor) for cost efficiency. **Figure 42** illustrates that despite the concentration being halved, the signal was still robust, and the signal window and Z' was still ideal for high throughput screening techniques. We altered the positive control from untagged BRAF$^{V600E/16mut_E667F}$ to 100 μM plumbagin, as the small molecule was easier to obtain in large quantities than recombinant protein, and we showed that it is a selective inhibitor in the TR-FRET assay environment.

We performed both the ChemBridge and ChemDiv library screens within the span of two weeks, performing 20 plates a day within that time span. **Figures 43a and 43b** show the results of both libraries. Using an NPI of 25% as our cutoff, the two screens gave a total of 148 hits. ChemDiv gave a total of 70 hits, and a hit rate of 0.625%. ChemBridge gave a total of 78 hits and a hit rate of 0.241%. As noted in the results, a number of small molecules also "activated" dimerization, indicated by a stronger fluorescent signal and, in turn, a negative NPI. However, this could have been due to interference with the FRET signal. We sorted the 148 hits into "chemotypes" and selected one or two molecules from

each group with the best NPI out of the group, giving us a total of 49 compounds, 22 from ChemDiv and 27 from ChemBridge for futher testing.

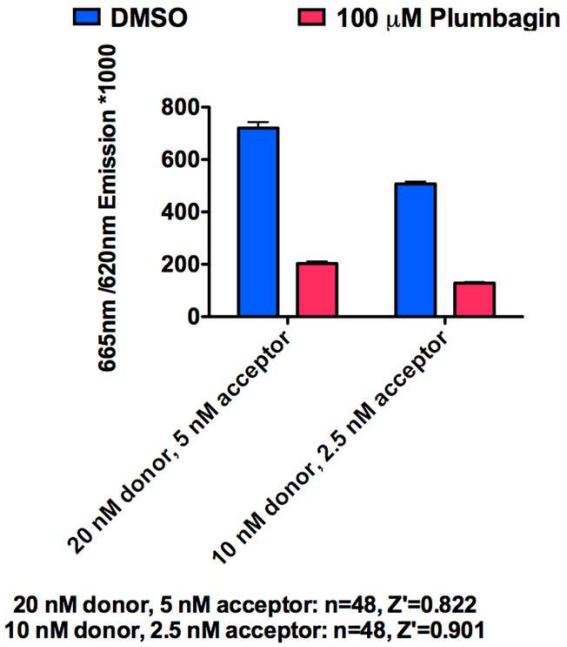

Figure 42 Fluorophore concentrations halved.

Halving the working concentrations of the donor and acceptor fluorophores in the screen, as well as using 100 μM plumbagin as a positive control, results in a Z' value suitable for high throughput screening (0.901).

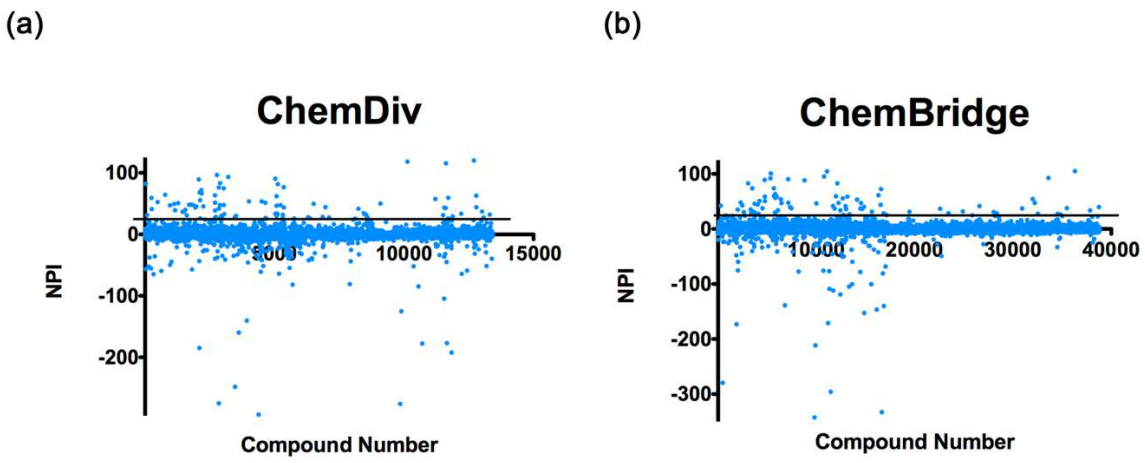

Figure 43 44,000 compound screen results.

(from previous page) (a) ChemDiv screen results, giving 70 hits with a cutoff of 25% NPI. (b) ChemBridge screen results, giving 78 hits with a cutoff of 25% NPI.

We ordered new stocks of each of the 49 compounds and prepared an automated dose response assay of each compound ranging from 46 nM to 100 μM against both the primary screen and the counter screen. Some compounds were not commercially available, and others did not fully dissolve in DMSO, taking the full list of testable compounds to 41. In performing the dose response assays, we looked for compounds that were able to hit the primary screen and not the counter screen. **Table 3** lists the results, including which compounds were not commercially available and which were not soluble in DMSO. **Table 4** lists the IUPAC names of the compounds in **Table 3**, in the same order. The total list of compounds that were able to be selective against the primary screen were 15, which are listed in **Table 5.** It should be noted that CD10 did hit the counter screen, but its IC_{50} was appreciably lower in the counter screen than in the primary screen. In selecting compounds

to move forward, we aimed for compounds that hit the primary screen with a max signal close to the positive control of plumbagin (listed as "max" and is the normalized max inhibition shown). We also avoided compounds with high Hill slopes, as this is indicative of a compound that can aggregate the protein in question (Feng et al., 2007). This left us with 8 compounds, and we next decided to repeat the dose response assay by hand with these compounds, increasing the concentration range of inhibitors to 300 μM to 586 nM to obtain a more accurate representation of IC_{50} values and Hill slopes (**Figure 44**). All 8 compounds hit the primary screen with IC_{50} values ranging from 2 μM to 34 μM. All of the compounds were also shown to be ineffective in the counter screen up to a concentration of 300 μM, except for CD10, which was able to inhibit BRAF with an IC_{50} of 205 μM.

Supplier	ID	Initial NPI	Available	Soluble	Primary	Counter	Name	Chemotype
ChemBridge	7532833	82.83773	Yes	Yes	Yes	No	CB1	thiophene
ChemBridge	95877291	41.78127	Yes	Yes	No	No	CB25	pyrazole
ChemBridge	38667363	30.79267	Yes	Yes	Yes	Yes	CB24	imidazole
ChemDiv	K029-0062	76.5445	No	N/A	N/A	N/A	N/A	imidazole
ChemBridge	9018218	47.59549	Yes	Yes	Yes	Yes	CB10	1,2,4-triazole
ChemBridge	9283140	72.48091	Yes	Yes	No	No	CB21	1,2,3-triazole
ChemBridge	9153534	47.21289	Yes	Yes	Yes	No	CB20	1,2,3-triazole
ChemDiv	M564-0134	49.60175	Yes	Yes	No	No	CD16	1,2-oxazole
ChemDiv	C201-1987	51.57056	Yes	Yes	Yes	No	CD8	1,2,4-oxadiazole
ChemBridge	9017718	90.30982	Yes	mostly	Yes	No	CB9	1,3,4-thiadiazole
ChemDiv	K783-6707	81.66144	Yes	Yes	Yes	No	CD14	1,3,4-thiadiazole
ChemBridge	7903556	88.90437	Yes	Yes	Yes	No	CB3	thioamide
ChemBridge	7916412	92.09573	Yes	Yes	Yes	No	CB4	thioamide
ChemDiv	0655-0099	59.22873	Yes	Yes	Yes	No	CD1	cyclic thioamide
ChemDiv	C201-1499	63.53421	Yes	Yes	Yes	No	CD7	cyclic thioamide
ChemDiv	C301-7412	62.83147	Yes	Yes	No	No	CD9	urea
ChemDiv	M509-0433	26.07941	Yes	Yes	Yes	Yes	CD15	urea
ChemDiv	8018-1737	66.5581	Yes	Yes	No	No	CD4	thiourea
ChemDiv	K783-5213	46.57137	Yes	Yes	Yes	No	CD13	thiourea
ChemDiv	D284-0238	93.24313	Yes	Yes	Yes	No	CD11	cyclic thiourea
ChemDiv	K241-0225	43.87642	Yes	Yes	No	No	CD12	cyclic thiourea
ChemDiv	1494-0327	31.23913	Yes	Yes	No	No	CD3	cyclic thiourea
ChemDiv	8014-2247	89.27625	No	N/A	N/A	N/A	N/A	cyclic thiourea
ChemDiv	8019-0869	45.41068	Yes	Yes	No	No	CD5	cyclic thiourea
ChemDiv	C200-3441	76.31184	No	N/A	N/A	N/A	N/A	1,4,8-triazaspiro[4.5]dec-3-ene-2-thione
ChemDiv	C200-3443	83.35142	Yes	Yes	No	No	CD6	1,4,8-triazaspiro[4.5]dec-3-ene-2-thione
ChemBridge	9144997	53.32442	Yes	Yes	No	No	CB19	7H-[1,2,4]triazolo[3,4-b][1,3,4]thiadiazine
ChemBridge	9104745	104.5595	Yes	Yes	Yes	Yes	CB13	benzothiazole
ChemBridge	9122006	82.91343	Yes	Yes	Yes	Yes	CB15	Thieno[2,3-b]pyridine
ChemBridge	9116291	42.0284	Yes	Yes	Yes	No	CB14	Thieno[2,3-b]pyridine
ChemBridge	27065701	28.61002	Yes	Yes	Yes	Yes	CB23	1H-Pyrrolo[2,3-b]pyridine
ChemBridge	79024647	105.1373	No	N/A	N/A	N/A	N/A	1H-Pyrrolo[2,3-b]pyridine
ChemDiv	T499-0675	118.2352	Yes	Yes	No	No	CD18	Various nitrogen-containing 6-5 ring systems
ChemDiv	P814-4725	41.6299	Yes	Yes	Yes	Yes	CD17	Various nitrogen-containing 6-5 ring systems
ChemDiv	C430-0042	120.0072	Yes	Yes	Yes	Yes (lower)	CD10	isoindole
ChemBridge	7954896	30.22385	Yes	Yes	Yes	Yes	CB6	isoindole
ChemDiv	0263-0418	41.07984	No	N/A	N/A	N/A	N/A	benzimidazole
ChemBridge	9157817	39.96184	Yes	Yes	Yes	No	CB21	quinazoline
ChemBridge	7697494	30.78429	Yes	Yes	Yes	No	CB2	quinazoline
ChemBridge	9131456	58.80107	Yes	Yes	Yes	Yes	CB18	quinoline
ChemBridge	76251720	37.21705	No	N/A	N/A	N/A	N/A	quinoline
ChemBridge	7958461	33.89854	Yes	No	N/A	N/A	CB7	4-oxo-4H-pyrido[1,2-a]thieno[2,3-d]pyrimidine
ChemBridge	7961079	63.35647	Yes	mostly	Yes	Yes	CB8	4-oxo-4H-pyrido[1,2-a]thieno[2,3-d]pyrimidine
ChemBridge	9126762	55.58708	Yes	Yes	No	No	CB16	4-oxo-1,4-dihydropyrido[1,2-a]pyrrolo[2,3-d]pyrimidine
ChemDiv	1391-0614	82.2714	Yes	Yes	Yes	Yes	CD2	benzopyrones
ChemBridge	9023017	39.59888	Yes	Yes	No	No	CB11	benzopyrones
ChemBridge	9128342	36.35136	Yes	No	N/A	N/A	CB17	unstructured
ChemBridge	9103442	95.37924	Yes	Yes	No	No	CB12	unstructured
ChemBridge	7928988	100.872	Yes	Yes	No	No	CB5	unstructured

Table 3. ChemBridge and ChemDiv screen results *(from previous page)*. A list of the 49 compounds that hit in the initial screen and were pulled out by chemotype. Their activity in both the primary and counter screen is listed, as well as company, ID number, initial NPI, availability, solubility, chemotype, and shorthand name.

supplier_ID	IUPAC name
7532833	methyl 2-amino-5-phenyl-3-thiophenecarboxylate
95877291	2-[1-(2-chlorophenyl)-3-methyl-5-oxo-1,5-dihydro-4H-1,2,4-triazol-4-yl]-N-cyclopropyl-N-[(1-methyl-1H-pyrazol-4-yl)methyl]acetamide
38667363	2-methyl-5-(2-pyridin-4-yl-1H-imidazol-1-yl)phenol
K029-0062	4-(4-methoxyphenyl)-1H-imidazole-1,2-diamine
9018218	N-(3-cyano-4,5,6,7-tetrahydro-1-benzothien-2-yl)-3-(4H-1,2,4-triazol-4-yl)benzamide
9283140	[5-methyl-1-(3-methylphenyl)-1H-1,2,3-triazol-4-yl]acetic acid
9153534	5-amino-1-(4-methylphenyl)-N-(3-oxo-1,3-dihydro-2-benzofuran-5-yl)-1H-1,2,3-triazole-4-carboxamide
M564-0134	1-[4-(5-amino-1,2-oxazol-3-yl)piperidin-1-yl]-3-(4-methoxyphenyl)propan-1-one
C201-1987	2-{3-[(4-chlorophenyl)methyl]-1,2,4-oxadiazol-5-yl}ethanethioamide
9017718	N-[5-(1,1-dimethylpropyl)-1,3,4-thiadiazol-2-yl]cyclohexanecarboxamide
K783-6707	5-(4-fluorophenyl)-1,3,4-thiadiazol-2-amine
7903556	1-(4-fluorophenyl)-4-[(2-methoxyphenyl)carbonothioyl]piperazine
7916412	4-{[3-chloro-5-methoxy-4-(2-propyn-1-yloxy)phenyl]carbonothioyl}morpholine
0655-0099	5-ethyl-4,6-dimethyl-2-sulfanylidene-1,2-dihydropyridine-3-carbonitrile
C201-1499	6-[4-(2-methoxyphenyl)piperazin-1-yl]-2,3-dihydropyridazine-3-thione
C301-7412	3-(2H-1,3-benzodioxol-5-yl)-1-(2,4-dihydroxypyrimidin-5-yl)urea
M509-0433	3-(2-{1-propyl-1H-pyrrolo[2,3-b]pyridin-3-yl}ethyl)-1-[3-(trifluoromethyl)phenyl]urea
8018-1737	3-[(2E)-1-methyl-1,2-dihydropyridin-2-ylidene]-1-phenylthiourea
K783-5213	3-benzyl-N-(3,5-dichlorophenyl)imidazolidine-1-carbothioamide
D284-0238	3-(2,3-dihydro-1,4-benzodioxin-2-yl)-4-ethyl-4,5-dihydro-1H-1,2,4-triazole-5-thione
K241-0225	4-tert-butyl-1-(4-chlorophenyl)-2,3-dihydro-1H-imidazole-2-thione
1494-0327	4-phenyl-3-(phenylamino)-4,5-dihydro-1H-1,2,4-triazole-5-thione
8014-2247	3-amino-1-phenyl-4,5-dihydro-1H-1,2,4-triazole-5-thione
8019-0869	5-benzyl-1-(6-methylpyridin-2-yl)-1,3,5-triazinane-2-thione
C200-3441	8-methyl-3-phenyl-1,4,8-triazaspiro[4.5]dec-3-ene-2-thione
C200-3443	3-phenyl-8-(propan-2-yl)-1,4,8-triazaspiro[4.5]dec-3-ene-2-thione
9144997	6-(1H-indol-3-yl)-3-(4-methylphenyl)-7H-[1,2,4]triazolo[3,4-b][1,3,4]thiadiazine
9104745	methyl 2-[(3-pyridinylcarbonyl)amino]-1,3-benzothiazole-6-carboxylate
9122006	ethyl 5-{[(3-aminothieno[2,3-b]pyridin-2-yl)carbonyl]amino}-2-chlorobenzoate
9116291	3-amino-N-(3-chloro-4-methoxyphenyl)thieno[2,3-b]pyridine-2-carboxamide
27065701	5-[6-(cyclopentylamino)-1H-pyrrolo[2,3-b]pyridin-4-yl]nicotinamide
79024647	N-piperidin-4-yl-4-(1,3-thiazol-2-yl)-1H-pyrrolo[2,3-b]pyridin-6-amine
T499-0675	1-(5-chlorothiophene-2-carbonyl)-3-[3-(2-methoxyethyl)-3H-imidazo[4,5-b]pyridin-2-yl]pyrrolidine
P814-4725	9-[1-(furan-2-carbonyl)pyrrolidin-3-yl]-8,9-dihydro-7H-purin-8-one
C430-0042	1-hydroxy-2-(2-methoxyethyl)-3-oxo-2,3-dihydro-1H-isoindole-5-carboxylic acid
7954896	2-(5-methyl-3-isoxazolyl)-1,3-dioxo-N-1,3-thiazol-2-yl-5-isoindolinecarboxamide
0263-0418	2-(4-aminophenyl)-5-chloro-1H-1,3-benzodiazol-6-amine
9157817	3-[(4-oxo-3,4-dihydro-2-quinazolinyl)methyl]-5,6,7,8-tetrahydro[1]benzothieno[2,3-d]pyrimidin-4(3H)-one
7697494	N-(6,7-dimethoxy-4-oxo-1,4-dihydro-2-quinazolinyl)benzamide
9131456	N-[4-(aminocarbonyl)phenyl]-4-hydroxy-3-quinolinecarboxamide
76251720	8-methoxy-5-[5-(pyrrolidin-1-ylcarbonyl)-2-furyl]quinoline
7958461	9-methyl-N-(5-methyl-3-isoxazolyl)-4-oxo-4H-pyrido[1,2-a]thieno[2,3-d]pyrimidine-2-carboxamide
7961079	N-1,3-benzodioxol-5-yl-4-oxo-4H-pyrido[1,2-a]thieno[2,3-d]pyrimidine-2-carboxamide
9126762	1-benzyl-N-methyl-4-oxo-1,4-dihydropyrido[1,2-a]pyrrolo[2,3-d]pyrimidine-2-carboxamide
1391-0614	3-{imidazo[1,2-a]pyridin-2-yl}-2H-chromen-2-one
9023017	2,4-dimethoxy-N-(2-oxo-2H-chromen-6-yl)benzamide
9128342	N-(4-chloro-2,5-dimethoxyphenyl)-5-oxo-5H-[1,3]thiazolo[3,2-a]pyrimidine-6-carboxamide
9103442	4-oxo-4-[(3-propoxyphenyl)amino]butanoic acid
7928988	2-{[1-(2-amino-5-ethyl-6-methyl-4-pyrimidinyl)-1H-diaziren-3-yl]thio}acetamide

Table 4. ChemBridge and ChemDiv screen results IUPAC names *(from previous page)*. Chemical names of hits from ChemBridge and ChemDiv screen, listed in the same order as in **Table 3**.

Name	ID	Min	Max	Hill Slope	IC_{50} (μM)
CD10	C430-0042	0.000	157	1.94	29.3
CD8	C201-1987	-1.38	152	1.86	98.5
CD1	0655-0099	0.430	55.5	1.75	39.4
CD7	C201-1499	2.02	7580	0.910	Ambiguous
CD11	D284-0238	0.210	74.1	2.05	37.0
CD14	K783-6707	2.29	89.0	3.75	16.8
CD13	K783-5213	0.990	83.7	3.15	22.4
CB9	9017718	-1.64	80.4	2.56	4.36
CB20	9153534	-4.59	43.0	1.09	57.3
CB2	7697494	-2.33	40.4	21.7	12.8
CB21	9157817	-3.37	44.5	2.69	32.8
CB14	9116291	-0.820	107	1.42	80.0
CB3	7903556	-0.970	3804	1.96	Ambiguous
CB4	7916412	-1.43	84.0	2.38	28.0
CB1	7532833	-1.59	80.2	2.92	23.1

Table 5 Initial hits *(from previous page)*. A list of the 15 compounds that hit in the initial screen and hit the primary screen in the dose response assay but not the counter screen. The ID number, Min, Max, IC_{50} and Hill slope from the dose response against the primary screen of each compound is listed. Max is the normalized maximum inhibition shown, while min is the normalized minimum inhibition shown. Compounds whose Max values were close to 100, had unambiguous IC_{50} values, and initial Hill slopes between 1 and 5 are listed in bold.

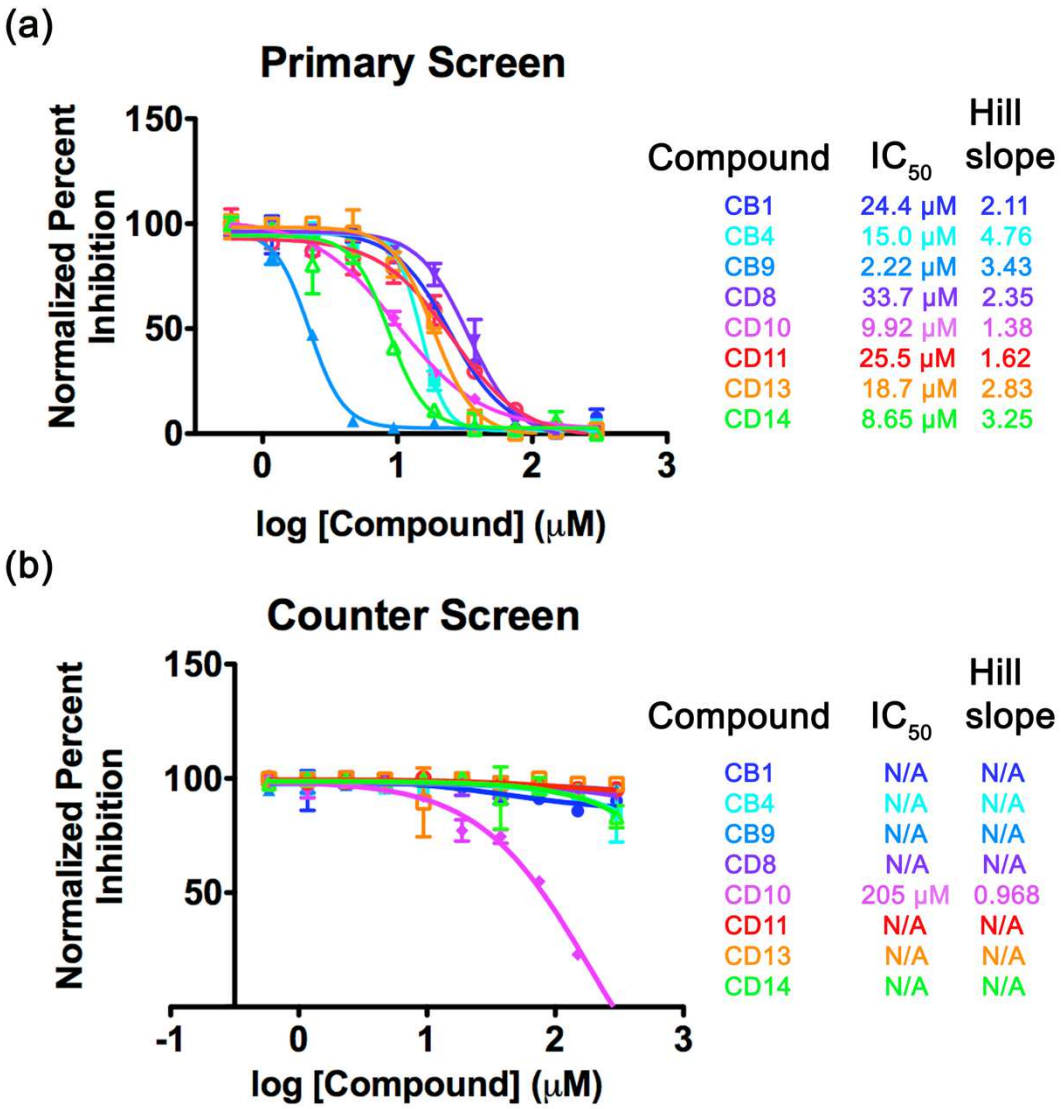

Figure 44 Dose response repeat.

(from previous page). (a) Primary screen dose response assay of 8 initial hit compounds, with IC_{50} values and Hill slopes listed, tested in duplicate. 95% confidence intervals for IC_{50} values are: CB1 (21.0 μM to 28.3 μM), CB4 (13.7 μM to 16.3 μM), CB9 (2.08 μM to 2.37 μM), CD8 (29.6 μM to 38.4 μM), CD10 (8.97 μM to 11.0 μM), CD11 (20.9 μM to 31.1 μM) CD13 (16.6 μM to 20.9 μM), and CD14 (7.42 μM to 10.1 μM). 95% confidence intervals for Hill slope values are: CB1 (1.53 to 2.69), CB4 (3.39 to 6.13), CB9 (2.66 to 4.21), CD8 (1.71 to 3.00), CD10 (1.19 to 1.57), CD11 (1.15 to 2.10) CD13 (1.98 to 3.68),

and CD14 (1.68 to 4.81). (b) Counter screen dose response assay of the 8 initial hit compounds, showing only CD10 hit against the counter screen. 95% confidence intervals for IC_{50} values are as follows: CD10 (70.8 μM to 591 μM). 95% confidence intervals for Hill slope values are as follows: CD10 (0.621 to 1.31).

4.3 Discussion

In conclusion, we have developed a high-throughput method for identifying small molecules that can disrupt the interaction between BRAF and its substrate, MEK. We have also developed a counter screen useful in determining whether these small molecules are non-specific inhibitors that affect the specific technology of the screen or if these inhibitors are specific towards the RAF/MEK interaction. In developing this screen, we have utilized a point mutation to make *E. coli* expressed BRAF able to interact with MEK in vitro and also have restored kinase activity in BRAF through this mutation. Finally, we have developed secondary assays useful in further confirming lead compounds and have identified chemotype structures that can be further analyzed for determining mode of inhibition.

Using secondary assays used for plumbagin and thymoquinone such as Differential Scanning Calorimetry (DSC), Differential Scanning Fluorimetry (DSF), ELISA based activity assays, and Analytical Ultracentrifugation (AUC) can help further confirm these compounds as lead hits that can be optimized to target MAPK signaling and, possibly, inhibitor resistant melanoma cell lines. While any compounds that inhibit the BRAF-MEK interaction will not be able to differentiate basal level MAPK signaling from BRAF-mutant

MAPK signaling, using chemical linking techniques such as those described in Chapter 2 and Chapter 3 of this thesis would be able to add selectivity to these compounds. Chemically linking vemurafenib, a $BRAF^{V600E}$-selective compound, to a compound that can bind to the surface of BRAF or MEK and hinder dimerization between these two proteins could have therapeutic benefits in inhibitor resistant cell lines and be more effective than in normal cells due to the selectivity of the vemurafenib inhibitor. We have shown that bivalent vemurafenib molecules are not potent in $BRAF^{WT}$ cells (Grasso et al., 2016), and this added selectivity could make these compounds powerful therapeutic tools in the clinic. BRAF-MEK dimerization inhibitors alone can also be powerful probes in exploring the effects of disrupting BRAF-MEK dimerization *in vitro* and in cells. Further confirming if these compounds affect BRAF signaling *in vitro* and testing their effects on MEK phosphorylation of ERK could help elucidate the binding mode of these compounds as well as elucidate the intricacies of the BRAF/MEK complex. Testing these inhibitors in cells to determine if resistant pathways could develop is also a use that can enlighten the field on further directing melanoma therapy.

4.4 Methods

4.4.1. Plasmids

DNA encoding the BRAF kinase domain residues 448-723 containing 16 solubilizing mutations (I543A, I544S, I551K, Q562R, L588N, K630S, F667E, Y673S, A688R, L706S, Q709R, S713E, L716E, S720E, P722S, and K723G) was ordered from Epoch Biolabs and

cloned into a Pet28a(+) vector encoding an N-terminal 6XHis Tag and a thrombin cleavage site between the protein and the tag. This construct was used as a template to create 6XHis-BRAF^{16mut_V600E}, 6XHis-BRAF^{16mut_E667F}, 6XHis-BRAF$^{V600E/16mut_E667F}$, FLAG-tagged BRAF^{16mut_E667F}, and 6XHis-FLAG-BRAF^{16mut}. This construct was also cloned into a PRSF vector with a GST-tag to create untagged BRAF^{16mut_V600E} and BRAF$^{V600E/16mut_E667F}$. These proteins were used in the TR-FRET assay, the ELISA based assay confirming that the E667F mutation restores kinase activity in the E. coli construct, DSF experiments, and DSC experiments.

A cDNA library for full length MEK was purchased from Dharmacon (Catalog # MHS 6278-211690391) and residues 63-393 were cloned into a pET-Duet vector containing a TEV protease cleavable N-terminal 6XHis tag. This construct was used in TR-FRET assays and thermal shift assays. The MEK construct spanned residues 45-393 and with replacement of the flexible linker region 264-307 with a 6-residue sequence SVQSDI, which was a gift from Dr. Donita Brady (University of Pennsylvania) and used for *in vitro* complexation of BRAF and MEK via size exclusion chromatography. Full length human MEK1 with an N-terminal GST fusion tag and a C-terminal His tag in a pGex-3t vector was provided by Dr. Michael Olson (Beatson Institute for Cancer Research, Glasgow, UK) and was used as the substrate for the BRAF *in vitro* kinase assays.

DNA encoding the BRAF kinase domain residues 442-724 was used as a template and cloned into a Pfastbac dual vector with mouse p50^{cdc37} full length as an expression chaperone for protein expression in baculovirus infected Sf9 insect cells. An N-terminal 6X-His tag was inserted into the plasmid, and this plasmid was used as a template to create mutant BRAF^{V600E}.

DNA encoding mouse NF-κB p65 residues 191-291 with an N-terminal 6XHis-tag was cloned into a pET-Duet vector. This construct was used in TR-FRET assays.

4.4.2 Protein Purification

6XHis-tagged $BRAF^{16mut}$ proteins were produced as previously described (Grasso et al., 2016). In brief, proteins were expressed in (DE3)RIL bacterial expression cells at 37 ºC and induced with 1mM IPTG overnight at 18 ºC, spun down the next day, and lysed in lysis buffer (50mM potassium phosphate pH 7.0, 250mM NaCl) with 1mM PMSF and DNaseI. The lysate was spun down at 19000 rpm for 30 minutes, and the supernatant was added to 7mL of TALON metal affinity resin (Takara) and left to incubate at 4 ºC for 1 hr. The supernatant was eluted via gravity column, and the resin was washed with 1 L of lysis buffer with 10 mM imidazole. The BRAF proteins were eluted with lysis buffer supplemented with 250 mM Imidazole. Protein was dialyzed into dialysis buffer (50 mM potassium phosphate pH 7.0, 5 mM EDTA pH 7.5, 1mM DTT (Dithiothreitol)) overnight and then applied to a 5 mL SP Sepherose cation exchange column followed by washing in dialysis buffer and elution in 50 mM potassium phosphate pH 7.0, 1 M NaCl, and 1 mM DTT. Peak fractions were run on an SDS-PAGE gel, pooled, concentrated, and applied to a Superdex S200 gel filtration column in a final buffer of 20 mM HEPES pH 7.0, 150 mM NaCl, 5% Glycerol and 10 mM DTT. Protein was concentrated to 5-10 mg/mL, flash frozen in liquid nitrogen, and stored in an -80 ºC freezer for future use. 6XHis-FLAG-tagged BRAF was purified in the same manner.

FLAG-tagged $BRAF^{16mut}$ proteins were expressed in (DE3)RIL bacterial expression cells at 37 ºC and induced with 1mM IPTG overnight at 18 ºC, spun down the next day, and

lysed in lysis buffer (50mM potassium phosphate pH 7.0, 250mM NaCl) with 1mM PMSF and DNaseI. The lysate was spun down at 19000 rpm for 30 minutes, and the supernatant was added to 15mL of M2 Anti-FLAG resin affinity resin (Sigma-Aldrich) and left to incubate at 4 ^{o}C for 2 hr. The supernatant was eluted via gravity column, and the resin was washed with 1 L of lysis buffer. The BRAF proteins were eluted with lysis buffer supplemented with 5 mL of 0.5 mg/mL 3X FLAG peptide (Sigma Aldrich). The resin was then washed with lysis buffer and the eluent was collected and monitored using Bradford reagent (Sigma Aldrich) until protein elution was complete. Protein was dialyzed into dialysis buffer (50 mM potassium phosphate pH 7.0, 1mM DTT (Dithiothreitol)) overnight and then applied to a 5 mL SP Sepherose cation exchange column followed by washing in dialysis buffer and elution in 50 mM potassium phosphate pH 7.0, 1 M NaCl, and 1 mM DTT. Peak fractions were run on an SDS-PAGE gel, pooled, concentrated, and applied to a Superdex S200 gel filtration column in a final buffer of 20 mM HEPES pH 7.0, 150 mM NaCl, 5% Glycerol and 10 mM DTT. Protein was concentrated to 3-5mg/mL, flash frozen in liquid nitrogen, and stored in an -80 ^{o}C freezer until future use.

GST-tagged BRAF^{16mut} proteins were expressed in bacteria as described for the His-tagged proteins, lysed in lysis buffer (50 mM KPi pH 7.0 and 250 mM NaCl) and incubated on Glutathione Resin at 4 ^{o}C for 1 hr. The protein on resin was then washed with 1L of lysis buffer and left on the resin and cleaved with TEV protease overnight and eluted the next morning in lysis buffer with 25 mM NaCl, run over both SP Sepharose and Q Sepharose ion exchange columns in tandem and the flow through collected. The protein was run over Ni-NTA resin pre-equilibrated with lysis buffer and the flowthrough was collected. The protein was then concentrated using a 10kDalton cutoff centrifugal filter unit (Millipore)

and chromatographed on a Superdex S200 gel filtration column in a final buffer of 20 mM HEPES pH 7.0, 150 mM NaCl, 10 mM Dithiothreitol and 5% glycerol. Protein eluted as a mixture of dimer and monomer and both species were pooled together, concentrated to 10mg/mL (~320 μM) and flash frozen in liquid nitrogen and stored for later use in a -80 ^{o}C freezer.

MEK$^{63-393}$ with an N-terminal 6XHis tag was expressed in DE(3) RIL bacterial expression cells at 37 ^{o}C, induced with 1mM IPTG overnight at 16 ^{o}C, spun down the next day, and lysed in lysis buffer 2 (25 mM Tris pH 7.5, 500mM NaCl, 5mM BME) supplemented with 1mM PMSF and DNAseI. The lysate was spun down at 19,000 rpm for 30 minutes and the supernatant was added to 10 mL of Ni-NTA metal affinity resin (Thermo Scientific) and left to incubate at 4 ^{o}C for 1 hr. The supernatant was then eluted via gravity column and the resin was washed with 1L of lysis buffer 2 treated with 20mM imidazole. The MEK protein was eluted with lysis buffer 2 supplemented with 300 mM imidazole. Protein was dialyzed into dialysis buffer (25 mM Tris pH 7.5, 25mM NaCl, 5 mM BME) overnight and then applied to a 5 mL Q Sepharose cation exchange column followed by washing in dialysis buffer and elution in 25 mM Tris pH 7.5, 5 mM BME, and 1 M NaCl. Peak fractions were run on an SDS-PAGE gel, pooled, concentrated using a 30k Dalton cutoff centrifugal filter unit (Millipore), and applied to a Superdex S200 gel filtration column in a final buffer of 20 mM HEPES pH 7.0, 150 mM NaCl, 5% Glycerol and 5 mM BME. Protein was concentrated to 5-10 mg/mL (200 μM), flash frozen in liquid nitrogen, and stored in an -80 ^{o}C freezer for future use.

$MEK^{45\text{-}393\ (\Delta 264\text{-}307/SVQSDI\ linker)}$ with an N-terminal 6XHis tag was expressed in DE(3) RIL bacterial expression cells at 37 ºC, induced with 1mM IPTG overnight at 17 ºC, spun down the next day, and lysed in lysis buffer 2 (25 mM Tris pH 7.5, 500mM NaCl, 5mM BME) supplemented with 1mM PMSF and DNAseI. The lysate was spun down at 19,000 rpm for 30 min. and the supernatant was added to 10 mL of Ni-NTA metal affinity resin (Thermo Scientific) and left to incubate at 4 ºC for 1 hr. The supernatant was then eluted via gravity column and the resin was washed with 1L of lysis buffer 2 treated with 20mM imidazole. The MEK protein was eluted with lysis buffer 2 supplemented with 300 mM Imidazole. Protein was dialyzed into dialysis buffer (25 mM Tris pH 7.5, 25mM NaCl, 5 mM BME) overnight while incubated with TEV protease in dialysis and then applied to a 5 mL SP Sepharose cation exchange column followed by washing in dialysis buffer and elution in 25 mM Tris pH 7.5, 5 mM BME, and 1 M NaCl. Peak fractions were run on an SDS-PAGE gel, pooled, concentrated, and applied to Ni-NTA resin pre-washed with lysis buffer 2. The flow through was collected, concentrated using a 30kDalton cutoff centrifugal filter unit (Millipore), and loaded onto a Superdex S200 gel filtration column in a final buffer of 20 mM HEPES pH 7.0, 150 mM NaCl, 5% Glycerol and 5 mM BME. Protein was concentrated to 5-10 mg/mL (200 μM) and then added to already purified untagged $BRAF^{V600E/16mut\_E667F}$. This complex was then loaded onto a Superdex S200 gel filtration column in a final buffer of 20 mM HEPES pH 7.0, 150 mM NaCl, 5% Glycerol and 5 mM BME and only the fractions containing stoichiometric amounts of BRAF and MEK were pooled together, concentrated to 5-10 mg/mL, and then flash frozen in liquid nitrogen and stored in an -80 ºC freezer for future use.

$BRAF^{WT}$ and $BRAF^{V600E}$ kinase domains were overproduced as N-terminally His-tagged proteins in insect cells. Briefly, protein constructs were coexpressed with $p50^{cdc37}$, pelleted, suspended in lysis buffer 3 (25 mM Tris pH 8.0, 250 mM NaCl, 5 mM Imidazole and 10% glycerol) treated with Complete EDTA-free protease inhibitor cocktail tablets (Roche) and DNaseI, lysed, centrifuged at 19,000 rpm for 30 min., and added to TALON metal affinity resin and incubated at 4 ºC for 1 hr. The protein on the resin was washed extensively with 1 L of lysis buffer 3 and eluted with 25 mM Tris pH 7.5, 250 mM NaCl, 250 mM imidazole, and 10% Glycerol. The protein was diluted into a low salt buffer containing 25mM Tris pH 8.0, 1 mM EDTA and 1 mM DTT and run on an SP Sepharose cation exchange column and eluted with a salt gradient from 50 mM NaCl to 1 M NaCl. Peak fractions were run on an SDS-PAGE gel and fractions containing protein were pooled, concentrated, and applied to a Superdex S200 gel filtration column and stored in a final buffer of 25 mM Tris pH 8.0, 300 mM NaCl, 1 mM DTT, and 10% glycerol. Protein was concentrated to ~0.5 mg/mL and flash frozen in liquid nitrogen and stored for later use in an -80 ºC freezer.

GST-MEK1 fusion protein used as a substrate in ELISA assays was expressed in (DE3) RIL cells at 37 ºC and induced with 0.5 mM IPTG at 15 ºC overnight. The cells were harvested and resuspended in lysis buffer 4 (20 mM HEPES at pH 7.0, 500 mM NaCl, 10 mM BME, 10 mM imidazole and 5% glycerol) supplemented with 1mM PMSF and DNaseI. The lysate was sonicated and spun down at 19,000 rpm for 30 min. and the supernatant was added to Ni-NTA resin and incubated at 4 ºC for 1 hr. The resin was washed extensively with lysis buffer 4 with 20 mM instead of 10 mM imidazole and eluted with lysis buffer 4 supplemented with 250 mM imidazole. Eluted protein was concentrated

and loaded onto a Superdex S200 16/60 gel filtration column into a final buffer of 20 mM HEPES pH 7.0, 150 mM NaCl, 10 mM BME and 5% glycerol. The protein eluted off the sizing column in two separate populations, and the second peak was collected, concentrated to ~20 mg/mL (~250 μM), and flash frozen in liquid nitrogen and stored in an -80 ºC freezer for future use.

NF-κB p65 residues 191-291 with an N-terminal 6XHis-tag was expressed in DE(3) RIL bacterial expression cells at 37 ºC, induced with 1mM IPTG overnight at 22 ºC, spun down the next day, and lysed in lysis buffer 5 (25 mM HEPES pH 7.5, 500 mM NaCl, 5mM BME) supplemented with 1 mM PMSF and DNAseI. The lysate was spun down at 19,000 rpm for 30 min. and the supernatant was added to 10 mL of Ni-NTA metal affinity resin (Thermo Scientific) and left to incubate at 4 ºC for 1 hr. The supernatant was then eluted via gravity column and the resin was washed with 1L of lysis buffer 5 treated with 20mM imidazole. The MEK protein was eluted with lysis buffer 5 supplemented with 300 mM imidazole. Protein was dialyzed into dialysis buffer (25 mM HEPES pH 7.5, 150 mM NaCl, 5 mM BME) overnight and concentrated the next day to ~600 μM and flash frozen in liquid nitrogen and stored in an -80 ºC freezer for future use.

4.4.3. In Vitro Kinase Assay

Compound inhibition of $BRAF^{WT}$ and $BRAF^{V600E}$ were performed using an ELISA assay. Briefly, GST-MEK fusion protein was diluted 3:1000 in Tris-buffered saline (25 mM Tris pH 7.5, 140 mM NaCl) treated with 0.05% Tween-20 (TBST), and diluted MEK was added to each well of a glutathione coated 96-well plate (Pierce #15240) and incubated at room

temp for 1 hr. with shaking. BRAF was diluted from frozen stocks (1:500 dilution for $BRAF^{WT}$ and 1:1000 dilution for $BRAF^{V600E}$) in 50 mM HEPES pH 7.0 and 50 mM NaCl. 2 μL of desired concentration of inhibitor was added to 100 μL of diluted BRAF in a 96 well "V" bottom plate (Corning #2897) and the inhibitor/protein mixture was incubated for 1 hr. at room temp. Glutathione plates were washed extensively with TBST and the protein-inhibitor mixture was added to the plate with a 100 μM final concentration of ATP in a buffer containing 50 mM HEPES pH 7.0, 200 mM NaCl, and 20 mM $MgCl_2$. The plate was incubated at 37 ^oC for 30 min. The reaction was washed from the plate and the plate was again washed with TBST. A 1:8000 dilution of primary antibody (p-MEK1/2 (S217/S221) rabbit antibody (cell signaling)) in TBST treated with 0.5% BSA was added to the plate and incubated for 1 hr. with shaking. The plate was then treated with multiple TBST washes and then incubated with a 1:10,000 dilution of secondary antibody (goat anti-rabbit IgG (H+L)-HRP (BioRad)) in TBST treated with 0.5% BSA for 1 hr. with shaking. The plate was washed extensively with TBST and Supersignal ELISA Pico Chemiluminescent Substrate (Pierce #37069) was added. The plate was read on a Promega GloMAX 96 Microplate Luminometer. Each curve was repeated in duplicate or triplicate, normalized using GraphPad Prism by selecting the largest value as the maximum and the lowest value as the minimum, and used to calculate IC_{50} values by using a log (inhibitor) vs response fit on Prism 5.0 (GraphPad). Error bars are indicative of the SEM of each point, and 95% confidence intervals are listed in the figure legends as calculated by GraphPad Prism.

4.4.4 Differential Scanning Fluorimetry (DSF) assays

Frozen aliquots of $BRAF^{V600E/16mut\_E667F}$ and MEK^{63-393} proteins were thawed and diluted in DSF Buffer (25 mM Hepes pH 7.0, 150 mM NaCl) to a final concentration of 5 μM (0.2 mg/mL) and 15 μL were added to the selected wells of a MicroAmp Optical 384 well plate (Applied Biosystems). Sypro Orange (5000X stock, ThermoFisher Scientific) was diluted 1:300 and 4 μL of that diluted stock was added to each well. 1 μL of inhibitor in 100% DMSO was added to each well to a final concentration of 100-300 μM and the plate was spun down and heated from 20 ºC to 95 ºC using a qPCR (ABI 7900 RealTime PCR) with a 1% ramp rate. Melting curves were generated from this data and analyzed by taking the first derivative of the curve. Data were analyzed and plotted using GraphPad. Each data set was performed in quadruplicate. One representative curve for each data point is shown in **Figure 40.**

4.4.5 Differential Scanning Calorimetry (DSC) assays

$BRAF^{16mut}$ was diluted to a final concentration of 37 μM in DSC Buffer (20 mM HEPES pH 7.0, 150 mM NaCl). 50 μL of either DMSO or inhibitor dissolved in 100% DMSO was added to 450 μL of $BRAF^{16mut}$ and degassed for 3 min. The protein/inhibitor or protein/DMSO mixture was then added to a MicroCal VP-Capillary DSC (Malvern) and blanked with 450 μL of DSC Buffer and 50 μL of DMSO. The protein (sample) and buffer (blank) were both heated from 10 ºC to 90 ºC with a scan rate of 60 ºC/hour and a filtering period of 10 seconds. The difference in heat required to raise the temperature of the sample as compared to the blank is measured as a function of temperature. The data was plotted using Origin 7.

4.4.6 Time Resolved- Fluorescence Resonance Energy Transfer (TR-FRET) assay "hooking experiment"

Frozen aliquots of FLAG-$BRAF^{16mut\_E667F}$ and 6XHis-MEK^{63-393} were thawed and each were diluted to 4X final concentrations in TR-FRET buffer (20 mM Tris pH 7.5, 140 mM NaCl, 0.05% Tween-20, and 0.2% BSA) and 2.5 µL of each protein were added to each well in a 384 well Proxi-Plate (Perkin Elmer). LANCE Eu-W1024-anti6XHis (AD011, Perkin Elmer) was diluted to 40 nM and mixed with 10 nM LANCE Ultra ULight Anti-FLAG (TRF0059M, Perkin Elmer) in TR-FRET buffer and 5 µL of fluorophore mixture was added to each well. The plate was then covered and left to sit at room temperature for 60 minutes and then read on a PerkinElmer EnVision Xcite plate reader at both 665 nm and 620 nm. The 665 nm emission signal was divided by the 620 nm emission and multiplied by 1000 to control for Europium loading.

4.4.6 TR-FRET assay 50:50 screen

Frozen aliquots of untagged $BRAF^{16mut\_V600E}$ and $BRAF^{V600E/16mut\_E667F}$ were thawed and 1 µL of 22µM $BRAF^{16mut\_V600E}$ was pipetted into half of a 384-well Proxi plate (Perkin Elmer) and 22 µM $BRAF^{V600E/16mut\_E667F}$ was added to the other half using the Janus Modular Dispensing Tool (MDT) P30 head (Perkin Elmer). Frozen aliquots of FLAG-$BRAF^{16mut\_E667F}$ and 6XHis-MEK^{63-393} were thawed and each were diluted to 50 nM final concentrations in TR-FRET buffer (20 mM Tris pH 7.5, 140 mM NaCl, 0.05% Tween-20, and 0.2% BSA) along with 20 nM LANCE Eu-W1024-anti6XHis (AD011, Perkin Elmer) and 5 nM LANCE Ultra ULight Anti-FLAG (TRF0059M, Perkin Elmer). 10 µL of protein-fluorophore mixture was then dispensed into 384 well plates using a MultiDrop

Combi reagent dispenser (Thermo Fisher). The plate was then left at room temperature for 90 min. and read on a Perkin Elmer EnVision XCite. The data was analyzed as described above.

4.4.6 TR-FRET assay Natural Product Pilot Screen

A frozen aliquot of untagged $BRAF^{V600E/16mut\_E667F}$ was thawed and 1 µL of 22µM $BRAF^{V600E/16mut\_E667F}$ was pipetted into rows 2 and 24 of three 384-well Proxi plates (Perkin Elmer) using the Janus MDT P30 head. Frozen aliquots of FLAG-$BRAF^{E667F}$ and 6XHis-MEK^{63-393} were thawed and each were diluted to 50 nM final concentrations in TR-FRET buffer (20 mM Tris pH 7.5, 140 mM NaCl, 0.05% Tween-20, and 0.2% BSA) along with 20 nM LANCE Eu-W1024-anti6XHis (AD011, Perkin Elmer) and 5 nM LANCE Ultra ULight Anti-FLAG (TRF0059M, Perkin Elmer). 10 µL of protein-fluorophore mixture was then dispensed into 384 well plates using a MultiDrop Combi reagent dispenser (Thermo Fisher). 50nL of 5mM small molecules from the Natural Product Pilot Screen were pipetted to the 384 well plates using the Janus MDT PinTool. The plate was then left at room temperature for 60 min. and read on a Perkin Elmer EnVision XCite. This was repeated for the counter screen, except FLAG-6XHis-$BRAF^{16mut}$ was added at a final concentration of 50 nM to 20 nM LANCE Eu-W1024-anti6XHis (AD011, Perkin Elmer) and 5 nM LANCE Ultra ULight Anti-FLAG (TRF0059M, Perkin Elmer) in TR-FRET buffer. Also, 1 µL of 300 µM NF-κB was added to rows 2 and 24 of each of the counter screen plates using the Janus MDT P30 head. The data was analyzed as described above and normalized by using positive (plumbagin) and negative (DMSO) controls. Any

inhibitors that hit with an NPI above 25% and did not hit the counter screen with more than 5% NPI were considered hits.

4.4.9 Dose Response assays by hand

Frozen aliquots of FLAG-BRAF^{16mut_E667F} and 6XHis-MEK$^{63-393}$ were thawed and each were diluted to 50 nM final concentrations in TR-FRET buffer (20 mM Tris pH 7.5, 140 mM NaCl, 0.05% Tween-20, and 0.2% BSA) along with 10 nM LANCE Eu-W1024-anti6XHis (AD011, Perkin Elmer) and 2.5 nM LANCE Ultra ULight Anti-FLAG (TRF0059M, Perkin Elmer). 10 μL of protein-fluorophore mixture was then added into a 384 well plate and 1 μL of inhibitor in 100% DMSO was added to each of the wells ranging from 586 nM to 300 μM for each inhibitor. Each inhibitor titration was performed in duplicate. Data was normalized with DMSO as a control and data was analyzed using GraphPad Prism using a nonlinear regression (curve fit) (log (agonist) vs response (variable slope)).

4.4.10 High Throughput screening

Compounds (50 nL) were transferred to low volume 384-well assay plates (Perkin Elmer 6008280) containing 5uL of assay buffer (25mM Tris pH7.5, 140mM NaCl, .05% Tween, and 0.2% BSA) using a 384, 50 nL slotted pin tool (V&P Scientific) and a JANUS Automated Workstation (Perkin Elmer). Compounds were added to a final concentration of 50 uM in 0.5% DMSO with negative control (DMSO) in columns 1 and 23, and positive control (100uM Plumbagin) in columns 2 and 24. Five microliters of premixed BRAF-MEK (50nM: 50nM ratio), protein-bead complex in assay buffer was added to the assay

plates using a Multidrop^{TM} Combi Reagent Dispenser (Thermo Scientific). Assay plates were incubated for 90 minutes at room temperature and fluorescence was measured on an EnVision Xcite Multilabel Plate Reader (PerkinElmer), using the TR-FRET measurement technology (Ex 320 nM and Em 620 and 665 nm, 300 us window, 60us delay).

4.4.11 Data Analysis using Tibco Spotfire Software

The EM665:Em620 ratio from DMSO and Plumbagin control wells were aggregated, respectively, and used to calculate z'-factors for each assay plate, as a measure of assay performance and data quality, with a z'-factor >0.5 representing acceptable data. Em665: Em620 values of sample wells were normalized to aggregate values from DMSO and Plumbagin plate control wells and expressed as normalized percent inhibition [NPI = (($DMSO_{avg}$-test well) / ($DMSO_{avg}$ - $Plumbagin_{avg}$) x 100)] and Z-score [Z= ($DMSO_{avg}$-Test well) / ($DMSO_{stddev}$].

For dose response experiments, Normalized Percent Inhibition (NPI) and log10 transformed drug concentration values were fit to a non-linear model with variable slope to define the IC50 values, Hill slope, and Area Under Curve (AUC).

4.4.12 Inhibitors

Plumbagin (P7262-250MG) and Thymoquinone (274666-1G) were purchased from Sigma Aldrich. Eseroline Fumarate (sc-202155) was purchased from Santa Cruz Biotechnology. Erythromycin (AC227330050) was purchased from Acros Organics. All hits from ChemBridge and ChemDiv were purchased directly from their respective companies.

4.4.13 Library

We screened ~44000 compounds from the 3 independent libraries, designed with assistance from medicinal and computational chemists. These 44,000 compounds were vetted from an initial set of 500,000 compounds for early stage lead-like characteristics (i.e. modified Lipinski rules, including MW<625 Da, LogP/LogD, Hydrogen bond donor/acceptors, chiral centers and PSA, functional groups, etc.). Additional substructure filters were applied to remove reactive groups (e.g. Michael acceptors) and compounds predicted to be PAINS. Lead Finder Clustering and MACCS fingerprinting was used to select a set of compounds to perform property based selection of a 50,000 compound set of which 43,000 were readily available from commercial vendors. The final library is comprised of 800 purified Natural Products (Microsource) with annotated biological activities, 11,137 compounds from ChemDiv's SMART library, 20,000 compounds from Chembridge's Core set, and 12,000 compounds from Chembridge's Express Pick set. The compound composition of the library can be characterized by an average MW of 350 Da, LogP/LogD of 2.5, Hydrogen Bond donors of 1, hydrogen bond acceptors of 4, chiral centers <1, and a PSA of 60, with ~25% of the library enriched with compounds with known pharmacophore content. Compounds are suspended in DMSO, arrayed in columns 3-22 of 384 well microplates, and stored at -20^{o}C. Library plates are thawed a maximum of 10X to maintain compound integrity.

Chapter 5- Conclusions and Future Directions

While the experiments within help elucidate important mechanisms in inhibitor resistance within the MAPK signaling pathway, there is still much work to be done in discovering a novel class of inhibitors that can bypass paradoxical activation. While the bivalent vemurafenib inhibitors were able to stabilize $BRAF^{V600E}$ in an inactive, artificially induced dimeric conformation, these inhibitors were ineffective against resistance in cells (Grasso et al., 2016). We hypothesize that this affect is due to $BRAF^{V600E}$'s ability to activate $BRAF^{WT}$ in cells (Heidorn et al., 2010; P. I. Poulikakos et al., 2010), indicating that our bivalent inhibitor must be further adapted to target $BRAF^{WT}$ while not losing selectivity. Our initial efforts were focused on chemically linking pan RAF inhibitor TAK632 with vemurafenib, creating an asymmetric RAF inhibitor capable of inhibiting activated $BRAF^{WT}$ while still maintaining selectivity towards mutant cells with vemurafenib. However, when this was tested with proof-of-principle bivalent TAK inhibitors, these inhibitors were found to drastically reduce TAK's potency in vitro. Monovalent TAK632, however, was able to induce the biologically relevant dimeric conformation of BRAF in vitro, even in the presence of surface mutations that are known to disrupt the dimer (Rajakulendran et al., 2009). These discoveries led us to believe that a chemically linked TAK/vemurafenib heterodimeric inhibitor would not be successful, because the chemical linking has drastically different effects depending on whether an αC-helix IN (TAK) or an αC-helix OUT (vemurafenib) inhibitor is used. Based on our experiments detailed above, focusing on chemically linking αC-helix OUT inhibitors will be more successful in stabilizing an inactive form. However, this is complicated by αC-helix OUT inhibitors being more specific towards $BRAF^{V600E}$ rather than $BRAF^{WT}$ or $CRAF^{WT}$. In moving forward, discovering inhibitors that can hit $BRAF^{WT}$ while not

inducing an αC-helix IN conformation would be integral in discovering a chemically linked RAF inhibitor that can "trap" RAF molecules and disrupt any possible transactivation. A bioluminescence resonance energy transfer (BRET) system has been developed for determining BRAF dimerization effects of various inhibitors (H Lavoie et al., 2013), and this can be used in conjunction with the ELISA based activity assay described above to determine if inhibitors can inhibit $BRAF^{WT}$ but not induce dimerization to the same effect as TAK632. Using these two techniques to monitor existing RAF inhibitors in the literature could lead to a new useful target to chemically link to vemurafenib, as well as help characterize existing inhibitors further to give a clear predictive model for whether inhibitors will induce paradoxical activation and inhibitor resistance.

While these methods are able to predict the effects of inhibitors within a cell, the field is limited by the lack of easily expressing and purifying full length BRAF. Furthermore, it is currently unknown how the N-terminal RBD and CRD domains of BRAF are able to interact with the kinase domain and inhibit activity. The N-terminus of BRAF is known to be able to inhibit the kinase domain *in trans* (Dent et al., 1995; Hugo Lavoie & Therrien, 2015), and using X-ray crystallography to elucidate how the N-terminus blocks the kinase domain is integral. The RBD of BRAF is able to be expressed and purified *in vitro* (Athuluri-Divakar et al., 2016), and I propose adapting this construct and expanding it to encompass regions that are then able to inhibit RAF kinase activity in vitro would give a good construct for crystallization. This can then be complexed with $BRAF^{16mut\_E667F}$ purified in *E. coli* and subjected to crystallization screens. These structural studies could help give the field a more in-depth picture at how transactivation functions.

While the TR-FRET screen was productive in determining hit compounds that are able to specifically disrupt the RAF/MEK signal, these inhibitors need to be further confirmed using ELISA based activity assays, DSF and DSC assays, and AUC studies to elucidate if they affect RAF or MEK kinase activity, which protein they are binding, and if they are truly disrupting the complex formation. These inhibitors are also just a subset of various inhibitors within group chemotypes, and further exploring the successful chemotypes can lead to a novel family of type-IV kinase inhibitors that can disrupt the interaction between BRAF and MEK (Müller et al., 2015). X-Ray crystallography can also be used to perform structure-based drug design to improve these inhibitors. They can then be chemically linked to vemurafenib to develop a selective class of kinase inhibitor that can be selective towards $BRAF^{V600E}$ while disrupting proliferation of the phosphorylation cascade in a synergistic fashion. The MEK/RAF heterodimerization can also further be exploited by developing chemically linked heterodimeric inhibitors that can target both BRAF and MEK at the same time. The crystal structure demonstrates that their dimer interface places the active site of BRAF within close proximity of the allosteric site of MEK (Haling et al., 2014). Chemically linking vemurafenib or another inhibitor to an allosteric MEK inhibitor such as cobimetinib can provide further diversity within MAPK pathway inhibitors that can target transactivation.

References

Acosta, A. M., & Kadkol, S. S. (2016). Mitogen-Activated Protein Kinase Signaling Pathway in Cutaneous Melanoma: An Updated Review. *Archives of Pathology & Laboratory Medicine*, *140*(11), 1290–1296. https://doi.org/10.5858/arpa.2015-0475-RS

Adams, P. D., Afonine, P. V., Bunkoczi, G., Chen, V. B., Davis, I. W., Echols, N., … Zwart, P. H. (2010). PHENIX: a comprehensive Python-based system for macromolecular structure solution. *Acta Cryst.*, *D66*, 213–221.

Afonine, P. V., Grosse-Kunstleve, R. W., Echols, N., Headd, J. J., Moriarty, N. W., Mustyakimov, M., … Adams, P. D. (2012). Towards automated crystallographic structure refinement with phenix.refine. *Acta Cryst.*, *D68*, 352–367.

Anforth, R. M., Blumetti, T. C. M. P., Kefford, R. F., Sharma, R., Scolyer, R. a., Kossard, S., … Fernandez-Peñas, P. (2012). Cutaneous manifestations of dabrafenib (GSK2118436): A selective inhibitor of mutant BRAF in patients with metastatic melanoma. *British Journal of Dermatology*, *167*(5), 1153–1160. https://doi.org/10.1111/j.1365-2133.2012.11155.x

Athuluri-Divakar, S. K., Vasquez-Del Carpio, R., Dutta, K., Baker, S. J., Cosenza, S. C., Basu, I., … Reddy, E. P. (2016). A Small Molecule RAS-Mimetic Disrupts RAS Association with Effector Proteins to Block Signaling. *Cell*, *165*(3), 643–655. https://doi.org/10.1016/j.cell.2016.03.045

Barker, W. C., & Dayhoff, M. O. (1982). Viral src gene products are related to the catalytic chain of mammalian cAMP- . dependent protein kinase. *Proceedings of the National Academy of Sciences of the United States of America*, *79*(May), 2836–2839.

Bollag, G., Hirth, P., Tsai, J., Zhang, J., Ibrahim, P. N., Cho, H., … Nolop, K. (2010). Clinical efficacy of a RAF inhibitor needs broad target blockade in BRAF-mutant melanoma. *Nature*, *467*(7315), 596–599. https://doi.org/10.1038/nature09454

Bollag, G., Tsai, J., Zhang, J., Zhang, C., Ibrahim, P., Nolop, K., & Hirth, P. (2012). Vemurafenib: the first drug approved for BRAF-mutant cancer. *Nature Reviews. Drug Discovery*, *11*(11), 873–886. https://doi.org/10.1038/nrd3847

Bonner, T. I., Kerby, S. B., Sutrave, P., Gunnell, M. a, Mark, G., & Rapp, U. R. (1985). Structure and biological activity of human homologs of the raf/mil oncogene. *Molecular and Cellular Biology*, *5*(6), 1400–1407. https://doi.org/10.1128/MCB.5.6.1400.Updated

Boulton, T. G., Nye, S. H., Robbins, D. J., Ip, N. Y., Radzlejewska, E., Morgenbesser, S. D., … Yancopoulos, G. D. (1991). ERKs: A family of protein-serine/threonine kinases that are activated and tyrosine phosphorylated in response to insulin and

NGF. *Cell*, *65*(4), 663–675. https://doi.org/10.1016/0092-8674(91)90098-J

Cargnello, M., & Roux, P. P. (2011). Activation and Function of the MAPKs and Their Substrates, the MAPK-Activated Protein Kinases. *Microbiology and Molecular Biology Reviews*, *75*(1), 50–83. https://doi.org/10.1128/MMBR.00031-10

Chen, R. H., Sarnecki, C., & Blenis, J. (1992). Nuclear localization and regulation of erk- and rsk-encoded protein kinases. *Molecular and Cellular Biology*, *12*(3), 915–927. https://doi.org/10.1128/MCB.12.3.915

Chen, V. B., Arendall, W. B., Headd, J. J., Keedy, D. A., Immormino, R. M., Kapral, G. J., … Richardson, D. C. (2010). MolProbity: all-atom structure validation for macromolecular crystallography. *Acta Cryst.*, *D66*, 16–21.

Chuang, E., Barnard, D., Hetfich, L., Zhang, X.-F., Avruch, J., & Marshall ', M. S. (1994). Critical Binding and Regulatory Interactions between Ras and Raf Occur through a Small, Stable N-Terminal Domain of Raf and Specific Ras Effector Residues. *Molecular and Cellular Biology*, *14*(8), 5318–5325. https://doi.org/10.1128/MCB.14.8.5318.Updated

Cook, S. J., & McCormick, F. (1993). Inhibition by cAMP of Ras-dependent activation of Raf. *Science*, *262*, 1069–1072.

Crews, C. M., & Erikson, R. L. (1992). Purification of a murine protein-tyrosine/threonine kinase that phosphorylates and activates the Erk-1 gene product: relationship to the fission yeast byr1 gene product. *Proceedings of the National Academy of Sciences of the United States of America*, *89*(17), 8205–8209. https://doi.org/10.1073/pnas.89.17.8205

Davies, H., Bignell, G. R., Cox, C., Stephens, P., Edkins, S., Clegg, S., … Futreal, P. A. (2002). Mutations of the BRAF gene in human cancer. *Nature*, *417*(6892), 949–954. https://doi.org/10.1038/nature00766

Dent, P., Reardon, D. B., Morrison, D. K., Sturgill, T. W., & Iol, M. O. L. C. E. L. L. B. (1995). Regulation of Raf-1 and Raf-1 Mutants by Ras-Dependent and Ras-Independent Mechanisms In Vitro. *Molecular and Cellular Biology*, *15*(8), 4125–4135.

Diaz, B., Barnard, D., Filson, a, MacDonald, S., King, a, & Marshall, M. (1997). Phosphorylation of Raf-1 serine 338-serine 339 is an essential regulatory event for Ras-dependent activation and biological signaling. *Molecular and Cellular Biology*, *17*(8), 4509–4516. https://doi.org/10.1128/MCB.17.8.4509

Emsley, P., Lohkamp, B., Scott, W. G., & Cowtan, K. (2010). Features and Development of Coot. *Acta Cryst.*, *D66*, 486–501.

Farrar, M. A., Alberola-Ila, J., & Perlmutter, R. M. (1996). Activation of the RAF1

kinase cascade by coumermcin-induced dimerization. *Nature*, *383*, 178–181.

Feng, B. Y., Simeonov, A., Jadhav, A., Babaoglu, K., Inglese, J., Shoichet, B. K., & Austin, C. P. (2007). A High-Throughput Screen for Aggregation-Based Inhibition in a Large Compound Library, 2385–2390.

Fetics, S. K., Guterres, H., Kearney, B. M., Buhrman, G., Ma, B., Nussinov, R., & Mattos, C. (2015). Allosteric effects of the oncogenic rasq61l mutant on raf-RBD. *Structure*, *23*(3), 505–516. https://doi.org/10.1016/j.str.2014.12.017

Flaherty, K. T., Infante, J. R., Daud, A., Gonzalez, R., Kefford, R. F., Sosman, J., … Weber, J. (2012). Combined BRAF and MEK Inhibition in Melanoma with BRAF V600 Mutations. *New England Journal of Medicine*, *367*(18), 1694–1703. https://doi.org/10.1056/NEJMoa1210093

Forbes, S. a., Bindal, N., Bamford, S., Cole, C., Kok, C. Y., Beare, D., … Futreal, P. A. (2011). COSMIC: Mining complete cancer genomes in the catalogue of somatic mutations in cancer. *Nucleic Acids Research*, *39*(SUPPL. 1), 945–950. https://doi.org/10.1093/nar/gkq929

Grasso, M., Estrada, M. A., Ventocilla, C., Samanta, M., Maksimoska, J., Villanueva, J., … Marmorstein, R. (2016). Chemically Linked Vemurafenib Inhibitors Promote an Inactive BRAFV600E Conformation. *ACS Chemical Biology*, *11*, 2876–2888. https://doi.org/10.1021/acschembio.6b00529

Greger, J. G., Eastman, S. D., Zhang, V., Bleam, M. R., Hughes, A. M., Smitheman, K. N., … Gilmer, T. M. (2012). Combinations of BRAF, MEK, and PI3K/mTOR Inhibitors Overcome Acquired Resistance to the BRAF Inhibitor GSK2118436 Dabrafenib, Mediated by NRAS or MEK Mutations. *Molecular Cancer Therapeutics*, *11*(4), 909–920. https://doi.org/10.1158/1535-7163.MCT-11-0989

Haling, J. R., Sudhamsu, J., Yen, I., Sideris, S., Sandoval, W., Phung, W., … Malek, S. (2014). Structure of the BRAF-MEK Complex Reveals a Kinase Activity Independent Role for BRAF in MAPK Signaling. *Cancer Cell*, *26*(3), 402–413. https://doi.org/10.1016/j.ccr.2014.07.007

Hanks, S. K., & Hunter, T. (1995). The eukaryotic protein kinase superfamily : kinase (catalytic) domain structure and classification. *The FASEB Journal*, *9*(8), 576–596.

Hanks, S., Quinn, a., & Hunter, T. (1988). The protein kinase family: conserved features and deduced phylogeny of the catalytic domains. *Science*, *241*(4861), 42–52. https://doi.org/10.1126/science.3291115

Heidorn, S. J., Milagre, C., Whittaker, S., Nourry, A., Niculescu-Duvas, I., Dhomen, N., … Marais, R. (2010). Kinase-Dead BRAF and Oncogenic RAS Cooperate to Drive Tumor Progression through CRAF. *Cell*, *140*(2), 209–221. https://doi.org/10.1016/j.cell.2009.12.040

Hopp, T., & Prickett, K. S. (1988). A short plypeptide marker sequence useful for recombinant protein identification and purification. *Nature Biotechnology*, *1542*, 33–36. https://doi.org/10.1017/CBO9781107415324.004

Hoshino, R., Chatani, Y., Yamori, T., Tsuruo, T., Oka, H., Yoshida, O., … Kohno, M. (1999). Constitutive activation of the 41-/43-kDa mitogen-activated protein kinase signaling pathway in human tumors. *Oncogene*, *18*(3), 813–822. https://doi.org/10.1038/sj.onc.1202367

Hu-Lieskovan, S., Mok, S., Homet Moreno, B., Tsoi, J., Robert, L., Goedert, L., … Ribas, A. (2015). Improved antitumor activity of immunotherapy with BRAF and MEK inhibitors in *BRAF* ^{V600E} melanoma. *Science Translational Medicine*, *7*(279), 279ra41-279ra41. https://doi.org/10.1126/scitranslmed.aaa4691

Hu, J., Stites, E. C., Yu, H., Germino, E. a, Meharena, H. S., Stork, P. J. S., … Shaw, A. S. (2013). Allosteric Activation of Functionally Asymmetric RAF Kinase Dimers. *Cell*, *154*(5), 1036–1046. https://doi.org/10.1016/j.cell.2013.07.046

Huleihel, M., Goldsborough, M., Cleveland, J., Gunnell, M., Bonner, T., & Rapp, U. R. (1986). Characterization of murine A-raf, a new oncogene related to the v-raf oncogene. *Molecular and Cellular Biology*, *6*(7), 2655–2662. https://doi.org/10.1128/MCB.6.7.2655.Updated

Hunter, T. (2009). Tyrosine phosphorylation: thirty years and counting. *Current Opinion in Cell Biology*, *21*(2), 140–146. https://doi.org/10.1016/j.ceb.2009.01.028

Ikawa, S., Fukui, M., Ueyama, Y., Tamaoki, N., Yamamoto, T., & Toyoshima, K. (1988). B-raf, a new member of the raf family, is activated by DNA rearrangement. *Molecular and Cellular Biology*, *8*(6), 2651–2654. https://doi.org/10.1128/MCB.8.6.2651.Updated

Illendula, A., Pulikkan, J. A., Zong, H., Grembecka, J., Xue, L., Sen, S., … Bushweller, J. H. (2015). A small-molecule inhibitor of the aberrant transcription factor CBFbeta-SMMHC delays leukemia in mice. *Science*, *347*(6223), 779–784. https://doi.org/10.1126/science.aaa0314

Jambrina, P. G., Rauch, N., Pilkington, R., Rybakova, K., Nguyen, L. K., Kholodenko, B. N., … Rosta, E. (2016). Phosphorylation of RAF kinase dimers drives conformational changes that facilitate transactivation. *Angewandte Chemie - International Edition*, *55*(3), 983–986. https://doi.org/10.1002/anie.201509272

Jänne, P. a., Gray, N., & Settleman, J. (2009). Factors underlying sensitivity of cancers to small-molecule kinase inhibitors. *Nature Reviews Drug Discovery*, *8*(9), 709–723. https://doi.org/10.1038/nrd2871

Johnson, D. B., Flaherty, K. T., Weber, J. S., Infante, J. R., Kim, K. B., Kefford, R. F., … Gonzalez, R. (2014). Combined BRAF (dabrafenib) and MEK inhibition

(trametinib) in patients with BRAFV600-mutant melanoma experiencing progression with single-agent BRAF inhibitor. *Journal of Clinical Oncology*, *32*(33), 3697–3704. https://doi.org/10.1200/JCO.2014.57.3535

Kabsch, W. (2010). XDS. *Acta Cryst.*, *D66*, 125–132.

Karaman, M. W., Herrgard, S., Treiber, D. K., Gallant, P., Atteridge, C. E., Campbell, B. T., … Zarrinkar, P. P. (2008). A quantitative analysis of kinase inhibitor selectivity. *Nature Biotechnology*, *26*(1), 127–132. https://doi.org/10.1038/nbt1358

Karoulia, Z., Wu, Y., Ahmed, T. A., Xin, Q., Bollard, J., Krepler, C., … Poulikakos, P. I. (2016). An Integrated Model of RAF Inhibitor Action Predicts Article An Integrated Model of RAF Inhibitor Action Predicts Inhibitor Activity against Oncogenic BRAF Signaling. *Cancer Cell*, *30*(3), 485–498. https://doi.org/10.1016/j.ccell.2016.06.024

Katz, M., Amit, I., & Yarden, Y. (2007). Regulation of MAPKs by growth factors and receptor tyrosine kinases. *Biochimica et Biophysica Acta - Molecular Cell Research*, *1773*(8), 1161–1176. https://doi.org/10.1016/j.bbamcr.2007.01.002

King, A. J., Arnone, M. R., Bleam, M. R., Moss, K. G., Yang, J., Fedorowicz, K. E., … Laquerre, S. G. (2013). Dabrafenib; Preclinical Characterization, Increased Efficacy when Combined with Trametinib, while BRAF/MEK Tool Combination Reduced Skin Lesions. *PLoS ONE*, *8*(7). https://doi.org/10.1371/journal.pone.0067583

Knapp, S., & Sundström, M. (2014). Recently targeted kinases and their inhibitors - The path to clinical trials. *Current Opinion in Pharmacology*, *17*(1), 58–63. https://doi.org/10.1016/j.coph.2014.07.015

Knighton, D. R., Zheng, J. H., Ten Eyck, L. F., Ashford, V. a, Xuong, N. H., Taylor, S. S., & Sowadski, J. M. (1991). Crystal structure of the catalytic subunit of cyclic adenosine monophosphate-dependent protein kinase. *Science (New York, N.Y.)*, *253*(5018), 407–414. https://doi.org/10.1126/science.1862342

Kolch, W., Heidecker, G., Lloyd, P., & Rapp, U. R. (1991). Raf-1 protein kinase is required for growth of induced NIH/3T3 cells. *Nature*, *349*, 426–428. https://doi.org/10.1038/349426a0

Kornev, A. P., Haste, N. M., Taylor, S. S., & Ten Eyck, L. F. (2006). Surface comparison of active and inactive protein kinases identifies a conserved activation mechanism. *Proceedings of the National Academy of Sciences*, *103*(47), 17783–17788. https://doi.org/10.1073/pnas.0607656103

Kyriakis, J. M., App, H., Zhang, X. F., Banerjee, P., Brautigan, D. L., Rapp, U. R., & Avruch, J. (1992). Raf-1 activates MAP kinase-kinase. *Nature*, *358*(6385), 417–421. https://doi.org/10.1038/358417a0

Lavoie, H., & Therrien, M. (2015). Regulation of RAF protein kinases in ERK signalling.

Nature Reviews Molecular Cell Biology, *16*(5), 281–298. https://doi.org/10.1038/nrm3979

Lavoie, H., Thevakumaran, N., Gavory, G., Li, J. J., Padeganeh, A., Guiral, S., … Therrien, M. (2013). Inhibitors that stabilize a closed RAF kinase domain conformation induce dimerization. *Nat Chem Biol*, *9*(7), 428–436. https://doi.org/10.1038/nCHeMBIO.1257

Lechtenberg, B. C., Mace, P. D., Sessions, E. H., Williamson, R., Stalder, R., Wallez, Y., … Pasquale, E. B. (2017). Structure-Guided Strategy for the Development of Potent Bivalent ERK Inhibitors. *ACS Medicinal Chemistry Letters*, *8*(7), 726–731. https://doi.org/10.1021/acsmedchemlett.7b00127

Lipinski, C.A.; Lombardo, F.; Dominy, B.W.; Feeney, P. J. (1997). Experimental and computational approaches to estimate solubility and permeability in drug discovery and development setting. *Advanced Drug Delivery Reviews*, *23*, 3–25. https://doi.org/10.1016/j.addr.2012.09.019

Liu, L., Lee, M. R., Kim, J. L., Whittington, D. A., Bregman, H., Hua, Z., … Norman, M. H. (2016). Purinylpyridinylamino-based DFG-in/αC-helix-out B-Raf inhibitors: Applying mutant versus wild-type B-Raf selectivity indices for compound profiling. *Bioorganic and Medicinal Chemistry*, *24*(10), 2215–2234. https://doi.org/10.1016/j.bmc.2016.03.055

Lyons, J., Wilhelm, S., Hibner, B., & Bollag, G. (2001). Discovery of a novel Raf kinase inhibitor. *Endocrine Related Cancer*, *8*(3), 219–225. https://doi.org/10.1677/erc.0.0080219

Ma, H., Deacon, S., & Horiuchi, K. (2008). The challenge of selecting protein kinase assays for lead discovery optimization. *Expert Opin Drug Discov.*, *3*(6), 607–621. https://doi.org/10.1109/TMI.2012.2196707.Separate

Manning, G., Whyte, D. B., Martinez, R., & Hunter, T. (2002). The Protein Kinase Complement of the Human Genome. *Science*, *298*(December), 1912–1934.

Marais, R., Light, Y., Paterson, H. F., Mason, C. S., & Marshall, C. J. (1997). Differential regulation of Raf-1, A-Raf, and B-Raf by oncogenic Ras and tyrosine kinases. *Journal of Biological Chemistry*, *272*(7), 4378–4383. https://doi.org/10.1074/jbc.272.7.4378

McCoy, A. J., Grosse-Kunstleve, R. W., Adams, P. D., Winn, M. D., Storoni, L. C., & Read, R. J. (2007). Phaser Crystallographic software. *J. Appl. Cryst.*, *40*, 658–674.

Moelling, K., Heimann, B., Beimling, P., Rapp, U. R., & Sander, T. (1984). Serine- and threonine-specific protein kinase activities of purified gag-mil and gag-raf proteins. *Nature*, *312*, 558–561.

Moriarty, N. W., Grosse-Kunstleve, R. W., & Adams, P. D. (2009). electronic Ligand Builder and Optimization Workbench (eLBOW): a tool for ligand coordinate and restraint generation. *Acta Cryst.*, *D65*, 1074–1080.

Morrison, D. K., Kaplan, D. R., Rapp, U., & Roberts, T. M. (1988). Signal transduction from membrane to cytoplasm : Growth factors and membrane-bound oncogene products increase Raf-1 phosphorylation and associated protein kinase activity. *Proceedings of the National Academy of Sciences of the United States of America*, *85*(December), 8855–8859.

Müller, S., Chaikuad, A., Gray, N. S., & Knapp, S. (2015). The ins and outs of selective kinase inhibitor development. *Nature Chemical Biology*, *11*(11), 818–821. https://doi.org/10.1038/nchembio.1938

Muslin, a. J., Tanner, J. W., Allen, P. M., & Shaw, a. S. (1996). Interaction of 14-3-3 with signaling proteins is mediated by the recognition of phosphoserine. *Cell*, *84*(6), 889–897. https://doi.org/10.1016/S0092-8674(00)81067-3

Nakamura, A., Arita, T., Tsuchiya, S., Donelan, J., Chouitar, J., Carideo, E., … Yoshida, S. (2013). Antitumor activity of the selective pan-RAF inhibitor TAK-632 in BRAF inhibitor-resistant melanoma. *Cancer Research*, *73*(23), 7043–7055. https://doi.org/10.1158/0008-5472.CAN-13-1825

Nakano, H., Kobayashi, E., Takahashi, I., Tamaoki, T., Kuzuu, Y., & Iba, H. (1987). Staurosporine inhibits tyrosine-specific protein kinase activity of Rous sarcoma virus transforming protein p60. *The Journal of Antibiotics*, *40*(5), 706–708. https://doi.org/10.7164/antibiotics.40.706

Nazarian, R., Shi, H., Wang, Q., Kong, X., Koya, R. C., Lee, H., … Lo, R. S. (2010). Melanomas acquire resistance to B-RAF(V600E) inhibition by RTK or N-RAS upregulation. *Nature*, *468*(7326), 973–977. https://doi.org/10.1038/nature09626

Ochoa, D., Bradley, D., & Beltrao, P. (2018). Evolution, dynamics and dysregulation of kinase signalling. *Current Opinion in Structural Biology*, *48*, 133–140. https://doi.org/10.1016/j.sbi.2017.12.008

Ohren, J. F., Chen, H., Pavlovsky, A., Whitehead, C., Zhang, E., Kuffa, P., … Hasemann, C. a. (2004). Structures of human MAP kinase kinase 1 (MEK1) and MEK2 describe novel noncompetitive kinase inhibition. *Nature Structural & Molecular Biology*, *11*(12), 1192–1197. https://doi.org/10.1038/nsmb859

Okaniwa, M., Hirose, M., Arita, T., Yabuki, M., Nakamura, A., Takagi, T., … Ishikawa, T. (2013). Discovery of a Selective Kinase Inhibitor (TAK-632) Targeting Pan-RAF Inhibition: Design, Synthesis, and Biological Evaluation of C-7- Substituted 1,3-Benzothiazole Derivatives. *Journal of Medicinal Chemistry*, *56*, 6478–6494. https://doi.org/10.1021/jm400778d

Omura, S., Iwai, Y., Hirano, a, Nakagawa, a, Awaya, J., Tsuchya, H., … Masuma, R. (1977). A new alkaloid AM-2282 OF Streptomyces origin. Taxonomy, fermentation, isolation and preliminary characterization. *The Journal of Antibiotics*, *30*(4), 275–282. https://doi.org/10.7164/antibiotics.30.275

Otwinowski, Z., & Minor, W. (1997). Processing of X-ray Diffraction Data Collected in Oscillation Mode. In C. W. Carter, Jr. & R. M. Sweet, Eds. (Ed.), *Method Enzymol.* (Vol. 276: Macro, pp. 307–326). New York: Academic Press.

Poulikakos, P. I., Persaud, Y., Janakiraman, M., Kong, X., Ng, C., Moriceau, G., … Solit, D. B. (2011). RAF inhibitor resistance is mediated by dimerization of aberrantly spliced BRAF(V600E). *Nature*, *480*(7377), 387–390. https://doi.org/10.1038/nature10662

Poulikakos, P. I., Zhang, C., Bollag, G., Shokat, K. M., & Rosen, N. (2010). RAF inhibitors transactivate RAF dimers and ERK signalling in cells with wild-type BRAF. *Nature*, *464*(7287), 427–430. https://doi.org/10.1038/nature08902

Poulikakos, P., & Rosen, N. (2011). Mutant braf Melanomas-Dependence and Resistance. *Cancer Cell*, *19*, 11–15.

Qin, J., Xie, P., Ventocilla, C., Zhou, G., Vultur, A., Chen, Q., … Marmorstein, R. (2012). Identification of a Novel Family of braf-V600E Inhibitors. *J. Med. Chem*, *55*, 5220–5230.

Rajakulendran, T., Sahmi, M., Lefrançois, M., Sicheri, F., & Therrien, M. (2009). A dimerization-dependent mechanism drives RAF catalytic activation. *Nature*, *461*(7263), 542–545. https://doi.org/10.1038/nature08314

Rapp, U. R., Goldsborough, M. D., Mark, G. E., Bonner, T. I., Groffen, J., Reynolds, F. H., & Stephenson, J. R. (1983). Structure and biological activity of v-raf, a unique oncogene transduced by a retrovirus. *Proceedings of the National Academy of Sciences of the United States of America*, *80*(July), 4218–4222. https://doi.org/10.1073/pnas.80.14.4218

Ray, L. B., & Sturgill, T. W. (1987). Rapid stimulation by insulin of a serine/threonine kinase in 3T3-L1 adipocytes that phosphorylates microtubule-associated protein 2 in vitro. *P Natl Acad Sci USA*, *84*(March), 1502–1506. https://doi.org/10.1073/pnas.84.6.1502

Rebocho, a. P., & Marais, R. (2013). ARAF acts as a scaffold to stabilize BRAF:CRAF heterodimers. *Oncogene*, *32*(26), 3207–3212. https://doi.org/10.1038/onc.2012.330

Rheault, T. R., Stellwagen, J. C., Adjabeng, G. M., Hornberger, K. R., Petrov, G., Waterson, A. G., … Kimberly, G. (2013). Discovery of Dabrafenib: A Selective Inhibitor of Raf Kinases with Antitumor Activity against B-Raf-Driven Tumors. *ACS Medicinal Chemistry Letters*, *4*, 358–362. https://doi.org/10.1021/ml4000063

Ritt, D. a., Zhou, M., Conrads, T. P., Veenstra, T. D., Copeland, T. D., & Morrison, D. K. (2007). CK2 Is a Component of the KSR1 Scaffold Complex that Contributes to Raf Kinase Activation. *Current Biology*, *17*(2), 179–184. https://doi.org/10.1016/j.cub.2006.11.061

Rossomando, a J., Payne, D. M., Weber, M. J., & Sturgill, T. W. (1989). Evidence that pp42, a major tyrosine kinase target protein, is a mitogen-activated serine/threonine protein kinase. *Proceedings of the National Academy of Sciences of the United States of America*, *86*(18), 6940–6943. https://doi.org/10.1073/pnas.86.18.6940

Rushworth, L. K., Hindley, A. D., Neill, E. O., & Kolch, W. (2006). Regulation and Role of Raf-1 / B-Raf Heterodimerization. *Mol Cell Biol*, *26*(6), 2262–2272. https://doi.org/10.1128/MCB.26.6.2262

Salama, A. K., & Kim, K. B. (2013). Trametinib (GSK1120212) in the treatment of melanoma. *Expert Opinion on Pharmacotherapy*, *14*(5), 619–627. https://doi.org/10.1517/14656566.2013.770475

Taylor, S. S., & Kornev, A. P. (2011). Protein Kinases: Evolution of Dynamic Regulatory Proteins. *Trends in Biochemical Sciences*, *36*(2), 65–77. https://doi.org/10.1016/j.tibs.2010.09.006.Protein

Thevakumaran, N., Lavoie, H., Critton, D. A., Tebben, A., Marinier, A., Sicheri, F., & Therrien, M. (2014). Crystal structure of a BRAF kinase domain monomer explains basis for allosteric regulation. *Nature Structural & Molecular Biology*, *22*(1), 37–43. https://doi.org/10.1038/nsmb.2924

Tran, N. H., Wu, X., & Frost, J. a. (2005). B-Raf and Raf-1 are regulated by distinct autoregulatory mechanisms. *Journal of Biological Chemistry*, *280*(16), 16244–16253. https://doi.org/10.1074/jbc.M501185200

Treiber, D. K., & Shah, N. P. (2013). Ins and outs of kinase DFG motifs. *Chemistry and Biology*, *20*(6), 745–746. https://doi.org/10.1016/j.chembiol.2013.06.001

Tsai, J., Lee, J. T., Wang, W., Zhang, J., Cho, H., Mamo, S., … Bollag, G. (2008a). Discovery of a selective inhibitor of oncogenic B-Raf kinase with potent antimelanoma activity. *Proceedings of the National Academy of Sciences of the United States of America*, *105*(8), 3041–3046. https://doi.org/10.1073/pnas.0711741105

Tsai, J., Lee, J. T., Wang, W., Zhang, J., Cho, H., Mamo, S., … Bollag, G. (2008b). Discovery of a selective inhibitor of oncogenic B-Raf kinase with potent antimelanoma activity. *Proceedings of the National Academy of Sciences of the United States of America*, *105*(8), 3041–3046. https://doi.org/10.1073/pnas.0711741105

Ünal, E. B., Uhlitz, F., & Blüthgen, N. (2017). A compendium of ERK targets. *FEBS*

Letters, *591*(17), 2607–2615. https://doi.org/10.1002/1873-3468.12740

Villanueva, J., Infante, J. R., Krepler, C., Reyes-Uribe, P., Samanta, M., Chen, H. Y., … Nathanson, K. L. (2013). Concurrent MEK2 Mutation and BRAF Amplification Confer Resistance to BRAF and MEK Inhibitors in Melanoma. *Cell Reports*, *4*(6), 1090–1099. https://doi.org/10.1016/j.celrep.2013.08.023

Villanueva, J., Vultur, A., & Herlyn, M. (2011). Resistance to BRAF inhibitors: Unraveling mechanisms and future treatment options. *Cancer Research*, *71*(23), 7137–7140. https://doi.org/10.1158/0008-5472.CAN-11-1243

Vojtek, A. B., Hollenberg, S. M., & Cooper, J. a. (1993). Mammalian Ras interacts directly with the serine/threonine kinase raf. *Cell*, *74*(1), 205–214. https://doi.org/10.1016/0092-8674(93)90307-C

Wagle, N., Emery, C., Berger, M. F., Davis, M. J., Sawyer, A., Pochanard, P., … Garraway, L. A. (2011). Dissecting therapeutic resistance to RAF inhibition in melanoma by tumor genomic profiling. *Journal of Clinical Oncology*, *29*(22), 3085–3096. https://doi.org/10.1200/JCO.2010.33.2312

Waizenegger, I. C., Baum, A., Steurer, S., Stadtmu ller, H., Bader, G., Schaaf, O., … Adolf, G. R. (2016). A Novel RAF Kinase Inhibitor with DFG-Out-Binding Mode: High Efficacy in BRAF-Mutant Tumor Xenograft Models in the Absence of Normal Tissue Hyperproliferation. *Molecular Cancer Therapeutics*, *15*(3), 354–365. https://doi.org/10.1158/1535-7163.MCT-15-0617

Walsh, D. A., Perkins, J. P., & Krebs, E. G. (1968). An Adenosine 3',5'-Monophosphate-dependent Protein Kinase from Rabbit Skeletal Muscle. *Journal of Biological Chemistry*, *243*(13), 3763–3766.

Wan, P. T. C., Garnett, M. J., Roe, S. M., Lee, S., Niculescu-Duvaz, D., Good, V. M., … Marais, R. (2004). Mechanism of activation of the RAF-ERK signaling pathway by oncogenic mutations of B-RAF. *Cell*, *116*(6), 855–867. Retrieved from http://www.ncbi.nlm.nih.gov/pubmed/15035987

Weisberg, E., Boulton, C., Kelly, L. M., Manley, P., Fabbro, D., Meyer, T., … Griffin, J. D. (2002). Inhibition of mutant FLT3 receptors in leukemia cells by the small molecule tyrosine kinase inhibitor PKC412. *Cancer Cell*, *1*(5), 433–443. https://doi.org/10.1016/S1535-6108(02)00069-7

Wellbrock, C., Karasarides, M., & Marais, R. (2004). The RAF proteins take centre stage. *Nature Reviews. Molecular Cell Biology*, *5*(11), 875–885. https://doi.org/10.1038/nrm1498

Wenglowsky, S., Moreno, D., Laird, E. R., Gloor, S. L., Ren, L., Risom, T., … Voegtli, W. C. (2012). Pyrazolopyridine inhibitors of B-RafV600E. Part 4: Rational design and kinase selectivity profile of cell potent type II inhibitors. *Bioorganic and*

Medicinal Chemistry Letters, *22*(19), 6237–6241. https://doi.org/10.1016/j.bmcl.2012.08.007

Wilhelm, S., & Chien, D. (2002). BAY 43-9006: Preclinical Data. *Current Pharmaceutical Design*, *8*(25), 2255–2257.

Wilhelm, S. M., Carter, C., Tang, L., Wilkie, D., McNabola, A., Rong, H., … Trail, P. A. (2004). BAY 43-9006 Exhibits Broad Spectrum Oral Antitumor Activity and Targets the RAF / MEK / ERK Pathway and Receptor Tyrosine Kinases Involved in Tumor Progression and Angiogenesis BAY 43-9006 Exhibits Broad Spectrum Oral Antitumor Activity and Targets the Pr. *Cancer Res*, *64*(19), 7099–7109. https://doi.org/10.1158/0008-5472.CAN-04-1443

Williams, N. G., Roberts, T. M., & Li, P. (1992). Both p21_ras_ and pp60_v-src_ are required, but neither alone is sufficient, to activate the Raf-1 kinase. *Proceedings of the National Academy of Sciences USA*, *89*(April), 2922–2926.

Wittmann, V., Takayama, S., Gong, K. W., Weitz-Schmidt, G., & Wong, C. (1998). Ligand Recognition by E- and P- Selectin: Chemoenzymatic Synthesis and Inhibitory Activity of Bivalent Sialyl Lewis x Derivatives and Sialyl Lewis x Carboxylic Acids. *J. Org. Chem.*, *63*, 5137–5143.

Xie, P., Streu, C., Qin, J., Bregman, H., Pagano, N., Meggers, E., & Marmorstein, R. (2009). The crystal structure of BRAF in complex with an organoruthenium inhibitor reveals a mechanism for inhibition of an active form of BRAF kinase. *Biochemistry*, *48*(23), 5187–5198. https://doi.org/10.1021/bi802067u

Zhang, B. H., & Guan, K. L. (2000). Activation of B-Raf kinase requires phosphorylation of the conserved residues Thr598 and Ser601. *EMBO J.*, *19*(20), 5429–5439.

Zhang, C., Spevak, W., Zhang, Y., Burton, E. A., Ma, Y., Habets, G., … Bollag, G. (2015). RAF inhibitors that evade paradoxical MAPK pathway activation. *Nature*, *526*(7574), 583–586. https://doi.org/10.1038/nature14982

Zhang, J., Chung, T. D. Y., & Oldenburg, K. R. (1999). A Simple Statistical Parameter for Use in Evaluation and Validation of High Throughput Screening Assays. *Journal of Biomolecular Screening*, *4*(2), 67–73.

Zhang, R., & Monsma, F. (2010). Fluorescence-based thermal shift assays. *Curr. Opin. Drug Discov Devel.*, *13*(4), 389–402.

Zhang, X. F., Settleman, J., Kyriakis, J. M., Takeuchi-Suzuki, E., Elledge, S. J., Marshall, M. S., … Avruch, J. (1993). Normal and oncogenic p21ras proteins bind to the amino-terminal regulatory domain of c-Raf-1. *Nature*, *364*(6435), 308–313.